Surface Defect Machining- A New Approach for Hard Turning

Waleed Bin Rashid

A dissertation Submitted for the degree of Doctor of Philosophy

Heriot-Watt University
Institute of Mechanical, Process and Energy Engineering (IMPEE)

August 2014

The copyright in this thesis is owned by the author. Any quotation from the thesis or use of any of the information contained in it must acknowledge this thesis as the source of the quotation or information.

ABSTRACT

Hard turning is emerging as a key technology to substitute conventional grinding processes, mainly on account of lower equipment cost, short setup time, and a reduced number of process steps. This is, however, being impeded by a number of challenges required to be resolved, including attainable surface roughness, surface deteriorations, surface residual stresses and metallurgical transformations on the machined steel surface (white layer).

In this thesis, a novel approach named Surface Defect Machining (SDM) is proposed as a viable solution to resolve a large number of these issues and to improve surface finish and surface integrity. SDM is defined as a process of machining, where a workpiece is first subjected to surface defects creation at a depth less than the uncut chip thickness; either through mechanical and/or thermal means; then followed by a normal machining operation so as to reduce the cutting resistance. A comprehensive understanding of SDM is established theoretically using finite element method (FEM). Also, an experimental study has been carried out for extensive understanding of the new technique. A good agreement between theoretical and experimental investigations has been achieved. The results show very interesting salient features of SDM, providing favourable machining outcomes. These include: reduced shear plane angle, reduced machining forces, lower residual stresses on the machined surface, reduced tool-chip interface contact length and increased chip flow velocity, as well as reductions in overall temperature in the cutting zone and changing the mechanism of chip morphology from jagged to discontinuous. However, the most prominent outcome is the improved attainable surface roughness. Furthermore, SDM shows the ability to exceed the critical feed rate and achieve an optical surface finish upto 30 nm. A scientific explanation of the improved surface roughness suggests that during SDM, a combination of both the cutting action and the rough polishing action help to improve the machined surface.

Based on these findings, it is anticipated that a component machined using the SDM method should exhibit improved quality of the machined surface, which is expected to provide tremendous commercial advantages in the time to come.

AKNOWLEDGEMENT

First and for most, I owe the greatest gratitude to my advisor, Prof. Xichun Luo, for his intellectual support and encouragement. His guidance has led this dissertation to be presented. I would also like to express my gratitude to Prof. James Ritchie for his knowledgeable advice and consistent input.

I am also very grateful for the Ministry of Higher Education, Kingdom of Saudi Arabia for their generous financial support.

All thanks to Dr. Saurav Goel for his unlimited support, wise advice, and his contribution to the joint publications. I also thank Dr. Jining Sun for his kind assistance and help whenever I needed.

I am indebted to my parents, my father and mother-in-law, and my brothers and sisters for their continued support.

Last but not least. I thank my wife and children for their endless love and patience.

Declaration Statement

ACADEMIC REGISTRY
Research Thesis Submission

Name*:*	Waleed Bin Rashid		
School/PGI:	IMPEE		
Version: *(i.e. First, Resubmission, Final)*	Final	Degree Sought (Award **and** Subject area)	PhD, Mechanical Engineering

---

Declaration

In accordance with the appropriate regulations I hereby submit my thesis and I declare that:

1) the thesis embodies the results of my own work and has been composed by myself
2) where appropriate, I have made acknowledgement of the work of others and have made reference to the work carried out in collaboration with other persons
3) the thesis is the correct version of the thesis for submission and is the same version as any electronic versions submitted*.
4) my thesis for the award referred to, deposited in the Heriot-Watt University Library, should be made available for loan or photocopying and be available via the Institutional Repository, subject to such conditions as the Librarian may require
5) I understand that as a student of the University, I am required to abide by the Regulations of the University and to conform to its discipline.

* *Please note that it is the responsibility of the candidate to ensure that the correct version of the thesis is submitted.*

Signature of Candidate*:*		Date:	/08/2014

Submission

Submitted By *(name in capitals):*	WALEED BIN RASHID
Signature of Individual Submitting:	
Date Submitted:	/08/2014

For Completion in the Student Service Centre (SSC)

Received in the SSC by *(name in capitals):*			
Method of Submission *(Handed in to SSC; posted through internal/external mail):*			
E-thesis Submitted (***mandatory for final theses***)			
Signature:		Date:	/08/2014

TABLE OF CONTENTS

Abstract.....i
Acknowledgement.....iii
Declaration statement.....iv
Table of Contents.....v
List of Tables.....viii
List of Figures.....ix
Abbreviation.....xi
Nomenclature.....xii
List of Publications by the Candidate.....xiii

CHAPTER 1 – INTRODUCTION.....1
1.1 Background and significance of the project.....1
1.2 Aim and objectives.....3
1.3 Structure of the thesis.....4
CHAPTER 2 – Literature review.....6
2.1 Introduction.....6
2.2 Definition and description of hard turning.....6
2.3 Machine tool requirements for hard turning.....7
2.4 Hard turning versus grinding.....8
2.5 Limitations of hard turning.....9
2.6 Workpiece materials used in hard turning.....9
2.7 Consideration of cutting tool materials.....10
  2.7.1 Cubic boron nitride (CBN).....12
  2.7.2 Polycrystalline cubic boron nitride (PCBN).....12
  2.7.3 Importance of tool geometry.....13
2.8 Tool wear and its mechanism during hard turning.....15
  2.8.1 Factors that influence tool tear and wear patterns.....16
2.9 Chip formation mechanism.....17
2.10 Cutting Forces observed in hard turning.....19
2.11 Surface integrity and roughness.....21
2.12 Surface defects.....25
  2.12.1 Side flow and pile-up edges.....28
  2.12.2 Weldament particles.....29
  2.12.3 Microchip debris/grooves/ridges.....30
2.13 Cutting parameters and optimization.....30
2.14 Numerical modelling of hard turning using FEA.....35
2.15 Summary.....37
CHAPTER 3 – Development of surface defect machining method for hard turning processes.....38
3.1 Introduction.....38
3.2 Description of the surface defect machining method.....38
3.3 Finite element modelling and constitutive deformation criterion.....42
  3.3.1 Fracture criterion and friction tool/chip interface.....44
3.4 Validations of FEM with experiments.....44
3.5 Temperature in the machining zone.....48
3.6 Stresses in the machining zone, residual stresses and chip morphology.....50
3.7 Summary.....53

CHAPTER 4 – Experimental design and proof-of-concept of SDM..............................54
4.1 Introduction…………………………………………………………………….....54
4.2 Machining experiments...54
4.2.1 Experimental design to obtain optimized machining parameters...................55
4.3 Multiple regression model...56
4.3.1 Comparison of Multiple Regression...61
4.4 Examination of proposed SDM experimentally in comparison to conventional hard turning…………………………………………….....................................63
4.4.1 Experimental Setup...63
4.4.2 Experimental parts assembly………………………………........................65
4.4.2.1 Material selection……………………………………………...........65
4.4.2.2 Laser ablation……………………………………………….................66
4.4.2.3 Dynamometer assembly…………………...67
4.4.2.4 Thermal camera assembly…………………….......................................68
4.5 Data collocation of the dynamometer………………………………....................69
4.6 Temperature in the cutting zone and chip morphology..71
4.7 Surface roughness...72
4.8 Summary.....……………………………………………………………...................73
CHAPTER 5 – Optimization of parametric design..75
5.1 Introduction...75
5.2 Taguchi method...75
5.3 Experimental details...77
5.4 Signal-to-noise (S/N) ratio analysis...79
5.5 Analysis of Variance 83
5.6 Confirmation experiments...85
5.7 Discussion on tool wear...87
5.8 Summary.....………………………………..89
CHAPTER 6 – SDM as a probe to ultra high precision machining................................90
6.1 Introduction……………………………………………………….........................90
6.2 Details of the experiment and the results……………………………….............90
6.3 The significant and critical feed rate observation………………….......................91
6.4 3D-2D surface topography analyses...93
6.5 SEM examination of the machined surface…………………………….............94
6.6 Theoretical analysis via FEM ....………………………………….........96
6.8 White layer in relation to SDM…………………………………………….........97
6.9 Classification of surface defects…………………………………….......98
6.10 Summary.....………………………………………………………………….........99
CHAPTER 7 – Finite element modelling of multi cutting passes................................101
7.1 Introduction…………………………………………….......................101
7.2 Simulation details………………………………………….........................101
7.3 Chip formation mechanism of SDM method……………………......................103
7.4 Workpiece temperature and residual stresses……………………….................106
7.4.1 Residual stresses....................……………………….................................108
7.5 Cyclic cutting forces……………………………………………….................109
7.6 Fatigue crack initiation of the cutting tool……………………….................111
7.7 Summary.....……………………………………………………….................115
CHAPTER 8– Conclusions and future work...117
8.1 Assessment of research contribution……………………………………………117
8.2 Conclusions of the research…………………………………………….........118
8.3 Recommendations for future work..120
List of References...122
Appendices...137

A. Comparison between surface defects machining and vibration assisted machining……...137
B. CNC G code program used in the experiments………………………………...139
C. Materails properties (Hardness and Composition)...140

LISTS OF TABLES

Table 2.1: Hard turning vs. conventional machining...6
Table 2.2: Major advantages of hard turning over grinding…………………………….7
Table 2.3: Different CBN tools and their properties (Dogra et al., 2010).....................13
Table 2.4: Qualitative characterization of various surface defects – adapted (Bailey, 1974, Zhou et al., 2011)..26
Table 2.5: Review of the work on surface deterioration..26
Table 2.6: Literature review of optimization studies on hard turning...........................30
Table 2.7: Finite element software used to study hard turning.....................................36
Table 2.8: Methods to determine the flow stress data...37
Table 3.1: Chemical composition of AISI 4340 steel (Coelho et al., 2007)..................43
Table 3.2: J-C constitutive parameters for AISI 4340 steel (52 HRC) (Coelho et al., 2007)...43
Table 3.3: Workpiece and cutting tool properties...43
Table 3.4: Simulation parameters..43
Table 3.5: Experimental and simulation results..45
Table 4.1: Experimental parameters...54
Table 4.2: Experimental data obtained from the hard turning trials...............................55
Table 4.3: Summary of data exponential...57
Table 4.4: Four normal equations for the model..57
Table 4.5: Multiple Regression models...59
Table 4.6: Standard deviation of the model with respect to experiments........................62
Table 4.7: Experimental parameters...64
Table 4.8: A comparison of the average surface roughness..73
Table 5.1: Cutting parameters and their levels...78
Table 5.2: Orthogonal array..78
Table 5.3: Experimental parameters...79
Table 5.4: Experimental results for surface roughness and S/N ratio............................80
Table 5.5: Response table mean S/N ratio for surface roughness factor........................81
Table 5.6: Results of the ANOVA for surface roughness..84
Table 5.7: Output of the confirmatory trial..85
Table 5.8: Experimental measurement of tool flank wear length V_b............................87
Table 6.1: Experimental parameters...90
Table 7.1: Constitutive equations and machining variables used in the FEA simulation for an elaborative testing on a range of materials...101
Table 7.2: Shear angle alteration from first cut and second cut..................................103
Table 7.3: Chip mechanism of D2 steel of two different hardnesses formed by the SDM method...104
Table 7.4: Second cut chip mechanism of SDM...106
Table 7.5: Average workpiece temperature obtained after the second cut..................107
Table 7.6: Summary of cutting forces obtained from simulated material...................110
Table 7.7: Summary of the values used in the Forman and Newman's equations......113
Table 7:8 Summary of Calculated results..114

LISTS OF FIGURES

Figure 1.1: Major advantages of hard turning (Hardinge Inc., 2014)............................1
Figure 1.2: Qualitative overview of the capability of hard turning and grinding (Klocke et al., 2005)...2
Figure 2.1: Comparison of conventional processing with hard turning 6
Figure 2.2: Characteristics of high-precision lathe suited for hard turning (Tönshoff et al., 2000)..6
Figure 2.3: Comparison of cost of turning versus grinding (Sandvikens, 2013)............7
Figure 2.4: Classification scheme for the various ferrous alloys (William, 2007)..........9
Figure 2.5: Different cutting tool properties (Hardinge Inc., 2014).............................11
Figure 2.6: Composition cycle of hard, brittle materials (Shaw, 2004).........................11
Figure 2.7: The variation of Knoop hardness with temperature for several hard materials (Hardinge Inc., 2014, Shaw, 2004)..12
Figure 2.8: Effect of tool geometry on performance parameters in hard turning (Dogra et al., 2011)..14
Figure 2.9: Type of edge preparations used in hard turning cutting tools (Özel et al., 2005)..14
Figure 2.10: Typical wear types observed on cutting tools (Lahiff et al., 2007)...........17
Figure 2.11: Classification of chip formation (Tönshoff et al., 2000)............................18
Figure 2.12: Chip morphology according to the hardness and the cutting speed (Poulachon et al., 2001)...19
Figure 2.13: Relationship between cutting forces and hardness of AISI 4340 steel workpiece (Matsumoto et al., 1987)..20
Figure 2.14: Achievable surface roughness and ISO tolerance in hard turning (Grzesik, 2011)..21
Figure 2.15: (a) Tensile residual stress (b) Compressive residual stress (Dogra et al., 2010)..23
Figure 2.16: Residual stress patterns in hard turned components (Tönshoff et al., 2000)..24
Figure 2.17: High speed camera image of the cutting zone showing a close up view of the machined surface – adapted (Pekelharing and Gieszen, 1971)................................28
Figure 3.1 Machining of porous material (Tutunea-Fatan et al., 2011).........................38
Figure 3.2 Pulse laser pre-treated machining proposed by Komanduri et al., (1982) and tool wear during LAM (Sun et al., 2010)..39
Figure 3.3: Development of surface defect machining method....................................40
Figure 3.4: (a) Patterning on a workpiece (b) Examples of patterns used to generate surface discontinuities on a workpiece..40
Figure 3.5: Schematic diagram indicating difference between the mode of deformation between a continuous material and a discontinuous material obtained from FEA.........41
Figure 3.6: Boundary conditions for the FEA model...42
Figure 3.7: Comparison of experimental and theoretical machining results while cutting AISI 4340 steel (52 HRC) with Al_2O_3 cutting insert having -5º tool rake angle............45
Figure 3.8: Evolution of cutting forces over 1.486 mm cutting length..........................47
Figure 3.9: Optimization of hardness, shear plane angle and friction force based on the experimental results (derived from the experimental data) (Matsumoto et al., 1986; Matsumoto et al., 1987; Wu and Matsumoto, 1990)...47
Figure 3.10: Temperature in the machining zone during surface defect machining........48
Figure 3.11: Temperature in the machining zone during ordinary HT process...............48
Figure 3.12: Temperatures in the machining zone using (a) conventional HT process (b) SDM method..49
Figure 3.13: von Mises stresses during surface defect machining.................................50

Figure 3.14: von Mises stresses during conventional machining...................................51
Figure 3.15: Comparison of residual stresses on the machined surface (*x*-direction) ….52
Figure 3.16: Velocity of cutting chips (V_c: Cutting velocity, V_f: Chip flow velocity, V_s: Shear velocity) during (a) surface defect machining and (b) ordinary HT process……. 52
Figure 4.1: Comparison of experimental surface roughness with Multiple Regression Model A...61
Figure 4.2: Comparison of experimental surface roughness with Multiple Regression Model E...62
Figure 4.3: Experimental setup...64
Figure 4.4: Trumpf CO_2 laser machining centre...66
Figure 4.5: Workpiece with holes made through laser...67
Figure 4.6: SEM image of the cross-section of the surface defect created by CO_2 laser, highlighting the damage depth caused by laser..67
Figure 4.7: Dynamometer assembly via special fixture to the tool holder......................68
Figure 4.8: Camera positioned inside the box to be protected from the chip, meanwhile, the suction mounted cup is used to fix both the camera and the box and the whole assembly is attached to the CNC wall...69
Figure 4.9: Experimental assembly..69
Figure 4.10: Cutting forces (a) proposed SDM (b) normal hard turning process...........70
Figure 4.11: Temperatures in the cutting zone (a) conventional HT process (b) SDM...71
Figure 4.12: Surface roughness using (a) conventional HT (b) proposed method..........72
Figure 5.1: Mean S/N ratio for various parameters (feed rate, depth of cut and cutting speed)...82
Figure 5.2: Close comparison of S/N ratio for cutting speed and depth of cut..............83
Figure 5.3: Measurement of the surface roughness using the optimal cutting parameters 86
Figure 6.1: Variation in Ra and Rz with respect to the feed rate during conventional machining and SDM..91
Figure 6.2: Quality of the machined surface (a) Talysurf measurement of the machined surface roughness (b) mirror finish smooth machined surface......................................92
Figure 6.3: Topography of the machined surface obtained using SDM.........................93
Figure 6.4: Topography of the machined surface obtained using classical HT.............93
Figure 6.5: 2D profile of the machined surface (a) SDM HT (b) classical HT...............94
Figure 6.6: Comparison of the surface topography obtained via SEM at a feed rate of 0.005 mm/ rev (a) surface defect machining method and (b) conventional hard turning 95
Figure 6.7: SEM examination of the machined surface quality obtained from machining at a feed rate of 0.03 mm/ rev...96
Figure 6.8: finite element analysis of the surface defect machining of hard steel (a) when depth of surface defects is less than the depth of cut and (b) depth of surface defects is larger than the depth of cut..97
Figure 6.9: Measurement of white layer on the finished machined surface....................98
Figure 6.10: Influence of surface defects on altering topography of machined surfaces 99
Figure 7.1: Schematic of FEA simulation...102
Figure 7.2: Saw tooth chip observed from the FEA simulations..................................103
Figure 7.3: Hardness effect on the chip formation (a) continuous chip (b) saw tooth chip…………………………………………………………………………….....104
Figure 7.4: Simulation results of the cutting zone temperature: conventional HT........107
Figure 7.5: Simulation results of the cutting zone temperature: SDM..........................107
Figure 7.6: Evolution of residual stresses...109
Figure 7.7: Cyclic force and amplitude for different hardness: conventional HT.........110

Figure 7.8: Cyclic force and amplitude for different hardness: SDM............................110
Figure 7.9: Cyclic stress on the cutting tool for different hardness: conventional HT..111
Figure 7.10: Cyclic stress on the cutting tool for different hardness: SDM..................111

Abbreviation

AISI	American Iron and Steel Institute
ANOVA	Analysis of variance
BCBN	Binder-less CBN
CBN	Cubic Boron Nitride
CBN-H	High content CBN
CBN-L	Low content CBN
CNC	Computer numerically controlled lathe
DOE	Design of experiments
FEM	Finite Element Method
GA	Genetic algorithm
HRC	Hardness on Rockwell ‘C’ Scale
HT	Hard turning
LAM	Laser Assisted Machining
MRR	Material Removal Rate
MSE	Mean squared error
N	Noise
NN	Neural Networks
OOB	Out of bag
PCBN	Polycrystalline Cubic Boron Nitride
RFR	Random forest regression
RPM	Rotation of spindle per minute
RSM	Response surface methodology
S	Signal
SDM	Surface Defect Machining
Var	Variation

Nomenclature

α	Constant (intercept)
ε_i	Normally distributed error
f	Feed rate
d	Depth of cut
β	Expected increment in the response
v	Cutting speed
R	Tool nose radius
Ra	Average value of machined surface roughness
Ra_i	Per unit change in surface roughness for ith experiment
F_f	Feed force
F_c	Cutting force
$\bar{\sigma}$	Flow stress
T	Workpiece temperature
T_{melt}	Workpiece melting temperature
$\bar{\varepsilon}$	Equivalent strain
σ_T	Maximum tensile stress
D	Damage
τ	Shear stress
μ	Friction factor
τ_0	Shear yield stress
S/N	Signal-to-Noise
$M.S.D$	Mean-square deviation
SS_T	Total sum of squared deviations
Vb	Flank wear length
$N_{\mathrm{P}red}$	The predicted number of load cycles for fatigue crack initiation
K_C	Fracture toughness

List of Publications by the Candidate

W. B. Rashid, S. Goel, **X. Luo** and J. M. Ritchie, Development of a surface defect machining method for hard turning processes, *Wear*, 2013, http://dx.doi.org/10.1016/j.wear.2013.01.048. Vol. 302 (1-2), 1124-1135.

Rashid, Waleed B, Saurav Goel, Xichun Luo, and James M Ritchie. "An Experimental Investigation for the Improvement of Attainable Surface Roughness During Hard Turning Process." *Proceedings of the Institution of Mechanical Engineers, Part B: Journal of Engineering Manufacture* 227, no. 2 (2013): 338-42.

Goel, Saurav, **Waleed Bin Rashid**, Xichun Luo, Anupam Agrawal, and VK Jain. "A Theoretical Assessment of Surface Defect Machining and Hot Machining of Nanocrystalline Silicon Carbide." *Journal of Manufacturing Science and Engineering, Transactions of ASME* , 2014, 136 (2), 021015, doi:10.1115/1.4026297

Goel, Saurav, Xichun Luo, Robert L. Reuben, and **Waleed Bin Rashid**. "Replacing Diamond Cutting Tools with CBN for Efficient Nanometric Cutting of Silicon." *Materials Letters* 68 (2012): 507-09.

Goel, Saurav, Xichun Luo, Robert L Reuben, and **Waleed Bin Rashid**. "Atomistic Aspects of Ductile Responses of Cubic Silicon Carbide During Nanometric Cutting." *Nanoscale research letters* 6, no. 1 (2011): 1-9.

Waleed Bin Rashid, Saurav Goel and Xichun Luo. "Enabling Ultra High Precision on Hard Steels Using Surface Defect Machining" Paper presented at the P7.16-Proceedings of the 14th EUSPEN International Conference – Dubrovnik – June 2014, 2014.

Saurav Goel, **Waleed B Rashid**, Amir Mir, Jining Sun and Xichun Luo. "Development of the Surface Defect Machining Method for Micro/Nano Scale Material Removal Processes " Paper presented at the P6.23-Proceedings of the 13th EUSPEN International Conference, 2013.

Waleed Bin Rashid, Saurav Goel, Xichun Luo, Jining Sun and James M Ritchie· "Achieving optical quality surface finish on hard steels by conventional machining". "To be submitted".

Waleed Bin Rashid, Saurav Goel and Xichun Luo. "Parametric design optimization of hard turning of AISI 4340 steel (69 HRC)". "To be submitted".

CHAPTER 1 – INTRODUCTION

1.1 Background and significance of the project

AISI-4340 steel is a kind of difficult-to-machine material widely used to manufacture parts for aerospace and automotive industries, as these parts often require specific surface properties such as wear resistance, low friction, and high strength and toughness. Surface roughness and surface integrity are especially important characterization parameters for these parts, since machining damage introduced into the surface can have a deleterious effect on component performance and consequently the lifetime of the component. Traditionally, the parts made of hardened steel are manufactured by following a special sequence of operations, starting from forming the material, annealing, hardening, and grinding to the fine finishing. Such a manufacturing cycle involves high lead time and is labour and cost intensive (Tönshoff et al., 2000, Grzesik, 2011, Steven, 2006). The emergence of a new material, known as cubic boron nitride (CBN), during the 1970s (Chou, 1994) led to the development in cutting tool technology which made it feasible to machine hardened steel parts over 45 HRC by a single point cutting tool on a turning machine, which is been known as “hard turning”, Figure 1.1. Current studies on hard turning are focused on investigations into chip formation, tool wear, tool geometry, surface integrity, and optimizing cutting forces by using experimental and theoretical methods.

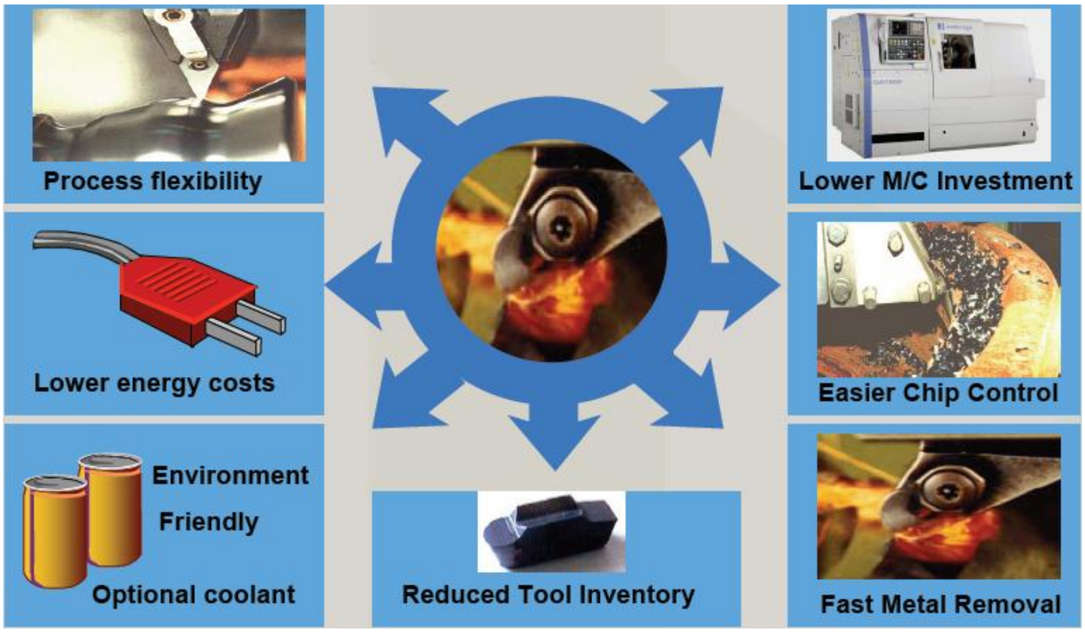

Figure 1.1: Major advantages of hard turning (Hardinge Inc., 2014)

However, some researchers still believe hard turning has further to go (Dogra et al., 2010). In their view, hard turning is not yet an independent process to replace grinding. Hard turning moreover, is impeded by a number of challenges requiring to be resolved to make it a complete replacement for the grinding process. Figure 1.2 shows a qualitative overview of the advantages of hard tuning and its limitations compared to the grinding processes and vice versa. It can be seen from Figure 1.2 that surface integrity and machined surface roughness are some of the prominent issues in hard turning, because rapid variations in the high deviatoric strains and/or temperature due to the movement of the cutting tool result in the generation of an amorphous layer of material, the details of which are not fully known.

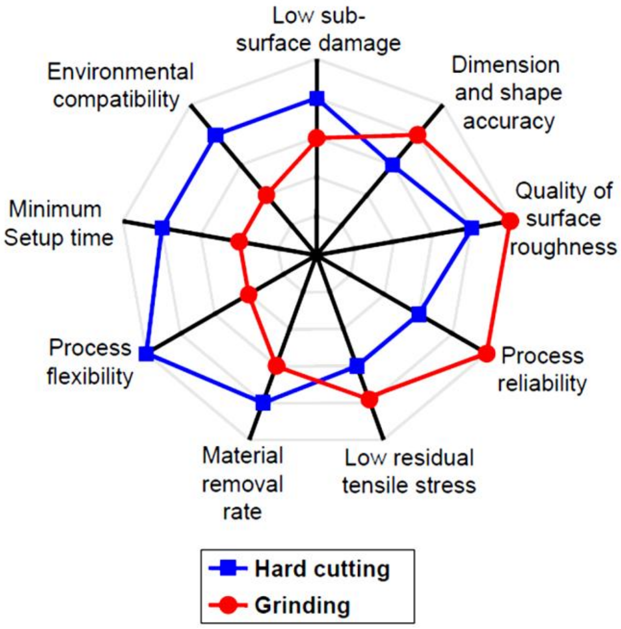

Figure 1.2: Qualitative overview of the respective capability of hard turning and grinding (Klocke et al., 2005)

Consequently, surface residual stresses, appearance of white layer and attainable machined surface roughness have lead to only partial success for the commercialization of HT. Therefore, several attempts have been made by researchers in the past to study the possibilities of solving some of these problems. The proposed solutions have been categorized as follows:

1- By optimization of the cutting parameters
2- By inclusion of microstructures in the cutting tool
3- By changing the geometry of the cutting tool and
4- By changing the mechanism of cutting

In this regard, this thesis will research a novel approach, referred as "surface defect machining", to alter the mechanism of cutting in order to enhance the machining capability of hard turning in terms of machined surface finish and surface integrity.

1.2 Aim and objectives

The aim of this study is to improve the hard turning process, particularly to improve the machined surface roughness and surface integrity as well as tool life through the development of a new machining approach named as surface defect machining (SDM). To achieve this aim, this research is divided into the following broad objectives:

1. Review of existing literature to develop an understanding of the previously published work on hard turning and to identify the key problems.
2. Proposition of a hypothesis to develop a new approach to manufacture hard steel components.
3. Testing the hypothesis through the numerical simulation and experiments to confirm the feasibility of the proposed idea, followed by a critical analysis of machining outcomes, such as comparison of cutting forces, chip morphology, machining temperature, chip flow velocity, residual stresses etc. and the formation of white layer.
4. Make generic suggestions for further improvements.

In order to achieve the above objectives, the following flow chart was followed:

1- Identification and selection of an appropriate material (workpiece and cutting tool) for analysis.
2- Formulating the new machining approach.
3- Selection of the tool for numerical modeling and simulation
4- Design of experiments and machining trials in conjunction with numerical simulations.
5- Analysis and comparison of results.

1.3 Structure of the thesis

To facilitate smooth learning to the readers, this thesis is organized in eight chapters detailed below:

1. Chapter One has presented a brief introduction to the hard turning process and also details the aim and objectives of the research.
2. Chapter Two reviews the literature concerning the topic and identifies the key gaps which created the niche for this research.
3. Based on the understanding developed from Chapter Two, a new method was developed which is termed “Surface Defect Machining” (SDM). This is introduced in Chapter Three. Alongside the concept of SDM, Chapter Three also presents some theoretical findings, through the use of finite element simulation.
4. Chapter Four describes the methodology of exploring the SDM method by finding the best cutting parameter through random trials based on widely suggested cutting parameters. A regression model, based on workpiece properties and the mathematical model provided by the finder of the cutting tool was used to compare the actual average surface roughness obtained experimentally by conventional hard turning and by the SDM method. The machines and tool used to carry out the experimental work are described in detail.
5. Chapter Five introduces the need for optimizing the cutting parameters through the design of experiments, or a method better known as the “Taguchi Method”, aimed to investigate the significant cutting parameters to be used in further experiments.
6. Chapter Six reports further experimental trials which were conducted after the determination of the significant cutting parameters and the results are highlighted and subjected to analysis. In this part of the work, the critical feed rate was indentified and 30 nm surface roughness was achieved using the SDM method.
7. Chapter seven reports a detailed investigation carried out to show the performance of SDM under multi-cutting passes. The chip mechanism of SDM and the effect of fatigue crack initiation are discussed as well.
8. Chapter Eight presents the conclusions and assessment of the thesis as well some recommended future work.

CHAPTER 2 – Literature review

2.1 Introduction

This chapter will review state-of-the-art hard turning with a particular focus on the limitations and capabilities of the process with respect to workpiece and tool materials, cutting parameters, importance of tool geometry, characteristics of the cutting chips, and other allied aspects of the process.

2.2 Definition and description of hard turning

Hard turning is a specialized process of machining used to manufacture (primarily by turning) hard ferrous alloys exhibiting hardness over 45 HRC by the use of a single point cutting tool (preferably CBN). Hard turning is considered to be one of the most promising operations to manufacture hard ferrous materials. It has gained popularity primarily on account of producing parts with reduced machining time and cost, due to eliminating some of the processing steps and procedures that were inherent in the previously used methods. A comparison of process chains using hard turning (eliminating the need for annealing and grinding (Dogra et al., 2010)) and conventional machining is shown in Figure 2.1. In general, the traditional way of processing hard steel involves an established sequence of operations i.e. forming, annealing, rough cutting, heat treatment and grinding. These processes consume significant amounts of time and cost (Tönshoff et al., 2000; Grzesik, 2011) The literature suggests no firm evidence of which is better. Experience suggests that it depends on the situation. Method number 1 uses CBN tool for both rough and finishing cutting because the part is already heat treated prior to cutting and it saves the set up time at an expense of increase cost of tooling. Method number 2 saves cost because the intent is to do away with the rough cut by inexpensive cutting tool material, prior to carrying out the finishing cut by the CBN tool. However, this method results in increased setup time since the heat treatment start after the rough cut therefore two set ups are used one for the rough cut and another one for the finish cut. Table 2.1 highlights the important differences between hard turning and conventional turning.

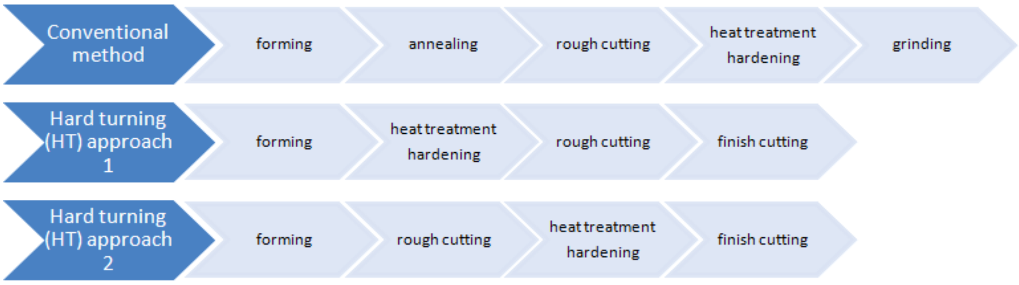
Conventional method
forming
annealing
rough cutting
heat treatment hardening
grinding
Hard turning (HT) approach 1
forming
heat treatment hardening
rough cutting
finish cutting
Hard turning (HT) approach 2
forming
rough cutting
heat treatment hardening
finish cutting

Figure 2.1: Comparison of conventional processing with hard turning

Table 2.1: Hard turning vs. conventional machining

Basis for Comparison	**Hard turning**	**Conventional turning**
Workpiece material hardness	Hard ferrous alloys hardened up to 45 HRC and above	Soft ductile materials hardness not exceeding 45 HRC
Cutting tool material	CBN	HSS, Carbides
Cutting tool geometry	Zero and negative rake angle	Positive rake angle
Temperature in the machining zone	Above 1000ºC	Less than 600ºC
Chip formation	Segmented/Serrated chip	Continuous chip

2.3 Machine tool requirements for hard turning

Hard turning involves high cutting forces and this warrants the requirement to have a rigid and strong machine tool. Some of the key features of a machine tool suited for such an operation are listed below and are also shown in Figure 2.2.

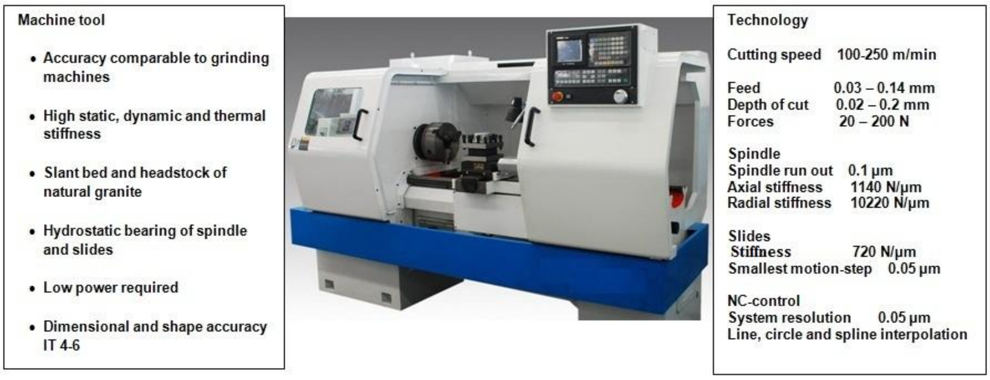
Machine tool

- Accuracy comparable to grinding machines
- High static, dynamic and thermal stiffness
- Slant bed and headstock of natural granite
- Hydrostatic bearing of spindle and slides
- Low power required
- Dimensional and shape accuracy IT 4-6

Technology

Cutting speed 100-250 m/min

Feed 0.03 – 0.14 mm
Depth of cut 0.02 – 0.2 mm
Forces 20 – 200 N

Spindle
Spindle run out 0.1 µm
Axial stiffness 1140 N/µm
Radial stiffness 10220 N/µm

Slides
Stiffness 720 N/µm
Smallest motion-step 0.05 µm

NC-control
System resolution 0.05 µm
Line, circle and spline interpolation

Figure 2.2: Characteristics of high-precision lathe suited for hard turning (Tönshoff et al., 2000)

1. Rigid and stiff machine tool
2. Better work-holding rigidity
3. Minimum vibration and controlled damping
4. Rigid tooling system
5. Appropriate cutting tools.

2.4 Hard turning versus grinding

Hard turning and grinding are two competing processes and this mandates the need to understand the precise differences between the two processes. A comparison of these two processes is shown in Table 2.2.

Table 2.2: Major advantages of hard turning over grinding

Differences	**Hard turning**	**Grinding**
Tool tip contact	Single point	Multi point
Setup time	Short	Long
Clamping operation	Single	Multiple
Material removal rate (MRR)	High	Low
Coolant	No	Grinding coolant
Machine surface profile	Periodic	Non- uniform
Finishing type	Deterministic	Iterative

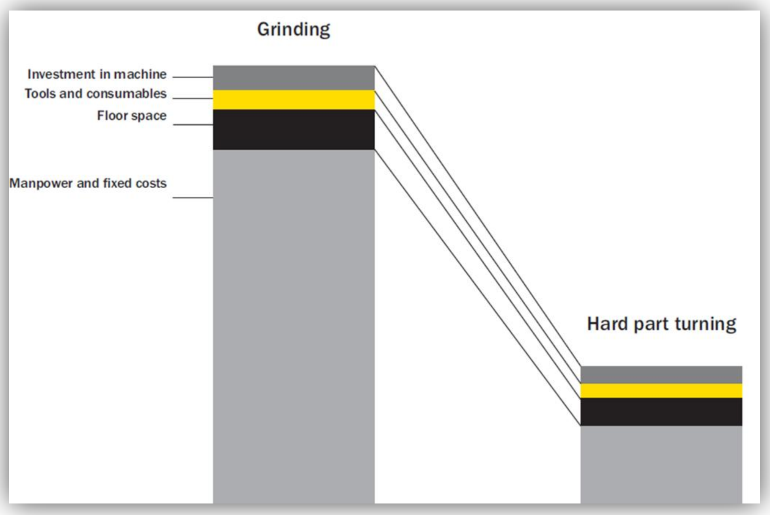

Figure 2.3: Comparison of cost of turning versus grinding (Sandvikens, 2013)

One of the most important considerations in manufacturing research is to develop processes which promote the long term vision of development of a manufacturing process that is socially sustainable and environmentally green. An advantage of HT over grinding is that since it can be carried out in dry conditions, it does not produce residual products, such as grinding sludge. When accessed on the same scale, the cost to execute a grinding operation turns out to be higher than that for hard turning, as shown in Figure 2.3 (Sandvikens, 2013, Hardinge Inc., 2014, Nakai, 1991). Furthermore, the material removal rate attainable during turning is an order of magnitude higher than that attainable during grinding, which ties in with the fact that hard turning offers the generation of complex geometries without compromising the form of accuracy, whereas specialized arrangements might be needed to attain the same result from grinding.

2.5 Limitations of hard turning

Despite the number of advantages HT offered over grinding, there are several bottlenecks limiting the HT process which have impeded its penetration in the commercial arena:

- The HT process provides a component which has relatively higher tensile residual stresses on the surface compared to those obtained from grinding operations.
- The science behind the formation of the white layer has not been clarified, so it warrants further investigation of the material science involved in manufacturing process.
- The HT process although more deterministic, provides an inferior machined surface finish compared to grinding.

2.6 Workpiece materials used in hard turning

HT is usually applied to parts made up of ferrous materials exhibiting hardness over 45 HRC, which includes hard steels (Dogra et al., 2010), bearing steels, alloy steels, die steels, high speed steels and alloy cast iron. Hardened steels due to their improved strength, wear resistance and fatigue strength provide a number of key benefits in engineering applications (König et al., 1993). There is a large demand worth 30-35 billion USD per year in the United States alone for application of hardened steels in bearings, camshafts, gears, cutting tools, dies, moulds etc. (Zhang, 2005). Such components find wide applications in the areas of transportation, energy generation and heavy duty engineering applications. Two of the most popular classes of hardened steel used in industries are AISI 52100 (used for bearing steel) and AISI 4340 (used in aircraft industry for the fabrication of structural components). For more information, a classification scheme for the various ferrous alloys is shown in Figure 2.4.

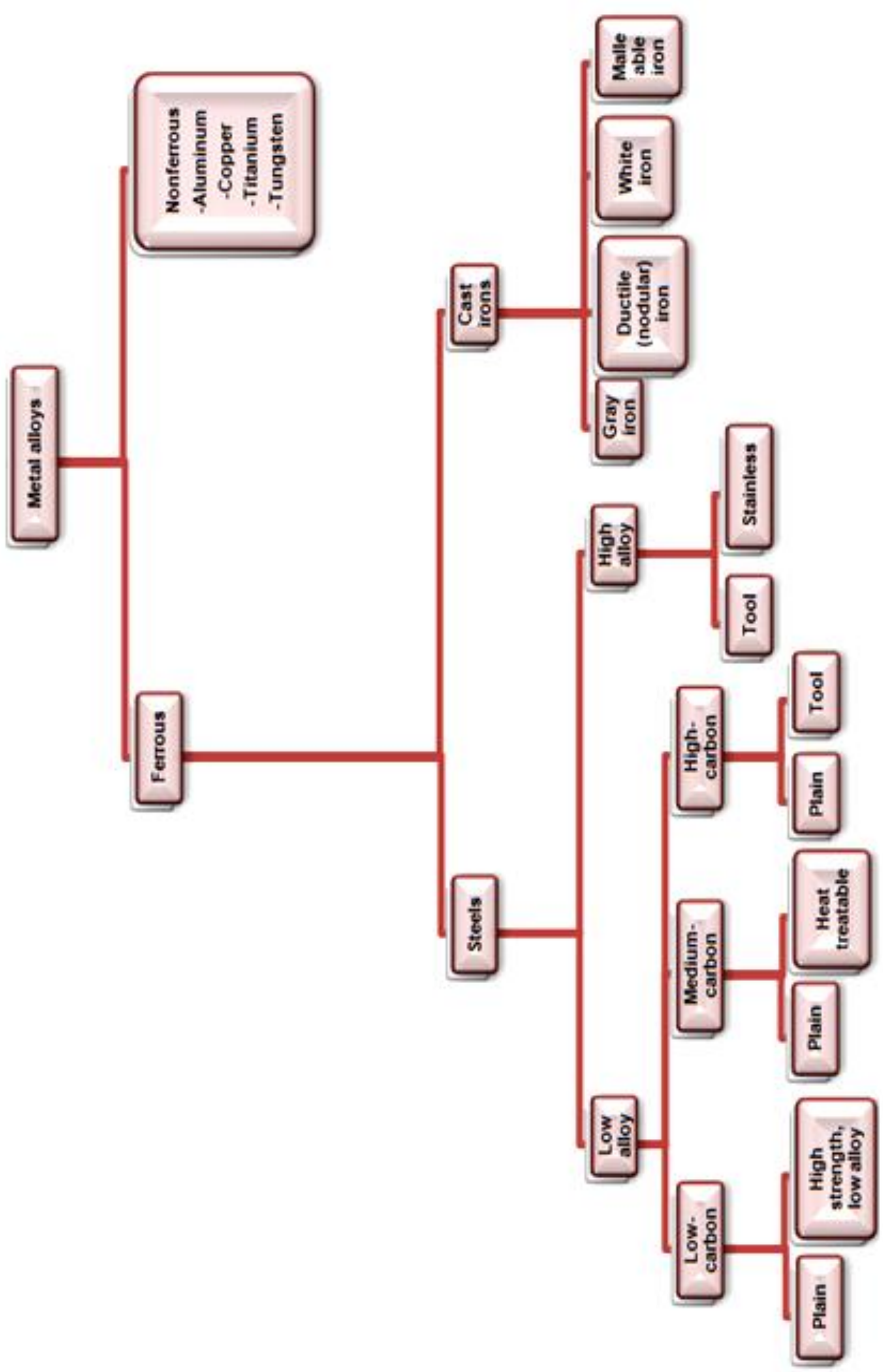
Metal alloys
Nonferrous
-Aluminum
-Copper
-Titanium
-Tungsten
Ferrous
Cast irons
Steels
Malleable iron
White iron
Ductile (nodular) iron
Gray iron
High alloy
Stainless
Tool
Low alloy
High-carbon
Tool
Plain
Medium-carbon
Heat treatable
Plain
Low-carbon
High strength, low alloy
Plain

Figure 2.4: Classification scheme for the various ferrous alloys (William, 2007)

2.7 Consideration of cutting tool materials

Selection of a cutting tool material is an important consideration in carrying out a successful hard turning operation. An ideal cutting tool must have high hardness, high hardness to modulus ratio, high thermal conductivity, high abrasive wear resistance and high thermal physical and chemical stability (Tönshoff et al., 2000). A hardness ratio of 5:1 between the cutting tool and the workpiece is normally recommended for machining (Ravindra, 2011). The development of the CBN tool during the early 1970 was a key came as a boon to facilitate hard turning process (Chou, 1994). Since then, there has been strong research focus on the development of the cutting tool in areas related to the importance of cutting tool geometry and the reduction of tool wear to provide longevity of tool life (Chou, 1994). A recent work by Wan et al. (2013) has proposed a method of a using radar chart–based method to assess material machinability to appropriately select a cutting tool. However, Al_2O_3/TiC ceramics, polycrystalline cubic boron nitride (PCBN) and CBN composites are the most commercially available cutting tool materials which are used in hard turning (shown in Figure 2.5). Furthermore, the cutting tool material must possess the following characteristics:

- Hot hardness: hardness, strength, and wear resistance should be retained at elevated temperatures so that the cutting tool does not undergo thermal softening induced deformations.
- Toughness: an ideal cutting tool should be able to withstand impact loading conditions such as those arising due to a sudden encounter with microstructures of the workpiece and should therefore be able to withstand dynamically varying fatigue conditions.
- Chemical stability
- High wear resistance

The composition tetrahedron (C, B, N, and Si) in Figure 2.6 shows that the hardest materials and compounds have been used as a cutting tool to cut difficult-to-machine materials. Diamond find ubiquitous use in wider applications because of its extreme hardness, high thermal conductivity and low sliding friction (Shaw, 2004). However, diamond is known to exhibit poor thermo-chemo-mechanical stability particularly against low carbon ferrous alloys (Komanduri and Shaw, 1975) and at elevated temperatures (Koskilinna, 2007).

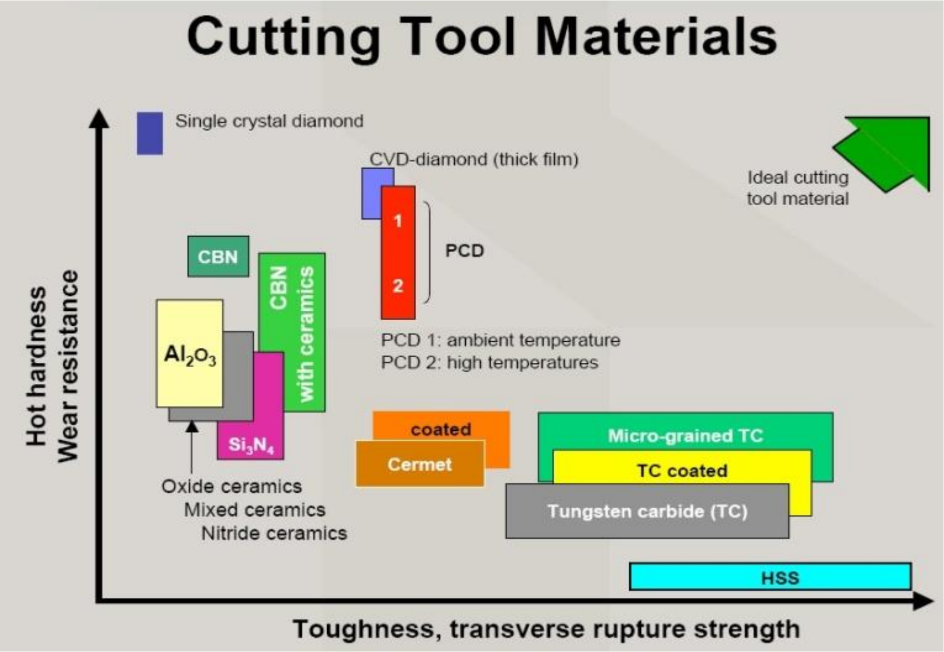

Figure 2.5: Different cutting tool properties (Hardinge Inc., 2014)

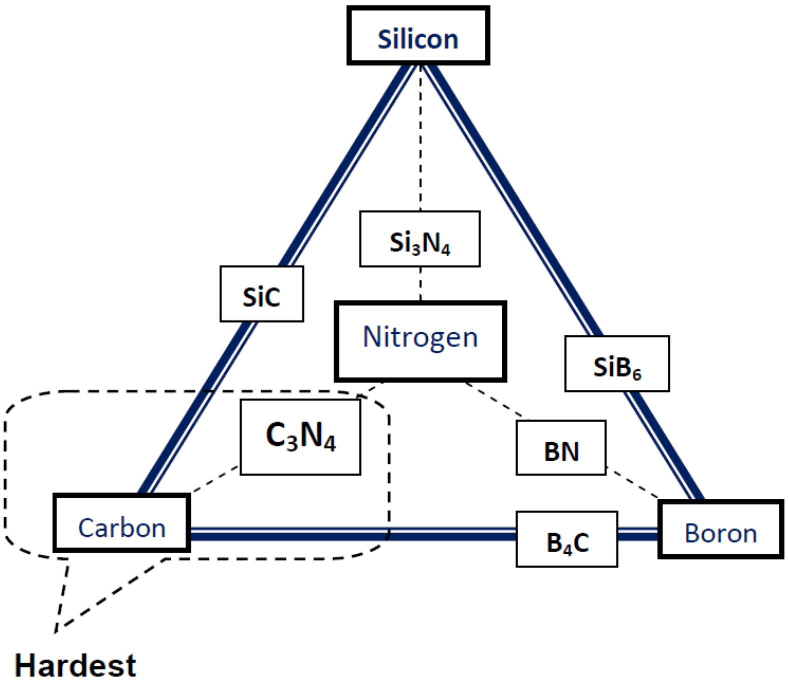
Silicon
Si3N4
SiC
Nitrogen
SiB6
C3N4
BN
Carbon
B4C
Boron
Hardest

Figure 2.6: Composition cycle of hard, brittle materials (Shaw, 2004)

It is surprising but true that diamond, the hardest available material wears catastrophically and extremely rapidly against low carbon ferrous alloys and pure iron (Narulkar, 2009).

2.7.1 Cubic boron nitride (CBN)

The most common tools used for hard turning are ceramics, carbides, CBN, and PCBN. However, CBN is the most widely used tool material in hard turning. It has high hardness and good thermal conductivity and it has low affinity towards ferrous alloys (Nakai, 1991). In fact, CBN is the second known hardest substance and its chemical stability makes it suitable in presence of hot iron. Indeed, CBN is more refractory than diamond to machine steels, as is evident from the plots shown in Figure 2.7. In fact, CBN is more stable at elevated temperatures of about 1300º C, where diamond is stable to only upto 800º C beyond which it starts showing significant reduction in hardness (Shaw, 2004).

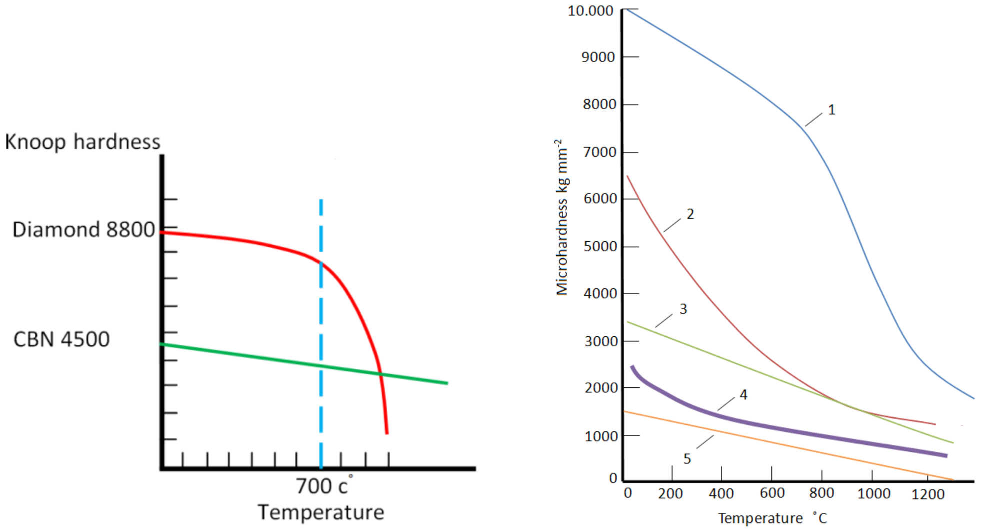

Figure 2.7: The variation of Knoop hardness with temperature for several hard materials:1, diamond; 2, CBN; 3,SiC; 4, Al_2O_3; 5, (92% Wc, 8% Co) (Hardinge Inc., 2014, Shaw, 2004)

2.7.2 Polycrystalline Cubic Boron Nitride (PCBN)

PCBN is a composite material of CBN grain with binder matrix, formed by sintering (Chou, 1994). In general, there are two categories of PCBN, depending on the CBN content. High CBN content tools consist of 90% volume of CBN grains with metallic binder (e.g., cobalt) known as CBN-H, and low CBN content tools which consist of 50-70% volume of CBN grains with ceramic binders (e.g., TiC, TiN) which are known as CBN-L. The higher percentage of CBN means higher toughness and hardness. Recent studies (Lahiff et al., 2007) have shown that CBN-H is better for rough hard turning whereas CBN-L is better for finish hard turning. Table 2.3 shows the classification of CBN (Dogra et al., 2010). The cutting performance of PCBN depends also on its CBN content, grain size, binder type, thermal conductivity and microstructure.

Type of CBN	CBN content (Vol. %)	CBN Grain size (μm)	Thermal conductivity (W/mK)	Type of binder
Low content CBN (CBN-L)	50-60	0.5-1	------------	Ceramic Binder (TiN, TiC)
High content CBN (CBN-H)	85-90	3-6	100-130	Metallic binder (e.g. cobalt)
Binder-less (BCBN)	> 99.9	< 0.5	360-400	Complete hBN

Table 2.3: Different CBN tools and their properties (Dogra et al., 2010)

2.7.3 Importance of tool geometry

Cutting tool geometry plays an important role in influencing the hard turning process. Figure 2.8 (Dogra et al., 2011) summarizes the effects of tool geometry: it is considered that the variation in tool geometry is one of the main factors that may enhance the performance of machining hard metal in terms of surface integrity, tool wear and material removal rate. The important factors in applying HT are the use of an appropriate rake angle in the cutting tools and preparation of the cutting edge (Özel et al., 2005). Normally four types of cutting edges are preferred for smooth HT operations, i.e. sharp, chamfer, hone or a combination of both chamfer and hone, as shown in Figure 2.9 (Özel et al., 2005). Significant differences were noted in the quality of the machined surfaced caused by the edge geometry in the studies carried out by Özel et al. (2005) and Chou et al. (2003). It was also shown experimentally that the residual stresses in the hard turning part were affected by cutting edge geometry and the hardness of the workpiece (Thiele, 2002).

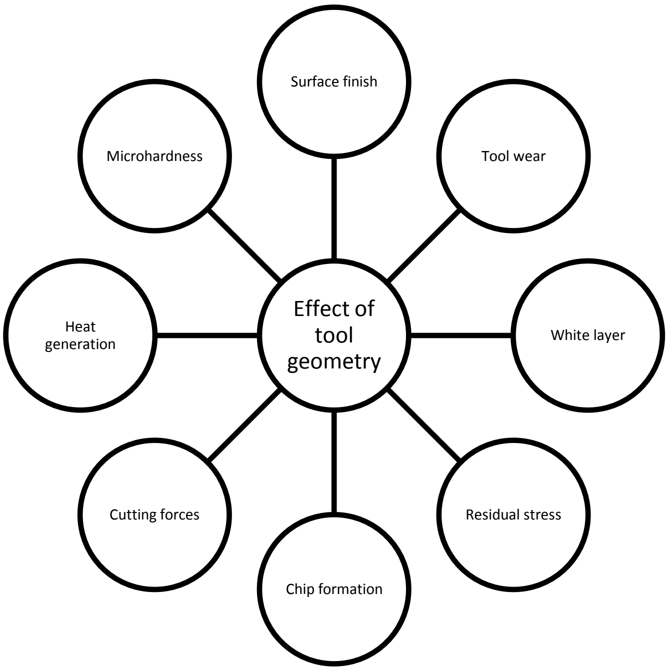
Surface finish
Microhardness
Tool wear
Heat generation
Effect of tool geometry
White layer
Cutting forces
Residual stress
Chip formation

Figure 2.8: Effect of tool geometry on performance parameters in hard turning (Dogra et al., 2011)

Chamfer only	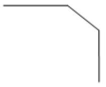
Hone only	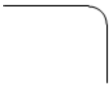
Sharp	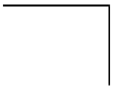
Chamfer and honed	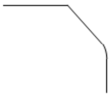

Figure 2.9: Type of edge preparations used in hard turning cutting tools (Özel et al., 2005)

Özel et al. (2005) conclude in their discussions that a chamfered edge could be useful to obtain better surface roughness when selecting higher cutting speed and high workpiece hardness. Also, the honed edge was recommended when higher cutting speed was selected to decrease tangential force.

2.8 Tool wear and its mechanism during hard turning

Tool wear is an important research topic in manufacturing research. A worn tool could damage the workpiece, which will increase the defective parts and may result in reduced productivity, beside the time consumed during the process. Therefore, it is very important to determine the tool life in order to achieve the complete targeted product on time. Furthermore, there are various factors affecting tool wear, such as cutting conditions, material properties of the workpiece and cutting tool geometry (Chou, 1994, Lahiff et al., 2007). According to Arsecularatne et al. (2006) there is no comprehensive theory available to date, that can substantiate and address the relation between cutting conditions, tool geometry, properties of the workpiece and tool life. For example, there exist a trade-off between tool life and material removal rate, where cutting speed will cause a rapid increase in the tool wear rate. Also, increasing depth of cut may increase the removal rate but on the other hand, reduce the tool life (Dawson and Kurfess, 2001). The cutting complexity of hard turning and extremely high temperature generated in the cutting zone make the wear mechanism complicated, because several processes involving chemical, mechanical and thermal processes may simultaneously exist. In the past, many experimental studies have been carried out and mathematical models of tool wear proposed for different tools and the wear processes categorized into abrasion, cohesion, adhesion, diffusion, attrition, and chemical reactions (Chou, 1994; Huang, 2002). In a process as complicated as hard turning, several mechanisms or one individual mechanism can cause tool wear (Chou, 1994, Lahiff et al., 2007, Arsecularatne et al., 2006). The following types are a major classification of such mechanisms.

(i) Abrasion Wear

When undesired hard particle chip moves over the rake face of the cutting tool, or due to spring-back when the flank face of the cutting tool rubs against the machined surface, then abrasive wear occurs (Chou, 1994, Lahiff et al., 2007). CBN grains of the cutting tool can easily be removed and exposed to more abrasion after the abrading of the binder material (Luo et al., 1999).

(ii) **Adhesion Wear**

The sliding of the cutting tool against the workpiece or the chip against the cutting tool causes adhesive wear to appear on the non-contact surface. The stresses and heat generated cause melting between the chip and the workpiece at the cutting tool edge (Lahiff et al., 2007, Luo et al., 1999). Then, welding occurs between the chip particles and the tool by plastic deformation due to high local pressure and temperature. After a while the welded particles fracture. This process can be repeated frequently and cause the tool to wear (Chou, 1994).

(iii) **Diffusion Wear**

The close contact and high temperature in the cutting zone area lead the atoms of the cutting tool to transfer either to the chip, the work piece, or both of them. The diffusion process depends upon forces and energy transfer between atoms and the solubility conditions (Chou, 1994). In PCBN, the binder is susceptible to this form of wear (Lahiff et al., 2007).

(iv) **Chemical wear**

Under high temperature and mechanical load chemical reactions take place between the workpiece and the cutting tool or the atmosphere (Chou, 1994, Lahiff et al., 2007, Luo et al., 1999). This may happen in the cutting area or in the area near it, causing a deposit on the tool surface (Lahiff et al., 2007, Luo et al., 1999). The chemical wear can form with adhesion wear, which makes the wear mechanism more complicated.

2.8.1 Factors that influence tool tear and wear patterns

A close examination of the used cutting tool reveals that there could be multiple locations which show distinct wear patterns. As shown in Figure 2.10, each location signifies a different type of tool wear. The main wear patterns observed during hard turning (detailed below) are flank wear, crater wear, notch wear and chipping (Chou, 1994, Huang and Dawson, 2005).

(i) Flank Wear

Flank wear occurs at the flank face of the cutting tool. The abrasion wear mechanism makes a significant contribution to flank wear due to the spring-back effect when the flank face of the cutting tool rubs against the machined surface (Chou, 1994, Lahiff et al., 2007). Flank wear significantly influences the surface finish and degrades the accuracy of the machined parts. Therefore, tool life can be indexed in terms of flank wear width (V_b) (Chou, 1994, Lahiff et al., 2007, Arsecularatne et al., 2006).

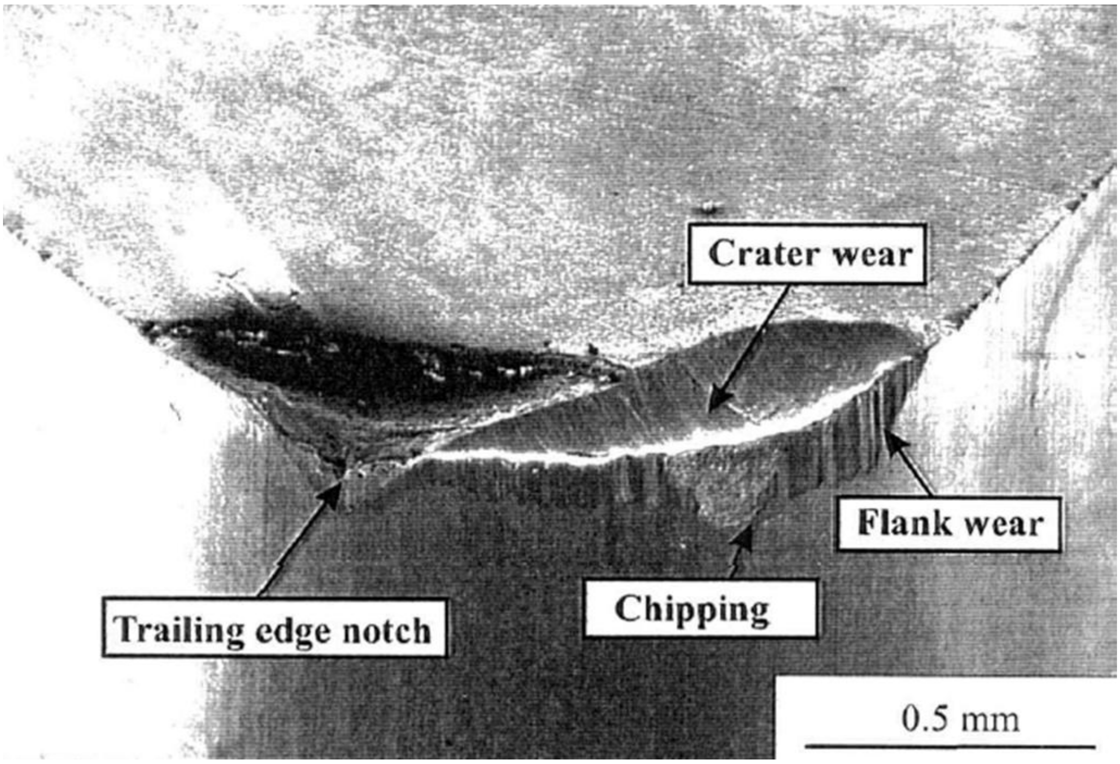

Figure 2.10: Typical wear types observed on cutting tools (Lahiff et al., 2007)

(ii) Crater Wear

Crater wear occurs at the rake face of the cutting tool. The movement of the cutting chips on the rake face of the cutting tool causes the tool to undergo the process of adhesion, abrasion or a combination of both. The reliability of the process is thus strongly influenced by crater wear due to the chipping or fracture of the tool edge (Lahiff et al., 2007). It may thus be seen that a lot of factors are involved in the mechanism of wear of the cutting tools. Further work is needed in order to understand the effect of the listed variables on the wear rates and tool life of the cutting tools (Dawson and Kurfess, 2001).

2.9 Chip formation mechanism

Cutting chips are the by-products of a machining process that results during the cutting process. In general, the classifications of various chips produced in machining are often divided into steady state or continuous chips and cyclic chips. The cyclic chips can be divided into three types: wavy chip, saw-tooth (segmented) chip, and discontinuous chip (Shaw and Vyas, 1998), as summarized in Figure 2.11.The type of cutting chips commonly observed during the hard turning operation is classified as segmented chips (Davies et al., 1997).

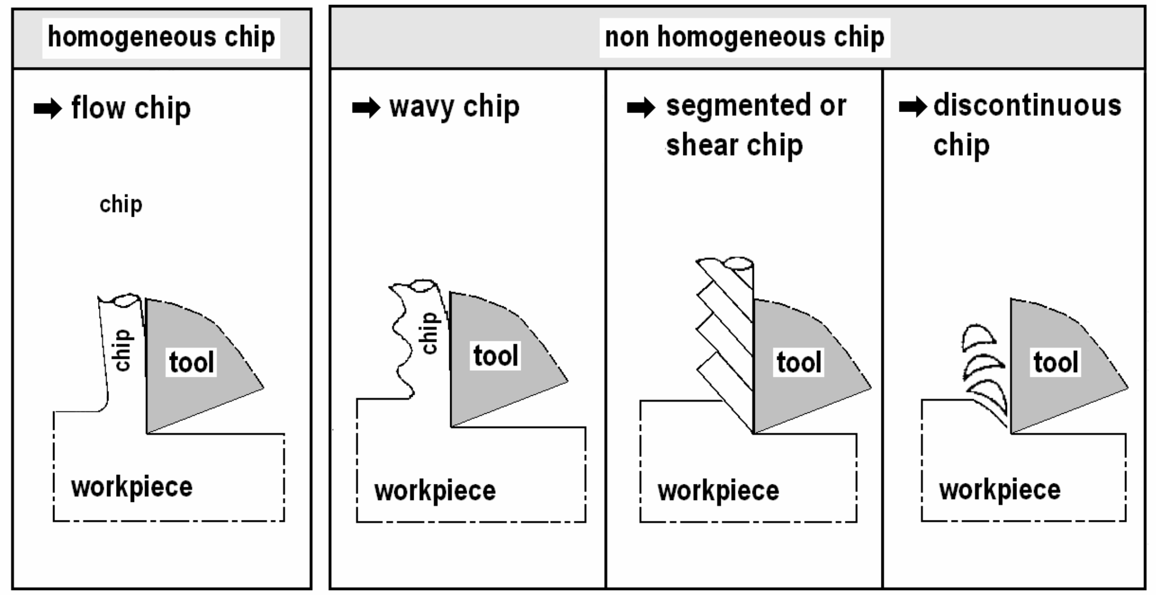
homogeneous chip
non homogeneous chip
➡ flow chip
➡ wavy chip
➡ segmented or shear chip
➡ discontinuous chip
chip
chip
tool
workpiece
chip
tool
workpiece
tool
workpiece
tool
workpiece

Figure 2.11: Classification of chip formation (Tönshoff et al., 2000)

Studying the chip formation mechanism is an essential step towards a better understanding of the different cutting conditions that result in these variations (König et al., 1993). If and when cutting forces vary periodically, this brings about a high wear rate and will eventually result in the deterioration of the machined surface finish (Davies et al., 1996, Komanduri, 1982). There are two popular theories concerning chip segmentation and a strong debate is evident between the theories presented by Shaw and Vyas. (1998) and Davies et al. (1997), Shaw affirming that the crack initiation and propagation causes the appearance of segmented chips while Davies believes adiabatic shear to be responsible behind the formation of segmented chips. Both of these theories are briefly reviewed below.

(i) Crack initiation theory

This theory suggests that the presence of deviatoric stresses such as those existing during machining causes the initiation of cracks at the free surface of the workpiece in the vicinity of the cutting zone. Once initiated, the crack propagates in a direction along a shear plane toward the tool tip until the compressive stress on the shear plane reaches a critical value, while the segmented chip tends to move along the rake face, due to the high plastic deformation brought by high compression. Finally, a new crack is initiated and the cycle repeats.

(ii) Adiabatic shear theory

The adiabatic theory suggests that the cutting tool attempts to indent the workpiece in the beginning, which develops a global stress field. When the induced maximum resolved shear stress causes the material to yield, the heat generated by the plastic deformation moves away from the primary shear zone and the yield strength therefore is reduced by thermal softening (Davies et al., 1997, Shaw and Vyas, 1998). Figure 2.12 shows an attempt that was made to correlate thermal softening with hardness (Poulachon et al., 2001). This study showed that the main parameters which influence the chip formation process are hardness of the workpiece and cutting speed. As the hardness increases to around 53 HRC, the crack begins to appear.

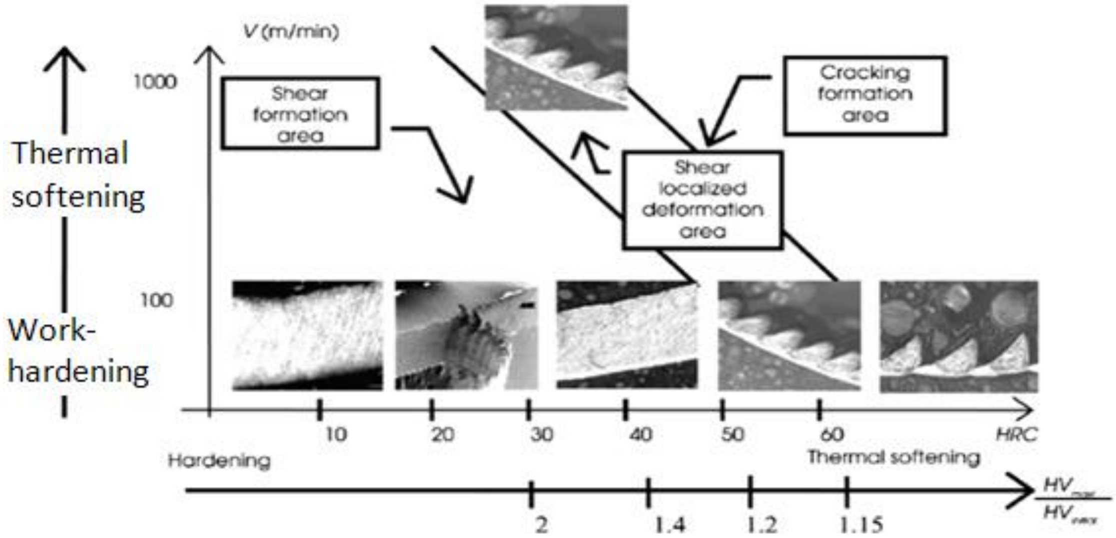
V (m/min)
1000
100
Thermal softening
Work-hardening
Shear formation area
Cracking formation area
Shear localized deformation area
10
20
30
40
50
60
HRC
Hardening
Thermal softening
2
1.4
1.2
1.15
HV_{max}/HV_{min}

Figure 2.12: Chip morphology according to the hardness and the cutting speed (Poulachon et al., 2001)

2.10 Cutting Forces observed in hard turning

Cutting forces can play a major role in influencing the cutting performance of the hard turning process. They are also important for thermal modelling, tool life estimation, chatter prediction and tool condition monitoring (Yong and Steven, 2005). Shaw and Vyas (1998) reported that cutting forces during hard turning fluctuated at a high frequency over of 10,000 Hz. The cutting force can be an important indicator in asserting the wear of the cutting tool. Cyclic force may lead to fatigue fracture, friction and high temperature. When cutting forces increase, it signifies an increase in the cutting temperature and tool wear. In hard turning, cutting forces also change with respect to the hardness of workpiece material (Matsumoto et al., 1987). The observation shown in Figure 2.13 highlights the variation in the forces with respect to hardness of the workpiece in which the trend shows three distinct regions. The first region starts from 29-39 HRC, the second from 40-49 HRC while the last appears to start beyond 50 HRC.

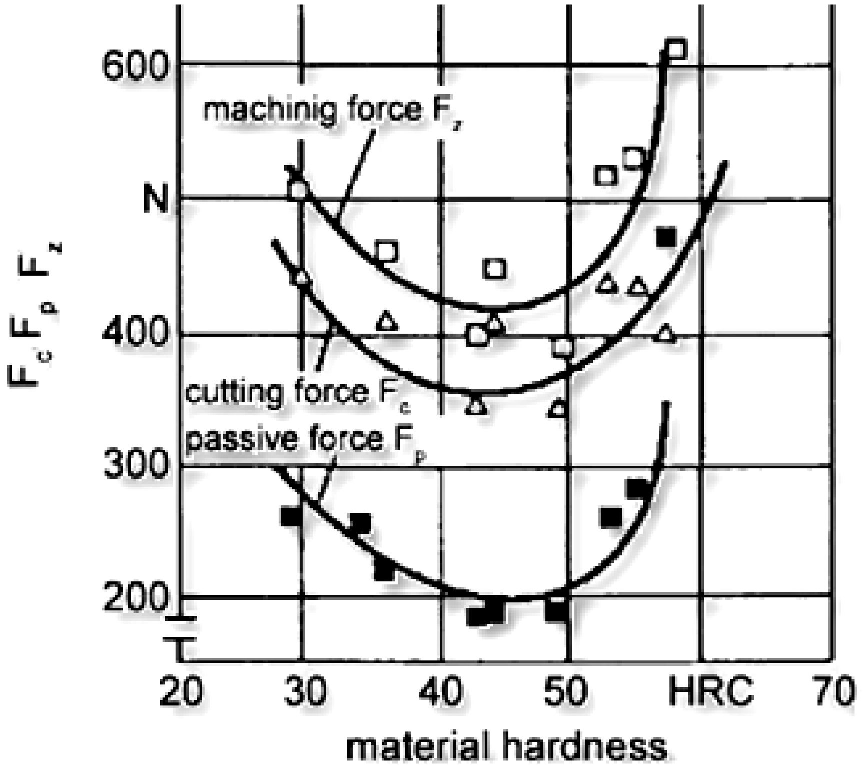

Figure 2.13: Relationship between cutting forces and hardness of AISI 4340 steel workpiece (Matsumoto et al., 1987)

Earlier, Chao and Trigger (1951) reported the same phenomenon. The interpretation of this phenomenon by Chao and Trigger was that the chip/tool interface temperature increased with an increase in the hardness of the workpiece. An experimental investigation also revealed a decrease in friction force and an increase in shear angle (Matsumoto et al., 1987). Chryssolouris (1982) offered different explanation for this phenomenon, when he cut maraging steels of different hardness. Chryssolouris suggests that yield stress increases when the hardness increased and the yield stress is reduced when cutting heat is generated. This is therefore still a grey area which needs additional studies to clarify the incongruence in the outcomes of the above studies.

2.11 Surface integrity and surface roughness

Surface quality of the finished workpiece can be assessed in terms of dimensional accuracy, surface finish, and surface integrity (Ko and Kim, 2001; El-Wardany et al., 2000). Compared to the earlier limitations reported by König et al. (1993) where geometric tolerances corresponding to IT6 and the surface qualities of Rtm 2-3µm are the maximum attainable, IT4 is now achievable through state-of-the-art HT processing (Tönshoff et al., 2000; Grzesik, 2011) as shown in Figure 2.14.

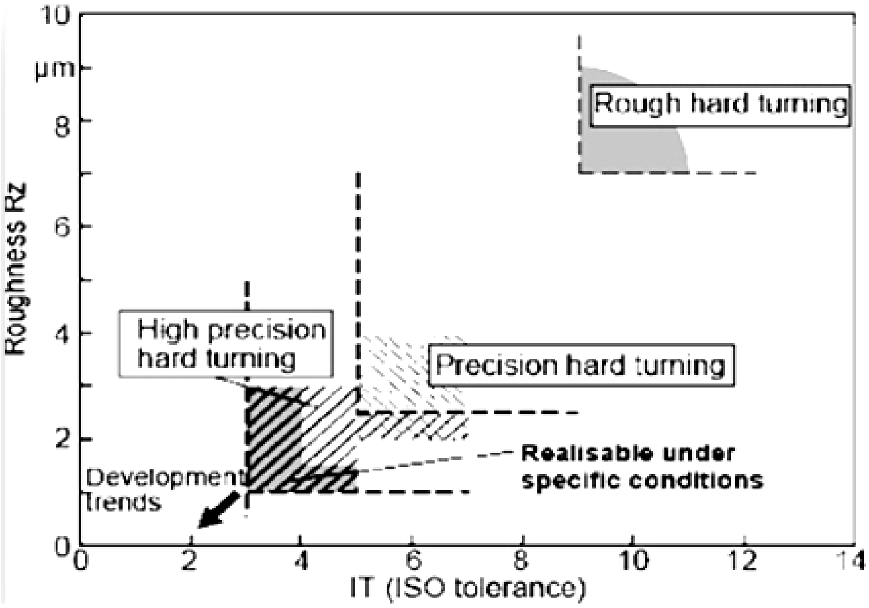

Figure 2.14: Achievable surface roughness and ISO tolerance in hard turning (Grzesik, 2011)

Variables such as cutting conditions, cutting tool geometry and workpiece and tool material properties are considered to be the major influential factors on the obtained surface roughness (Ko and Kim, 2001). Most importantly, a good surface finish is a major industrial requirement, which influences the marginal utility of a finished component, characterized by its finished quality (Tönshoff et al., 2000, Özel and Karpat, 2005). Therefore, the HT process has yet to meet the same level of machined surface roughness in order to compete with that attainable through grinding, i.e. an Ra of 0.1 µm (König et al., 1993). Earlier, an attainable surface finish (Ra) of 0.3µm was reported on a steel part exhibiting high hardness in the range of 50-70 HRC (Grzesik et al., 2007). El-Wardany et al. (2000) used a modern CNC lathe (10HP spindle, 1600rpm maximum speed motor) to machine a D2 tool steel with a hardness of 60 to 62 HRC using polycrystalline cubic boron nitride (PCBN) cutting tool at a depth of cut 0.4 mm and different feeds. The *Ra* values obtained were 0.3, 0.5 and 1 µm for feed rates of

0.05, 0.1 and 0.2 mm/rev respectively. Chou et al. (2003) used a BZN8100 cutting tool (0.8 mm nose radius, 5° clearance angle, 25×0.1 mm chamfer and a negative rake angle of 30°) to turn AISI 52100 (61-63 HRC hardness) steel with a fixed feed rate of 12.5 µm/rev, different ranges of cutting speed of 60, 120, 240 m/min and different ranges of depth of cut of 10, 50, 250 µm. They reported an average surface roughness of 0.4 µm. Özel et al. (2005) used a high-precision CNC lathe (Romi Centtur 35E) to execute the HT process using a depth of cut of 0.254 mm and feed rate of 0.05-0.08 mm/rev to obtain an average surface roughness (Ra) of 0.29 µm and 0.38 µm respectively. It is thus evident that the attainable surface finish using HT is still unsatisfactory, and has yet to reach the benchmarks attained by grinding. Hence, an improved surface finish is still a goal for the HT process. Some of the major issues which still need to be addressed are:

(i) White Layer

The consequence of machining hardened steel is the alteration of the microstructure and properties of the workpiece material at the machined surface and subsurface level (Davies et al., 1997). This layer appears to be white under optical microscopy (Barry and Byrne, 2002). The hardness of the white layer is more than the bulk material. Literature suggests that the extent of the formation of white layer could vary between 0.4 µm to 20 µm (Dogra et al., 2010). Despite several experiments, the nature of the white layer is not fully understood and hence it needs further investigation as well (Dogra et al., 2010). Schwach and Guo (2006) studied the effect of surface integrity on the rolling contact fatigue (RCF) of hardened AISI 52100 steel. Their results showed that a component free of a white layer could have six times longer life than a component with the presence of white layer. This could be even worse when the surface contains cracks and voids which could propagate easily due to tensile stress and could accelerate component failure. To avoid this premature failure, it is important that the average value of the machined surface roughness and the quality of the machined surface should be free from defects such as cracks or cavities.

(ii) Residual Stresses

Residual stresses are considered as the remains of the effects induced in a loaded body even after all the external loads are removed. The effect of residual stress on fatigue life of a machined part makes it worthwhile to make proper assessment of the residual stresses induced during the hard turning process. The residual stress profile attributes, including both magnitude and direction along the depth below the machined surface, are believed to significantly affect the service life of the component. Residual stress could be tensile or compressive in nature. Tensile residual stress reduces the material's performance, whereas the compressive residual stresses have beneficial effects on the fatigue life and crack propagation. As shown in the Figure 2.15, compressive stresses tend to close the crack. On the other hand, tensile stress acts the opposite way, towards opening the crack.

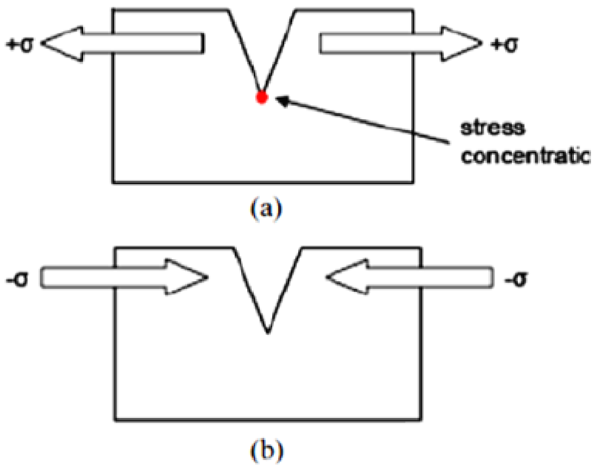

Figure 2.15: (a) Tensile residual stress (b) Compressive residual stress (Dogra et al., 2010)

Sadat and Bailey (1987) and Sadat (1990) analysed the residual stress distribution on the surface of the AISI 4340 workpiece after turning. They measured residual stress distribution using a deflection etching technique. It was found that the absolute value of the residual stresses at the machined surface were low, but increased with increasing depth of the workpiece, to a maximum value, before ultimately reducing to zero. Figure 2.16 shows the trend of residual stress with increased tool wear. From their work, it appears that increased tool wear typically results in large residual tensile stresses near the surface. With the developmental research exploring the avenue of hard turning as an alternative to grinding (Shaw, 2004), significant research is needed to explore the influence of residual stresses on the service life of the component.

The other factors which affect residual stress distribution in finish hard turning are:

- Tool geometry: including nose radius and edge preparation, chamfer angle and length hone radius.
- Cutting parameters, including cutting speed feed rate and depth of cut,
- Cutting tool wear progression.
- Workpiece material hardness.

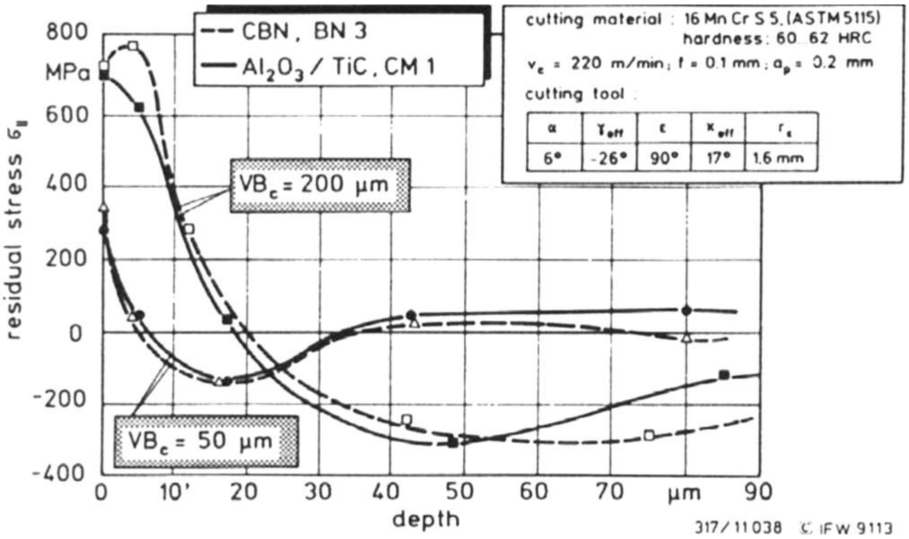

Figure 2.16: Residual stress patterns in hard turned components (Tönshoff et al., 2000)

The effect of workpiece hardness on surface integrity has also been identified by Wu and Matsumoto (Matsumoto et al., 1987, Wu and Matsumoto, 1990). Their research showed that material hardness has a significant effect on the pattern of residual stress. Also, the change in residual stress pattern was mainly caused by the change in the shear plane angle during the chip formation process. The shear angle was found to increase with respect to the material hardness. Jacobson, (2002) conducted experiments on hardened M50 steel (61HRC), using different tools with variation of depth of cut. The experimental result consistently showed compressive stress at the surface but the depth of cut did not affect the amount of residual stress generated. They also showed that higher negative rake angle and smaller nose radius created more compressive residual stress profile. Thiele and Melkote (1999) and Thiele (2002) conducted experimental studies on hardened AISI 52100 steel for finish turning to unravel the effect of cutting edge geometry on the workpiece subsurface deformation and residual stresses. Polycrystalline cubic boron nitride (PCBN) inserts with edge hones and chamfers were used as the cutting tools. Their results revealed that large edge hone tools produced deeper and more compressive residual stresses profiles in comparison to the small edge hone or chamfered tools. It is also very important to highlight some of the concerns that restrict significant exploitation of HT for many other reliable engineering components. The foremost of these is unexpected failure of machined components obtained from HT, due to the existence of tensile residual stresses on the machined surface and, in some cases, the magnitude and penetration depth of compressive stress is low (Tönshoff et al., 2000; Bartarya and Choudhury, 2012; Dogra et al., 2010; Suresh et al., 2013). Such failure is believed to be on account of the formation of the white layer both on and beneath the finished machined surface (Bartarya and Choudhury, 2012; Guo and Sahni, 2004; Barry and Byrne, 2002; Chou and Evans, 1999; Aramcharoen and Mativenga, 2008) or the existence of tensile residual stresses on the machined surface (Thiele, 2002; El-Wardany et al., 2000a; El-Wardany et al., 2000b; Wu and Matsumoto, 1990; Kishawy and Elbestawi, 2001; Matsumoto et al., 1999). Together, white layer and tensile residual stress impose serious threats to the potential fatigue life of the component (Warren and Guo, 2009; Guo et al., 2009; Guo et al., 2010). To avoid this premature failure, it is important that the machining process should induce minimum residual stress, the average value of the machined surface roughness should be low and the quality of the machined surface should be free from defects such as cracks or cavities. A recent literature review by Bartarya and Choudhury (2012) indicates that one of the key limitations of HT is the low magnitude of compressive stresses at the finished machined surface. El-Wardany et al. (2000a; 2000b) mentioned that high tensile residual stresses generated at the finished machined surface could be minimized by selection of proper depth of cut.

2.12 Surface defects

The degradation of the finished machined surface is often referred to as “surface deterioration”, which is mainly due to excessive plastic side flow, build-up of the workpiece material and microchips formed during the course of HT. Amongst other types of surface deterioration mechanisms, plastic side flow dominates the majority of the research discussion relating to HT. However, there are also several other forms of surface deterioration mechanisms observed, which appear in the form of cracks, grooves, cavities and the formation of hard dynamic particles due to the high machining temperature. In his seminal work, Bailey (1974) identified and characterized some of the types of surface damage on HT quenched and tempered AISI 4340 steel (56 HRC). He categorized the surface defects into coarse and fine scale, as tabulated in Table 2.4. This showed that coarse scale defects are associated with continuous chip formation that can be observed to appear in the form of weldament particles on the machined surface, whereas fine-scale defects are associated with discontinuous chip formation and mostly appear in the form of cavities, surface tearing and microcracks on the surface (Bailey, 1976).

Table 2.4: Qualitative characterization of various surface defects – adapted (Bailey, 1974, Zhou et al., 2011)

Coarse-Scale Defects	Fine-Scale Defects
Side flow/pile-up	Micro-Cracking
Weldament particles (hard dynamic particles)	Surface tearing
Microchip debris	Cavities
Grooves	Plastic flow
Ridges	Deformation of the grains

In his subsequent work Bailey (1977) established that the nature of the surface region was influenced primarily by two important factors, namely, the high temperature generated during the course of machining and the frictional conditions existing at the interface between the workpiece and the tool cutting edge. A summary of similar related work with different outcomes is tabulated in Table 2.5. It is evident from Table 2.5 that much of the past work has focused on attempting to relate the surface damage to machining parameters, such as depth of cut, cutting speed and feed rate as well as tool rake angle and tool nose radius (Bailey, 1977, El-Wardany and Elbestawi, 1998, Kishawy and Elbestawi, 1999, Liu and Melkote, 2006). Bailey (1977) studied the effect of tool nose radius, tool wear and feed rate as the primary factors which influences the occurrence of side flow.

Table 2.5: Review of the work on surface deterioration

Workpiece	**Observations/ conclusions**	**Reference**
Inconel 718	Observation of a wide range of surface damage (side flow, pile-up material, grooves and ridges and micro-cracking).	(Zhou et al., 2011)
A15083-H116	Surface roughness model involving consideration of plastic side flow.	(Liu and Melkote, 2006)
AISI 4615	SEM examination revealed presence of surface damage due to different cutting conditions.	(Kishawy and Elbestawi, 1999)

General category	Presents a phenomenological analysis of material side flow in hard turning.	(El-Wardany and Elbestawi, 1998)
Hardened steel (60 HRC)	Proposed material side flow dependent on the cutting conditions and tool geometry	(El-Wardany et al., 1993)
Annealed 18% nickel maraging steel (28 HRC)	Confirmed the presence of coarse and fine scale defects.	(Bailey, 1977)
Quenched and tempered AISI 4340 steel (56 HRC)	Comprehensive explanation of the effects of cutting speed, tool wear and land length on surface integrity.	(Bailey, 1976)
AISI 4340 steel	Surface defects categorized into coarse and fine scale defects (table 1).	(Bailey, 1974)
Plain carbon steel	Concluded that side flow and pile-up in metal cutting are responsible for poor surface roughness quality.	(Selvam and Radhakrishnan, 1973)
CK 45 steel (SAE 1045)	During finish turning, surface microchips are displaced in a direction opposite to the feed direction and eventually these form burrs.	(Pekelharing and Gieszen, 1971)
General	Identified factors affecting surface roughness such as the formation of a pile-up, swelling of the work material, vibration and tool wear.	(Sata, 1966)

Kishawy and Elbestawi (1999) used a full factorial experimental design of cutting parameters with three different nose radius cutting tools and different cutting edges including sharp, honed and chamfered tools to study the effect of process parameters on material side flow during hard turning. Generally, fine scale defects do not contribute to the surface roughness as much as the coarse scale defects; therefore, it was important to identify and characterize all such defects which are commonly observed during the hard turning process. Selvam and Radhakrishnan (1973) observed that side flow and welded materials were major factors influencing the machined surface roughness. The following section will discuss all the major categories of coarse scale defects commonly observed on a HT finished machined surface.

2.12.1 Side flow and pile-up edges

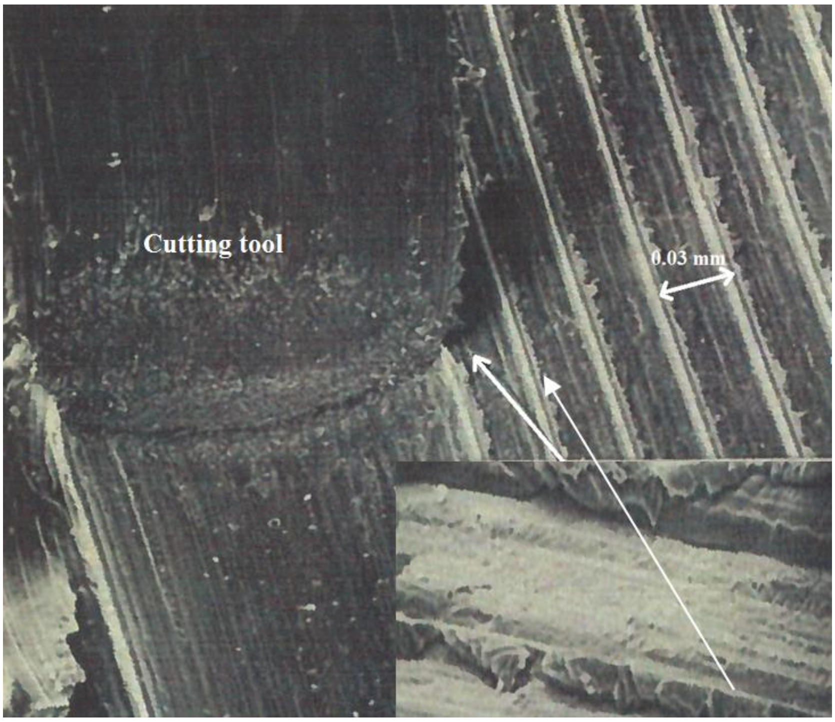

Figure 2.17: High speed camera image of the cutting zone, showing a close up view of the machined surface – adapted (Pekelharing and Gieszen, 1971)

In their pioneering work, Pekelharing and Gieszen (1971) presented photographic evidence of the occurrence of the pile-up and side flow, with the aid of a high speed imaging camera (as shown in Figure 2.17). They demonstrated that the workpiece material displaced sideways by the cutting tool in any cutting operation is analogous to the observations that can be found during a classical indentation process. As shown in Figure 2.17, the direction of the side flow on the machined surface always appears to be in a direction opposite to the direction of the feed rate. This is because, when the tool is engaged in the cutting operation, it will tend to push the material on both sides of the cutting edge. On the finished machined surface, the direction of the material displaced is opposite to the direction of the feed rate whereas it is along the direction of the feed rate on the uncut surface. Advancing the cutting tool removes the uncut portion of the material and leaves the displaced material on only one side which is in a direction opposite to the feed motion of the tool. This pile-up can be removed by the cutting tool during the course of machining, leading to abrasion, surface corrosion and micro-cracking (El-Wardany and Elbestawi, 1998). Furthermore, the adhered material is hard and has a tendency to abrade and therefore tends to wear down the working surface in its immediate contact (Kishawy and Elbestawi, 1999). Also, it is important to distinguish plastic side flow and piled up edges. Plastic side flow can be defined as the excess material that flows along the side of the tool while cutting chips flow along the rake face. In fact, it is the plastic side flow that eventually forms a burr along the feed mark ridges during the course of machining. In contrast, pile-up is an outcome of the excessive compressive strain causing the material (side flow and the pristine material) to appear as if it is bulging on the surface. Essentially, these two terms can also be compared in terms of strain rates, i.e. plastic side flow is strained more in comparison to the piled-up edges. Liu and Melkote (2006) and Sata (1966) state that, together, side flow and pile-up are the most important types of surface deterioration which influence the surface roughness up to 6 µm. Kishawy and Elbestawi (1999) suggest two plausible explanations for material side flow. The first is that the material is ploughed between the tool flank face and the machined surface at an instant when the chip thickness becomes smaller than a certain critical value. In the second mechanism, the plastically deformed material will be pushed to the sides of the tool, due to the high temperature and pressure in the cutting zone, which eventually appears as side flow. El-Wardany and Elbestawi (1998) found that side flow is heavily influenced by the nose radius of the cutting tool, feed motion and progression of the tool wear, which results in a change of profile of the cutting tool. Other researchers, Kishawy and Elbestawi (1999) and T. Sata and Shaw (1964) mention that cutting speed has a significant influence on material side flow. Bresseler et al. (1997) postulate that tool geometry is the most important factor in influencing this and Shaw (2004) found that plastic side flow was very significant at fine feed rates and could thus be partly responsible for the rise in surface roughness at considerably small feed rates.

2.12.2 Weldament particles

Weldaments are small globular particles formed during the process of welding between extremely fine and fractured edges of hard steel in the workpiece, due to the high temperature arising during the cutting process. The growth of weldament particles is strongly dependent on the growth and extent of fracture of built-up edges. Such particles could potentially be referred to as hard dynamic particles and are deemed to be harder than the pristine materials (Cai et al., 2007a, Cai et al., 2007b). Dynamic hard particles and weldaments have been recognized to have the tendency to cause abrasive cutting tool wear, which can eventually deteriorate the quality of the machined surface finish. During the abrasive action process, they may also travel along the cutting edge of the tool, thereby drawing a trajectory of their motions on the finished machine surface. This trajectory eventually appears as small grooves on the finished machine surface. When such a part is subjected to contact interactions, these dynamic hard particles may become source of abrasion to the part they come into contact with.

2.12.3 Microchip debris/grooves/ridges

In an investigation into hardened AISI 4340 steel, an explanation on the formation of the microchip was offered by Bailey (1976). It was pointed out that there could be an instance where there was formation of secondary chips of relatively smaller length (referred to as microchips). These microchips can be classified into three categories.

The first form of microchips is those which leave a groove behind them on the finished machined surface without making a physical separation from the bulk workpiece. Another category of microchips are those which leave their impressions on the surface and also separate from the workpiece in the form of small debris. The final form of the microchip is an outcome of the formation of a Beilby layer of material, as a consequence of interaction between the cutting tool and the workpiece to form a microchip in either of the above categories. Bresseler et al. (1997) point out such microchips could undergo the subsequent action of machining or welding depending on the cutting conditions and may thus worsen the finished surface. Also, they are nominally hard and brittle and are thus tend to accelerate tool wear. All of these categories of microchips eventually leave their marks as grooves and ridges on the finished machined surface.

From this brief review, it appears that there are many factors which may be responsible in influencing surface roughness in hard turning. Therefore, research is required to investigate and analyses the dominance of individual parameters to assert the extent they have on surface roughness.

2.13 Cutting parameters and optimization

Table 2.6: Literature review of optimization studies on hard turning

Work material	Tool material	Optimization tools	Variables studied

AISI 52100	Ceramic inserts of aluminium oxide and titanium carbonitride (Singh and Rao, 2007)	ANOVA + RSM	Cutting velocity, feed, effective rake angle, and nose radius
	CBN cutting tool (Özel et al., 2005)	ANOVA + NN	Cutting speed, feed, workpiece hardness, cutting edge geometry
Aluminium alloy 390, Ductile case iron, Medium carbon steel, alloy steel, inconel	Carbide cutting tool (Mital and Mehta, 1988)	Correlation analysis	Cutting speed, feed and nose radius
AISI 4140 steel	TiC coated tungsten carbide (Sundaram and Lambert, 1981, Sundaram and K LAMBERT, 1981)	Rotatable design + Multiple regression	Cutting speed, feed, depth of cut, time of cut
	Al_2O_3 + TiCN mixed ceramic (Aslan et al., 2007)	ANOVA +Taguchi	Cutting speed, feed, and depth of cut
Mild steel	TiN-coated tungsten carbide (CNMG) (Suresh et al., 2002)	RSM + GA	Speed, feed, depth of cut and nose radius
SCM alloy 440 steel	Al_2O_3 + TiC (Thamizhmanii et al., 2007)	ANOVA +Taguchi	Cutting speed, feed, and depth of cut
SPK alloyed steel	Sintered carbide (Mehrban et al., 2008)	ANOVA + DOE	Cutting speed, feed,

			and depth of cut
AISI D2 Steel	Ceramic wiper inserts (Özel et al., 2007)	Multiple Regression + NN	Cutting speed, feed, and cutting time
AISI 4340 steel (below 60 HRC)	TiC/TiCN/Al_2O_3 coated carbide tipped (Suresh et al., 2012)	Multiple Regression + Taguchi + RSM	Cutting speed, feed, and depth of cut
	Zirconia toughened alumina (ZTA) cutting (Mandal et al., 2012)	RSM + ANOVA	Cutting speed, feed, and depth of cut
	CBN, ceramic and carbide tools (Çydaş, 2010)	Taguchi + ANOVA + Tukey- Kramer comparison, correlation tests	Cutting speed, feed rate, depth of cut, workpiece hardness, and tool types
AISI H11 steel	CBN tool (Aouici et al., 2012)	ANOVA + RSM	Cutting speed, feed rate, depth of cut, workpiece hardness

In hard turning, the preferred cutting conditions suggested are cutting speeds between 100 and 250 m/min, a low feed rate in the range of 0.05 to 0.2 mm/rev and a depth of cut less than 0.25 mm (Bartarya and Choudhury, 2012). Besides these machining parameters, there are numbers of excellent studies reported in the literature regarding optimization of surface roughness using Taguchi methods. Among others shown in Table 2.6, Yang and Tarng (1998) are notable as the first to present a systematic study on application of the Taguchi method to the turning operation. They used three factors namely, feed rate, cutting speed and depth of cut with three different values for each factors called levels. While some researchers used the Taguchi experimental design method for the purpose of optimizing turning parameters for minimizing surface roughness, and obtaining dimensional accuracy and long life of the cutting tool (Davim, 2001, Davim, 2003, Lin, 2004, Manna and Bhattacharyya, 2004, Yih-fong, 2006) others used it for the exploration of the effect of feed rate, cutting speed, and depth of cut on surface finish (Kirby, 2006, Cirstoiu, 2005, Feng and Wang, 2003, Özel et al., 2005a, Vernon and Özel, 2003). Across these studies, it was Tamizharasan et al. (2006) who presented a rather anomalous finding that the depth of cut and the feed rate have negligible and little respective effect on the surface finish, which presents an opportunity for a reassessment of this finding. The second step in the Taguchi method is to determine the number of levels for each factor. (Zhang et al., 2007) selected three levels for three factors cutting speed (0.5 m/sec, 2.5 m/sec, 4.5 m/sec), feed rate (0.05 mm/rev, 0.15 mm/rev, 0.25 mm/rev), and depth of cut (0.025 mm, 0.08 mm, 0.135 mm) to investigate the attainable surface integrity for hardened bearing steel. They found that feed rate has the most important impact on surface finish; cutting speed has the most important impact on the depth of sub-surface damage and residual stress. The average surface roughness achieved by them was in the range of 0.165-0.475 µm. Özel et al. (2005) used four factors and two levels, a total of 16 runs which they replicated 16 times to end up with 256 tests. They used a high-precision rigid CNC lathe (Romi Centur 35E) for longitudinal hard turning. Hardened AISI H13 steel bar and 16 inserts were used for each run, with similar machining parameters. They arrived at a minimum average surface roughness of about 0.25 µm. Thiele and N. Melkote (1999) used three factors, full factorial design to determine the effects of workpiece hardness and tool edge geometry on surface residual stresses in finish hard turning, using CBN tools. The ANOVA they carried out showed that, although the cutting edge geometry and feed rate impact surface roughness, the interaction between the hardness and feed rate is also significant. Aslan et al. (2007) combined the effects of three cutting parameters, namely, cutting speed, feed rate, and depth of cut by employing Taguchi techniques on two performance measures of surface roughness (Ra) and flank wear (V_b). Three levels were selected for each factor thus making a total of 27 runs for turning 63 HRC AISI 4140 steel with an uncoated Al_2O_3+TiCN cutting tool. Their results showed that cutting speed is the most significant factor in influencing the wear of the cutting tool: i.e. an increase in cutting speed causes high tool wear. Davim and Figueira (2007) used orthogonal arrays for three factors and three levels for each factor. They conducted a total of 27 runs to investigate the machinability of cold work tool steel D2 by hard turning. Their ANOVA and S/N ratio showed that obtained surface roughnesses, Ra, were between 0.26 and 1.48 µm and that cutting speed is the most influencing parameter for tool wear. Similarly, Chou et al. (2003) examined tool performance based on the measured surface roughness and tool flank wear. They used two factors with three levels, namely, cutting speed (60, 120, and 240 m/min), depth of cut (10, 50, 250 µm) and the feed rate was fixed at 12.5 µm/rev. The results of the machining experiment of 62 HRC AISI 52100 showed that low CBN content tools (CBN-L) generated better surface finish and a lower flank wear rate than high CBN (CBN-H). The average surface roughness, Ra, obtained by the CBN-L was in the range of 0.2-0.4 µm. Xueping et al. (2009) used L9 orthogonal arrays to optimize hard turning process parameters in inducing subsurface compressive residual stress. Three levels for each cutting condition were selected, i.e. cutting speed (0.5, 2.5, 4.5 m/s), depth of cut (0.025, 0.080, 0.135mm), and feed rate (0.05, 0.15, 0.25 mm/rev). The optimal combination was found to be 0.5m/s, 0.135 mm and 0.25 mm/rev for cutting speed, depth of cut and feed rate, respectively. Bouacha et al. (2010) investigated the machinability of the AISI 52100 (64 HRC) by applying an L27 Taguchi orthogonal array for three factors and three levels i.e. cutting speed (125,176, 246 m/min), feed rate (0.08, 0.12, 0.16 mm/rev) and depth of cut (0.15, 0.3, 0.45 mm). Their ANOVA results show that surface roughness is significantly influenced by feed rate and cutting speed. The average surface roughness obtained was 0.19-0.77 µm and the optimum cutting parameters they suggest are 246 m/min, 0.08 mm/rev and 0.15 mm for cutting speed, feed rate and depth of cut, respectively. Asiltürk and Akkuş (2011) applied the Taguchi method to minimize surface roughness (Ra, Rz) for hard turning. Three factors and three levels were selected to machine AISI 4140 (51 HRC). While implementing a L9 orthogonal array, they used cutting speeds of 90, 120, 150 m/min, feed rate of 0.18, 0.27, 0.36 mm/rev and depth of cut of 0.2, 0.4, 0.6 mm. They showed that the feed rate has the most significant effect on Ra and Rz. Besides all the above work, Suresh et al. (2013) have reviewed a great deal of literature concerning hard turning studies, carried out between the years 2001 and 2008. They have listed all the cutting parameters and levels of each parameter used in each study. An interesting observation from this review is that much of the research has used a feed rate of 0.05 mm/rev as the minimum feed rate in their experiments and the lowest average surface roughness obtained was 0.2 µm. In another review, Bartarya and Choudhury (2012) reviewed cutting conditions used by various researchers in hard turning and found the range of feed rate chosen was between 0.05-0.2 mm/rev.

2.14 Numerical modelling of hard turning using FEA

Studying the machining process through computer simulation is another approach which reduces the cost of experimental investigation. The cutting process is a very complicated process that involves elastic/plastic deformation and fracture at high strain rates under the effect of high temperature, which causes the material properties to vary during the machining process. Thus, analytical modelling will be time consuming and tedious for such a complex process (Dornfeld et al., 2006). However, numerical modelling and computer simulation using finite element analysis (FEA) has become a popular tool to model machining processes. While only a few studies are evident involving the use of FEA on hard turning, no work has been done on hard turning that involves molecular dynamics simulation. In 1984, Lwate was the first to use software developed for metal forming analysis within an Eulerian framework to study machining. In the middle of the 1980s, an updated Lagrangian elastic-plastic analysis was used, and the chip/work separation criterion at the cutting edge became an issue. At that time, neither a realistic friction model nor coupling of the elastic-plastic to thermal analysis was included. The 1990s saw the development of non-steady analysis, from transient to discontinuous chip formation, the first three-dimensional analyses and the introduction of adaptive meshing techniques, particularly to cope with flow round the cutting edge of a tool. By the late 1990s, several FEM codes had been developed. There are two types of analysis in which a continuous medium can be described as Eulerian and Lagrangian. In a Lagrangian analysis, the computational grid deforms with the material, whereas in an Eulerian analysis, this is fixed in space. The Lagrangian calculation embeds a computational mesh in the material domain and solves for the position of the mesh at a discrete point in time. Updated Lagrangian formation with continuous remeshing has been used in the simulation of continuous and segmented chip formation in machining processes. The arbitrary Lagrangian-Eulerian ALE technique is a new approach which combines the features of pure Lagrangian and Eulerian analyses. The ALE formation is also utilized in simulating machining, to avoid the frequent remeshing required for chip separation (Arrazola and Ozel, 2008, Childs, 2000). Furthermore, FEA can also be used for process optimization for producing favourable surface integrity, cutting forces, and chip flow and chip morphology (Guo and Liu, 2002). Moreover, the use of commercially available software packages has increased dramatically over the last fifteen years. In recent years, several options have emerged to use commercially available softwares to study hard turning processes. These studies are shown in Table 2.7.

Table 2.7: Finite element software used to study hard turning

Software used in hard turning	Researchers using FAM to study hard turning
DEFORMTM	Klocke et al. (2001); Yen (2004); Umbrello et al. (2004); Hua et al. (2005)
AdvantEdgeTM	(Marusich and Ortiz, 1995); (Lundblad, 2000); (Davies and Burns, 2001); (Nouari et al., 2003); (Özel, 2003); (Bil et al., 2004);
ABAQUS/ExplicitTM	(Guo and Liu, 2002), (Guo and Barkey, 2004); (Guo and Yen, 2004); (Ng et al., 2002); (Bäker, 2006); (Bäker et al., 2003); (Chuzov et al., 2002) ; (Chuzhov et al., 2003)
FORGE 2TM	(Ng et al., 1999)

The reliability of a FEA based model is heavily dependent on the constitutive flow stress criterion used to describe and predict the deformation of the workpiece in terms of strain, strain rate, temperatures, as well as friction parameters between tool and work material interfaces. Childs (1998) reported using a range of strains, strain rate and temperature parameters to simulate the hard turning process with strain rates up to 10^6 s^{-1}, strains up to 4 and temperatures up to 1000° C, while Oyane et al. (1967) used strain rates in the range of 500 s^{-1}. The representation of any flow stress data should be limited to the exact material (microstructure and heat treatment) being tested. In other words, materials with nominally the same chemical composition but manufactured differently are more likely to have different mechanical behaviour (i.e. different flow stress curves).

In the literature, there are several methods available which are used to predict the flow stress of any material, as shown in Table 2.8.

Table 2.8: Methods to determine the flow stress data

Method's founder and users	Name of the methods
(Mathew and Arya, 1993); (Lei et al., 1999); (Kopac et al., 2001)	Orthogonal turning experiments
(Shatla, 1999); (Shatla et al., 2001a); (Shatla et al., 2001b)	inverse mapping of Oxley's machining theory
(Oxley and Young, 1989)	orthogonal slot milling tests
(Stevenson, 1997); (Kopac et al., 2001)	compression and cutting tests
(Kumar et al., 1997); (Özel and Altan, 2000); (Shatla, 1999); (Shatla et al., 2001a); (Shatla et al., 2001b); (Huang, 2002); (Ramesh, 2002); (Sartkulvanich et al., 2004)	FEA and experiments

2.15 Summary

An extensive review has been offered in this chapter to give the essential background about the hard turning process relevant to the proposed work in the thesis. The advantages and the limitations of hard turning have been highlighted. The need to improve the process in terms of its surface roughness and surface integrity was discussed based on many previous studies by experts in the field. From the review it is clear that the surface side flow is a problem associated with the machined component and no solution has been proposed to solve this problem. Also, it is clear that previous work was focused on the investigation of the limitations and the problems of the process without suggesting a method of resolving these. In the next chapter a new method is proposed to solve many of the issues related to hard tuning. The theoretical and experimental work will be explained in detail in the next two chapters.

CHAPTER 3 – Development of a surface defect machining method for hard turning processes

3.1 Introduction

In this chapter, the aim is to develop a novel machining method to ease the manufacturing of hard steel. A method named “surface defect machining” (SDM) is developed and a preliminary study is made on AISI 4340 hardened steel using FEA simulation. The simulation models were validated using previously published data during conventional hard turning, which became the basis of extending the simulation to test the SDM method. The following section comprehensively describes the SDM method in detail.

3.2 Description of the surface defect machining method

The proposed SDM method was developed to tie together the combined advantages of the porosity machining method (Tutunea-Fatan et al., 2011) and pulse laser pre-treated machining (Komanduri et al., 1982)

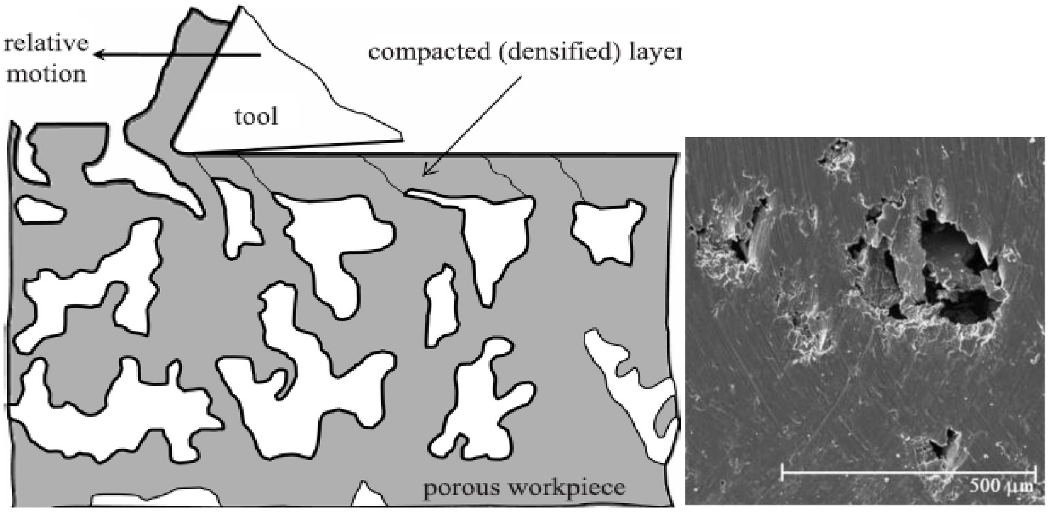

Figure 3.1 Machining of porous material (Tutunea-Fatan et al., 2011)

As shown in Figure 3.1, porous sintered materials such as filters, pressure regulators, phonic silencers and heat exchangers exhibit poor machinability (Tutunea-Fatan et al., 2011). It is believed that the stresses developed during machining the porous material pushes its particles into the vacant pores, which causes the formation of the layer of quasi-continuous material having no porosity on top of the machined surface. Therefore, an increase in porosity causes a decrease in micro hardness and a subsequent reduction in the required cutting energy. The problem with machining porous material is the random porosity contained on the workpiece: thus the cutting tool will be exposed to a short fatigue life. However, the proposed method, SDM, will generate controlled porosity on the workpiece surface, less than the programmed depth of cut, to avoid this problem.

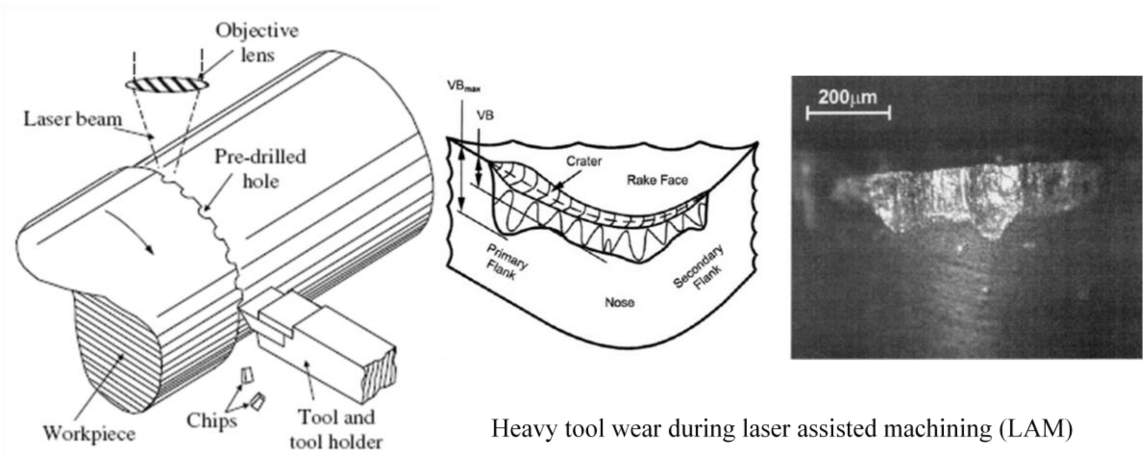

Figure 3.2 Pulse laser pre-treated machining proposed by Komanduri et al. (1982) and tool wear during LAM (Sun et al., 2010)

On the other hand, there is also a method patented in 1982, known as pulse laser pre-treated machining (Komanduri et al., 1982), as illustrated in Figure 3.2, where the machining of titanium and high temperature alloys was demonstrated to reduce the volume of the material required to be removed which was done with the aid of pulse laser drilling using an ultra high power laser ablation method. However, both of these methods have their own limitations, such as the fact that during porosity machining, the depth of discontinuities below the uncut chip thickness will present a risk to the tool life, due to high impact loads. Similarly, poor laser power control can cause the premature degradation, accelerated dissolution-diffusion and adhesion wear of the tool tip. SDM is a hybrid method meant to provide better control and quality of the machined surface, as shown in Figure 3.3. Taking advantage of both the above methods became the key motivation for development of the SDM method. Thus defined, SDM is a process of machining where a workpiece is first subjected to surface defects creation at a depth less than the uncut chip thickness, either through mechanical and/or thermal means and then followed by a normal machining operation. The process of generating surface defects can be carried out using a patterning tool to produce any desired defect shape, as shown in Figure 3.4a.

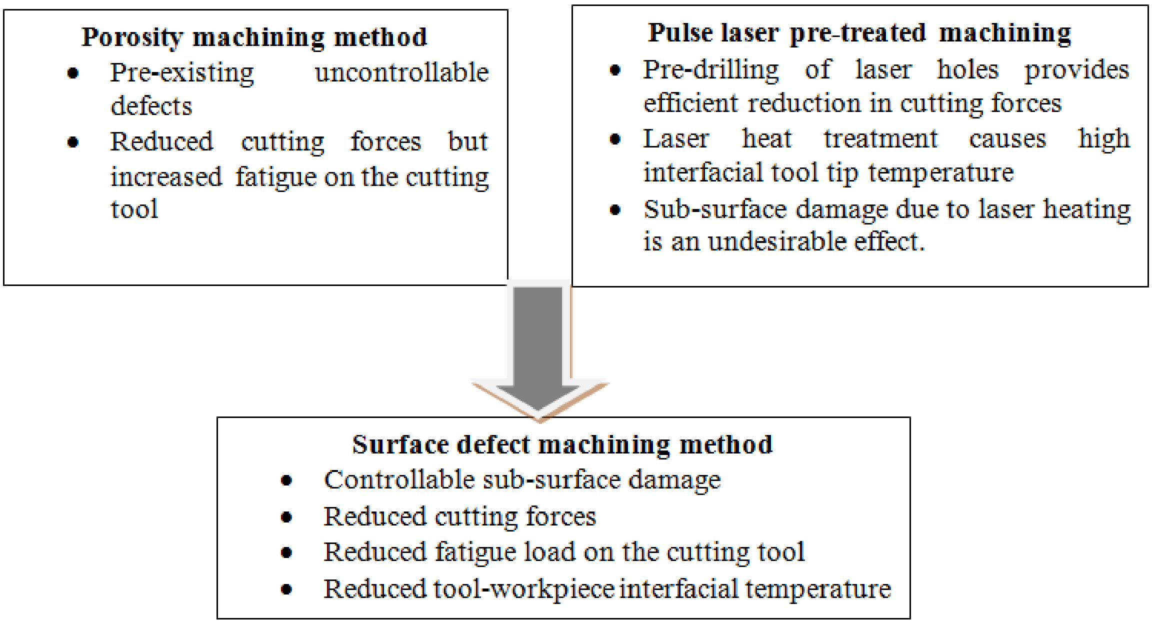

Porosity machining method

- Pre-existing uncontrollable defects
- Reduced cutting forces but increased fatigue on the cutting tool

Pulse laser pre-treated machining

- Pre-drilling of laser holes provides efficient reduction in cutting forces
- Laser heat treatment causes high interfacial tool tip temperature
- Sub-surface damage due to laser heating is an undesirable effect.

Surface defect machining method

- Controllable sub-surface damage
- Reduced cutting forces
- Reduced fatigue load on the cutting tool
- Reduced tool-workpiece interfacial temperature

Figure 3.3: Development of the surface defect machining method

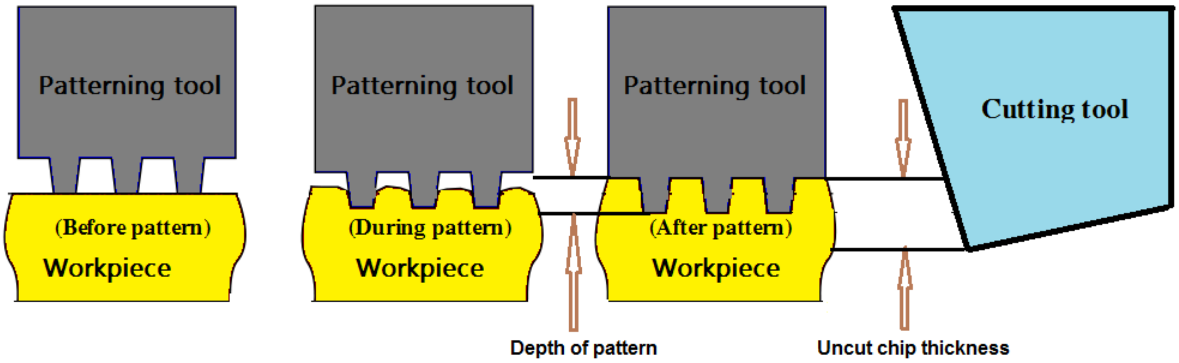
Patterning tool
(Before pattern)
Workpiece
Patterning tool
(During pattern)
Workpiece
Patterning tool
(After pattern)
Workpiece
Cutting tool
Depth of pattern
Uncut chip thickness

(a)

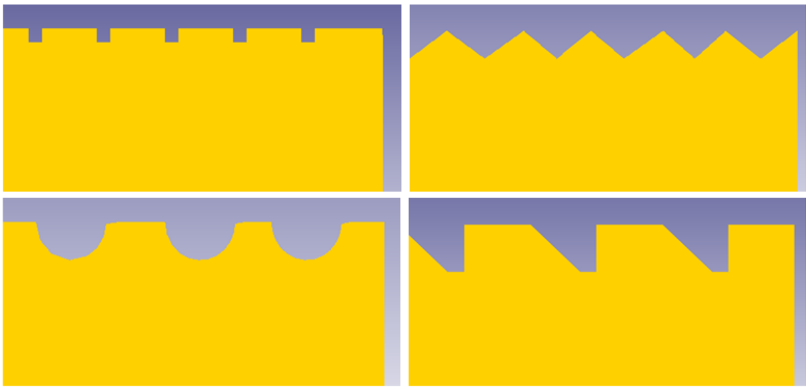

(b)

Figure 3.4: (a) Patterning on a workpiece (b) Examples of patterns used to generate surface discontinuities on a workpiece

It is anticipated that the shape of these defects (shown in Figure 3.4b) may also play a significant role in governing the mechanism of deformation in the cutting zone of the workpiece. Since this is only a preliminary investigation, the scope of this thesis is only to conduct preliminary feasibility trials and highlight the potential advantages of using the SDM method. Although, drilling, threading, ablation or combinations of these methods can be used for processing such defects; laser ablation possesses a peculiar advantage in the domain of hard turning, in that any sub-surface deformation arising due to laser heating can be eliminated during the heat treatment process stage. Therefore, the proposed method is potentially superior to using laser heating and subsequent thermal softening machining (Komanduri et al., 1982), which is referred to as laser assisted machining (LAM). The working principle underlying the proposed SDM method is that the cutting chips in a HT process are often observed to be serrated and continuous; as such, they can collide with the machined surface or the cutting tool and thus are capable of damaging the surface quality of the part being machined.

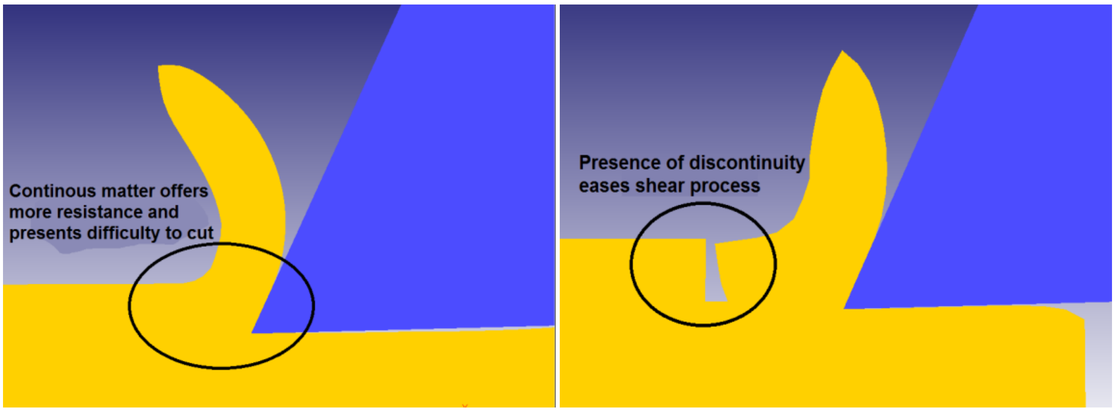
Continous matter offers more resistance and presents difficulty to cut
Presence of discontinuity eases shear process

Figure 3.5: Schematic diagram indicating difference between the mode of deformation between a continuous material and a discontinuous material obtained from FEA simulation

Moreover, the deformation of a continuous material will always require more energy than a discontinuous material. As a result, surface discontinuities break the energy barriers associated with the critical deformation load and provide a chip breaking mechanism, as shown schematically in Figure 3.5. Therefore, surface defects allow easy shearing and breaking of the cutting chips into small segments which reduces the overall cutting resistance. In the subsequent section, the application of finite element simulation to hard turning using conventional and the SDM method is presented and discussed.

3.3 Finite element modelling and constitutive deformation criterion

A comprehensive understanding of the SDM technique could only be made through a rigorous theoretical analysis. Accordingly, an assessment of the SDM method was made using the finite element analysis (FEA) to compare the conventional hard turning of AISI 4340 steel (52 HRC), using an Al_2O_3 insert, with the SDM method, using a Lagrangian implicit code. Figure 3.6 shows the configuration developed for the FEA model generated by applying surface defects. The model was subjected to fixed boundary conditions on the ends, as shown. The direction of cutting force (F_x) and feed force (F_y) which are normally used to compare the machining processes are also highlighted.

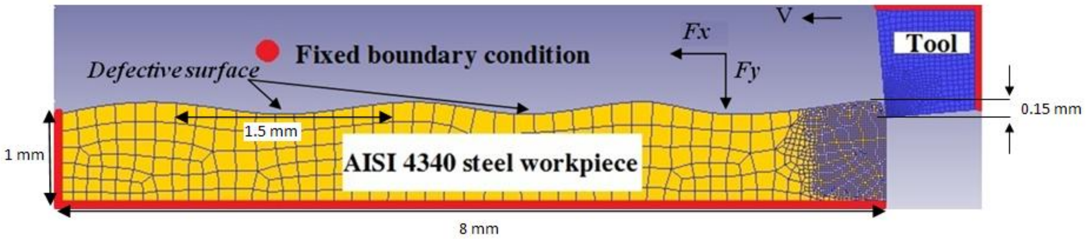

Figure 3.6: Boundary conditions for the FEA model

For a more accurate description of the cutting process of the AISI 4340 workpiece, a Johnson-Cook constitutive equation (Johnson and Cook, 1985) was employed as follows:

$$\bar{\sigma} = \underbrace{(A + B\bar{\varepsilon}^{n})}_{\text{Elasto}-\text{plastic term}} \underbrace{\left[1 + C\ln\left(\frac{\dot{\bar{\varepsilon}}}{\dot{\bar{\varepsilon}}_0}\right)\right]}_{\text{Viscosity term}} \underbrace{\left[1 - \left(\frac{T - T_{room}}{T_{melt} - T_{room}}\right)^{m}\right]}_{\text{Softening term}} \tag{3.1}$$

where $\bar{\sigma}$ is the flow stress (MPa), $\bar{\varepsilon}$ is the plastic strain, $\dot{\bar{\varepsilon}}$ is the strain rate (s^{-1}), $\dot{\bar{\varepsilon}}_0$ is the reference plastic strain rate (s^{-1}), T is the workpiece temperature (° C), T_{melt} is the workpiece melting temperature (° C), T_{room} is the ambient temperature (20° C), coefficient A (MPa) is the yield strength, B (MPa) is the hardening modulus, C is the strain rate sensitivity coefficient, n is the hardening coefficient and m is the thermal softening coefficient. The chemical composition of AISI 4340 steel, curve coefficients for Johnson and Cook model, properties of the cutting tool and the workpiece material and the machining parameters employed in the FEA simulation are shown in Tables 3.1, 3.2, 3.3 and 3.4 respectively (Coelho et al., 2007). The configuration of the FEA model and machining parameters were selected in a way that enabled the simulation results to be compared readily with the previously published experimental results (Coelho et al., 2007; Matsumoto et al., 1986).

Table 3.1: Chemical composition of AISI 4340 steel (Coelho et al., 2007)

AISI	**C**	**Mn**	**P, max**	**S, max**	**Nb**	**Ni**	**Cr**	**Mo**	**W**
4340	0.43	0.83	0.025	0.02	7.8	1.71	0.79	0.25	0.55

Table 3.2: J-C constitutive parameters for AISI 4340 steel (52 HRC) (Coelho et al., 2007)

A (MPa)	**B (MPa)**	**N**	**C**	**m**
950	725	0.375	0.015	0.625

Table 3.3: Workpiece and cutting tool properties

Property	**Unit**	**AISI 4340 steel workpiece**	**Al_2O_3 cutting tool**
Density	Kg/m^3	7850	3890
Young's modulus	GPa	205	375
Fracture Toughness	$MPa.m^{1/2}$	50	4
Poisson's ratio	-	0.3	0.22
Specific heat	J/KgK	750	880
Thermal conductivity	W/mK	44	35

Table 3.4: Simulation parameters

Simulation type	2D – FEA Simulation
Workpiece material (8 mm × 1 mm)	AISI 4340 steel with 52 HRC
Cutting tool tip	Al_2O_3
Cutting speed/ Surface speed	91 m/min
Uncut chip thickness	0.15 mm
Cutting tool rake angle	-5º
Cutting tool clearance angle	5º
Tool edge	Extremely Sharp
Surface defects (depth and width) with interspacing 0.3 mm	0.1 mm and 1.5 mm

3.3.1 Fracture criterion and friction tool/chip interface

The cutting chips start flowing on the rake face of the cutting tool when the applied stress reaches the value of flow stress. During the simulation, the well-known Cockroft and Lathem's criterion (Cockcroft, 1968) was employed, which states that the damage (D) occurring during the plastic deformation is the amount of work done by applied equivalent strain ($\bar{\varepsilon}$) multiplied by the ratio of maximum tensile stress (σ_T) to von Mises flow stress ($\bar{\sigma}$).

$$D = \int_0^{\bar{\varepsilon}_f} \frac{\sigma_T}{\bar{\sigma}} d\bar{\varepsilon} \qquad (3.2)$$

The critical damage value is calculated for each element under deformation at each time-step, by the code. Once the damage value in an element reaches the critical value, a crack is initiated in two steps: (i) this element is deleted with all the parameters related to it, including the element connectivity definition and the strain and stress values; (ii) the rough boundary produced by element deletion is smoothed by cutting out the rough angle and adding new points (Coelho et al., 2007). Thus, by comparing *D* with D_{max}, the material fracture criterion is assessed. In order to evaluate *D* at each time step the equation of *D* is discretized as follows:

$$D = \int_0^{\bar{\varepsilon}_f} \frac{\sigma_T}{\bar{\sigma}} \frac{d\bar{\varepsilon}}{dt} dt = \int_0^{t_f} \frac{\sigma_T}{\bar{\sigma}} \dot{\bar{\varepsilon}} dt \cong \sum_0^{t_f} \frac{\sigma_T \dot{\bar{\varepsilon}} \Delta t}{\bar{\sigma}} \qquad (3.3)$$

where $\dot{\bar{\varepsilon}}$ is the equivalent strain rate (s^{-1}) which is calculated from the individual principal strain-rate components and Δt, the variable time increment. For friction modelling, the following constant shear hypothesis was considered:

$$\tau = \mu \tau_0 \qquad (3.4)$$

where τ is the shear stress, μ is the friction factor and τ_0 is the shear yield stress ($\tau_0 = \sigma_0 / \sqrt{3}$). Based on this FEM model, cutting forces, stresses, temperature and velocity in the machining zone are presented and discussed in the subsequent sections.

3.4 Validations of FEM with experiments

Regardless of whether executing the conventional HT process, or the proposed SDM method, the cutting forces have remained one of the most important indicators of the outcome of the machining process used to characterize the performance of the process (Tutunea-Fatan et al., 2011). Figure 3.7 and Table 3.5 present a comparison of the cutting forces obtained under normal cutting conditions through the HT process, without any surface defects (experimentally and theoretically) and by inclusion of the surface defects on the workpiece obtained from the FEA simulation. These parameters were used intentionally, so as to compare the FEA results with an experimental study made by Matsumoto et al. (1987). The maximum error between the FEA simulation results and the experimental results were up to 16% in the friction forces, whereas only a 6% error was observed in the average cutting forces. As shown in Table 3.5 and Figure 3.7, the simulation results are in reasonable agreement with the reported experimental results, and thus became the basis for the extension of this model to test the feasibility of the SDM method merely by addition of the surface defects on the workpiece.

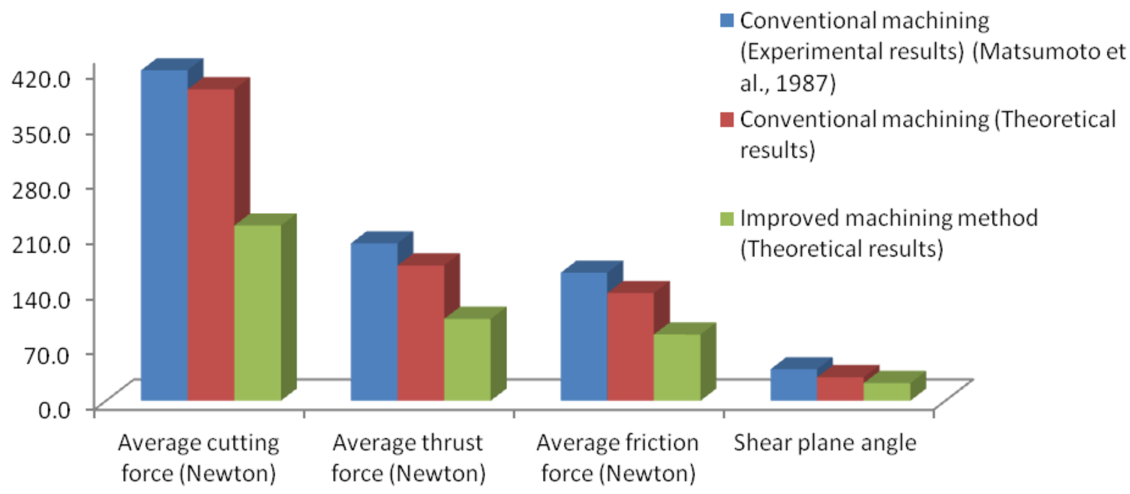

Figure 3.7: Comparison of experimental and theoretical machining results while cutting AISI 4340 steel (52 HRC) with Al_2O_3 cutting insert having -5º tool rake angle

Table 3.5: Experimental and simulation results

	Average cutting force (N)	**Average feed force (N)**	**Average friction force (N)**	**Shear plane angle**
Hard turning with conventional method (Experimental results) [93]	420.0	200.0	162.6	40.0°
Hard turning with conventional method (Simulation results)	395.8	171.9	136.8	29.9°
Approximate percentage error between experimental and simulation results	6%	14%	16%	-
Surface defect machining method (Simulation results)	222.6	104.0	84.2	27.9°

Approximate percentage reduction (theoretical) observed between conventional and proposed method of machining	22%	35%	38%	2°

Simulation results of the SDM method and conventional machining (HT) are also shown and compared in Table 3.5. It may be seen that compared to the conventional HT process, the SDM method shows a reduction in average cutting forces by up to 22% and other forces in the range of 35-40%. Furthermore, a reduction in the shear plane angle from 29.9° to 27.9° is also noticed.

In addition, Figure 3.8 presents the evolution of the cutting forces obtained from the simulation comparing both cases, i.e. a normal HT operation and SDM method. It can be seen that the cutting forces (F_x) are indeed higher than the feed forces (F_y). A significant drop in both cutting forces is observed when the cutting tool encountered the surface defects. This intermittent reduction in the cutting load is favourable for tool longevity, as it aids in the reduction of the local temperature at the cutting edge, which will be discussed further in later sections. Based on these results, it is plausible to presume that the deformation of material becomes more prone to shear (during SDM) which causes a reduction in the shear plane angle. In order to confirm this proposition, a plot was made, Figure 3.9, using the previously reported experimental machining data on AISI 4340 steel (Matsumoto et al., 1986; Matsumoto et al., 1987; Wu and Matsumoto, 1990). This plot shows a strong link between the shear plane angle, the friction forces and the material's hardness. As evident from Figure 3.9, there is a steep range of shear plane angles, which provides the most amenable healthy cutting conditions. It can also be seen that the material's hardness tends to influence the shear plane angle and the consequent friction forces during the machining of AISI 4340 steel. For the same AISI 4340 steel, the friction forces were lower for 44-52 HRC hardened steel, where the shear plane angle was in a range of 28°-34°. This observation strongly suggests that the shear plane angle influences the HT process. Through the proposed SDM method, a reduction in shear plane angle was achieved, which explains the improved machinability of the work material during the process. As seen earlier, using the proposed SDM method, a reduction in shear plane angle of up to 2° is observed using the current configuration of machining parameters. The reduction in the cutting force further testifies to the improved mechanism of deformation. Furthermore, the reduced shear plane angle signifies an increased cut chip thickness and a higher strain rate which makes the deformation process easier. This is further analysed and demonstrated in the subsequent sections.

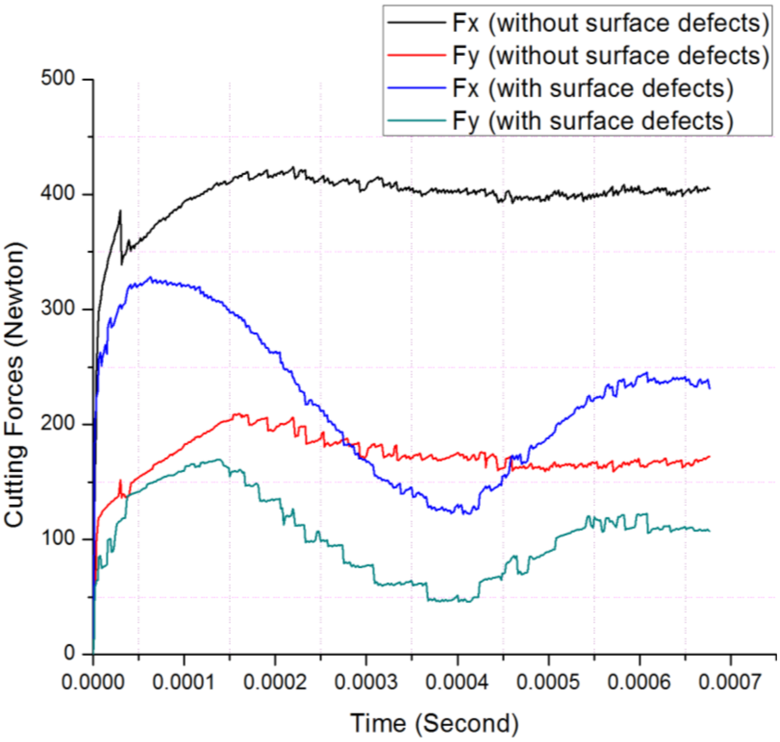

Figure 3.8: Evolution of cutting forces over 1.486mm cutting length

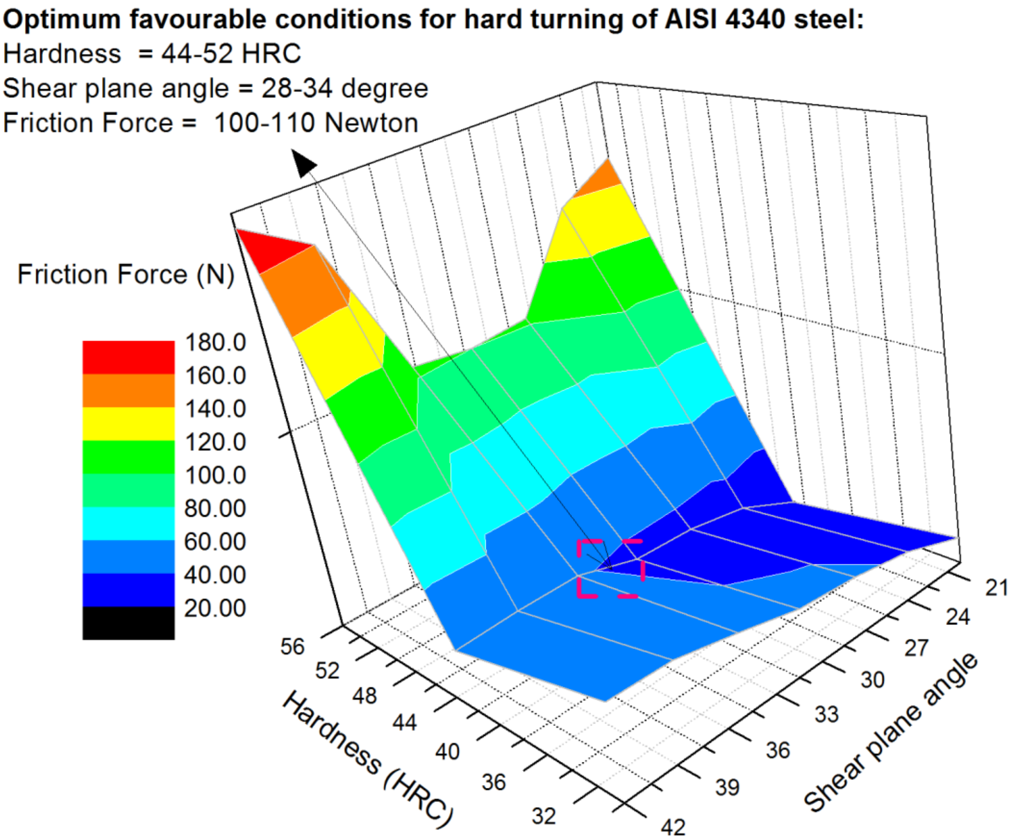

Optimum favourable conditions for hard turning of AISI 4340 steel:

Hardness = 44-52 HRC

Shear plane angle = 28-34 degree

Friction Force = 100-110 Newton

Figure 3.9: Optimization of hardness, shear plane angle and friction force, based on the experimental results (derived from the experimental data) (Matsumoto et al., 1986; Matsumoto et al., 1987; Wu and Matsumoto, 1990)

3.5 Temperature in the machining zone

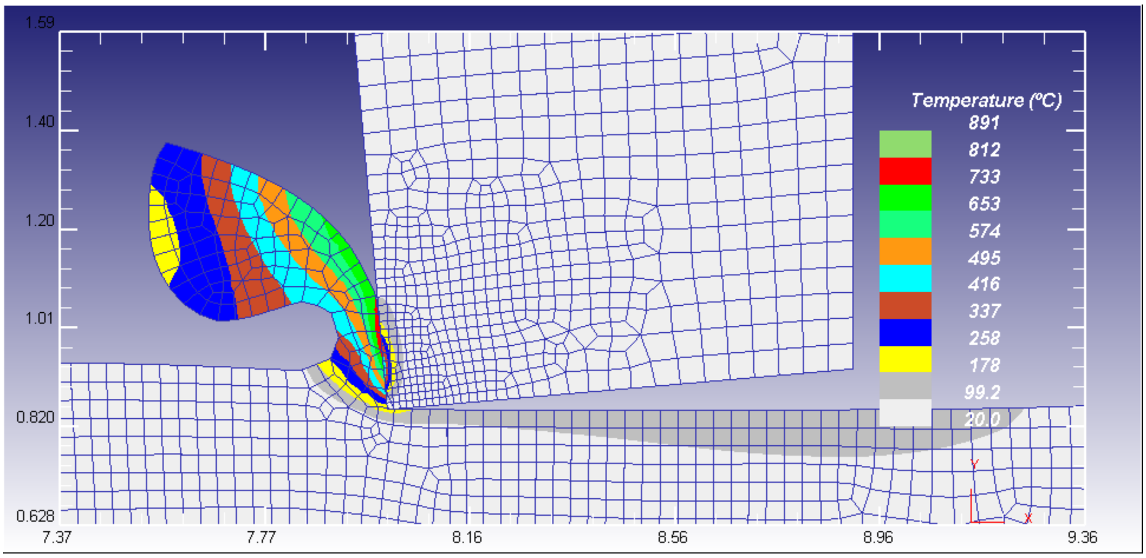

Figure 3.10: Temperature in the machining zone during surface defect machining

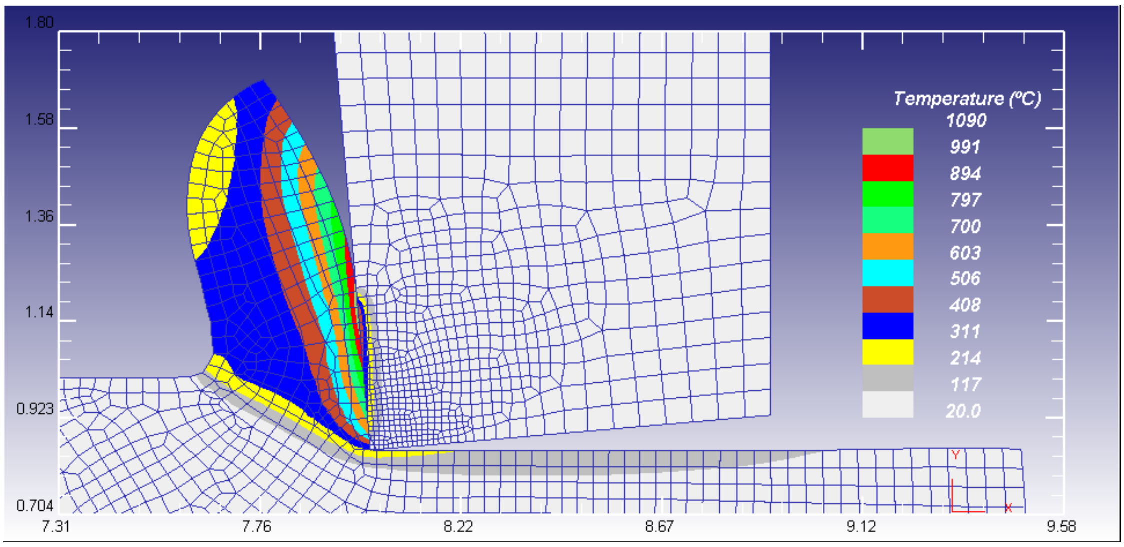

Figure 3.11: Temperature in the machining zone during ordinary HT process

Figures 3.10 and 3.11 present a comparison of the temperature in the machining zone during SDM and during the conventional machining process. As expected, due to the reduced cutting forces and a reduction in the volume of material removal, a drop in the temperature in the machining zone can be seen, which is indeed in accordance with the experimental trials in the following chapter. Due to the high hardness of the workpiece, the cutting temperature can reach up to a value of 1090º C within a 1.486 mm length of cut. This magnitude of high temperature was particularly evident on the section of those cutting chips which are in the direct contact with the rake face of the cutting tool. In contrast to this, the temperature in the shear zone of the workpiece was only about 200º

C. This suggests that thermal softening does not play an important role during the hard turning process, as also indicated by Shaw (2004). It is indeed the concentrated shear that contributes to the chip formation during the HT process. Although a reduction of the overall temperature is observed in the simulation and in the experiment, the peak magnitude of the temperature on the tool tip remained high using the SDM method, as shown in Figure 3.12. The contact length of the tool-chip interface in the SDM method and the normal HT method is found to be different. From Figure 3.12, it can be seen that the tool-chip interface contact length in the case of the SDM method is reduced to 0.22 mm from 0.39 mm observed in the normal machining method. Due to the low contact length, a low heat dissipation rate can be expected which is likely to be responsible for the high peak-value of the temperature on the tool tip using SDM.

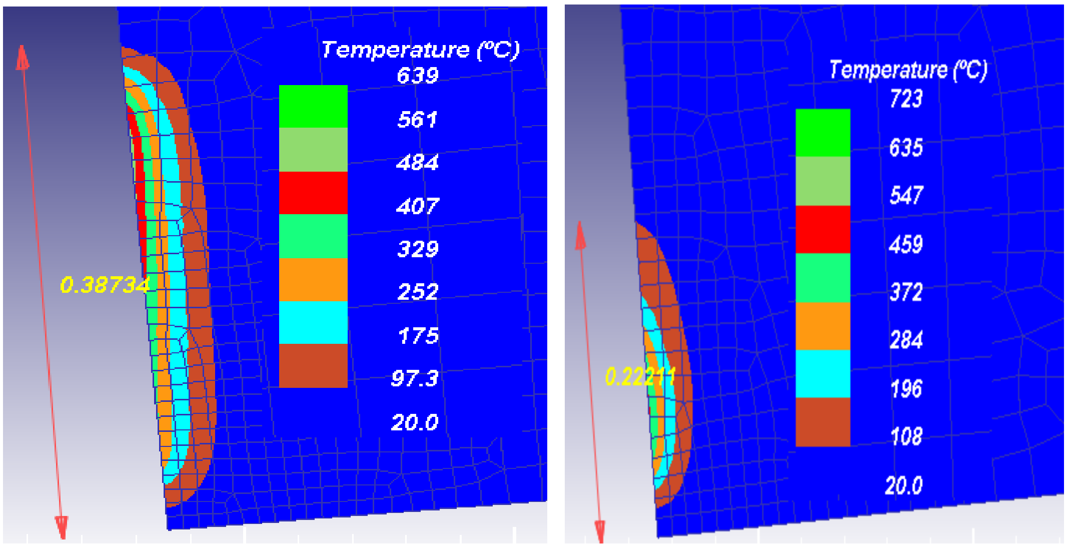

Figure 3.12: Temperatures in the machining zone using (a) conventional HT process (b) SDM method

However, the effect of this high temperature on the tool tip can be considered negligible, since a CBN cutting tool, which is normally used for practical HT operations, is known to exhibit good stability, even at higher temperatures of up to 1300º C (Shaw, 2004). Since, the value of peak temperature, 723º C, is much less than the stability temperature range of 1300º C of CBN, the reduced interface friction tool-chip contact length will not cause any thermal instability on the cutting edge of the CBN tool during the SDM process.

3.6 Stresses in the machining zone, residual stresses and chip morphology

Figures 3.13 and Figure 3.14 present a comparison of the von Mises stresses in the workpiece between surface defect machining and conventional hard turning operations after a 1.486 mm of length of cut. The local magnitude of the von Mises stress in the shear zone of the workpiece during SDM was found to be slightly higher (1520 MPa) than the normal HT operation (1360 MPa). However, unlike the normal HT method, SDM shows high stress concentration in the cutting zone, which causes relatively easier deformation of the work piece. Also evident is that a residual stress in the range of 136-271 MPa surrounded the machining zone in the case of ordinary HT method, deep into the sub-surface, which was not the case with the SDM method. This could lead to the possibility of residual stresses in the workpiece after the machining process, something which has often been cited as a reason for criticising the HT process when it is compared to grinding (König et al., 1993; El-Wardany et al., 2000a; El-Wardany et al., 2000b). To quantify this, the stresses in the *x*-direction were calculated by considering a portion of an element of the workpiece fixed since the beginning of the simulation. That is to say that the dynamic fluctuation of the stress in the machined surface of the workpiece is calculated with respect to the movement of the cutting tool.

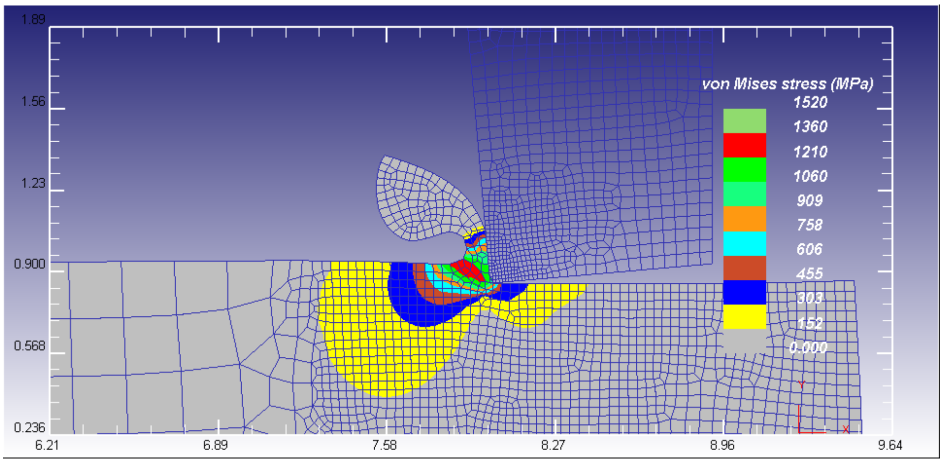

Figure 3.13: Von Mises stresses during surface defect machining

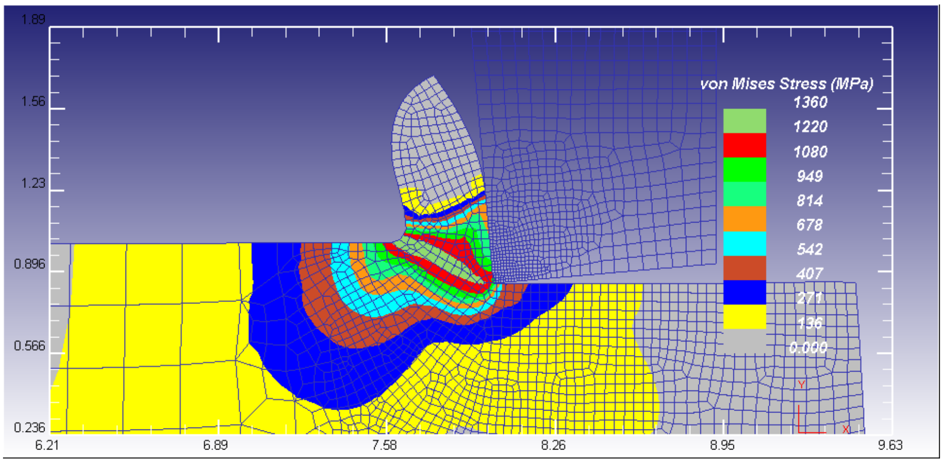

Figure 3.14: Von Mises stresses during conventional machining

The stresses left out on the machined surface after the simulation run can thus be considered as the residual stresses introduced by the action of machining. The abscissa in Figure 3.15 represents the time duration in which the cutting tool moves past the point of observation. It can be seen from Figure 3.15 that this portion of the workpiece is subjected to a high degree of compression in the vicinity of the tool, during the course of cutting. After the tool advances beyond the portion of the element being cut, the stresses left on and underneath the machined surface are of tensile (positive sign) nature. Also, during the SDM process (136 MPa), the residual stresses are found to reduce slightly compared to those obtained during the ordinary HT operation (174 MPa). Early research speculated on finding compressive residual stresses in contrast to the tensile residual stresses being found in Matsumoto et al. (1987) and Wu and Matsumoto (1990) work, so that it is in line with another finding of Brinksmeier et al. (1982); those compressive residual stresses may have arisen due to the forming process carried out prior to machining and were not accounted for when analyzing residual stresses in the machined workpiece specimen after the machining operation. Based on the analytical stress theory, it is firmly believed that if a residual-stress-free specimen is machined with the HT process, only tensile residual stresses will be observed on and underneath the machined surface. This eliminates the possibility of finding compressive residual stress even under the white layer formation. The previous research suggests that the white layer formation impedes the release of tensile stresses to come to the surface and, hence, becomes of a compressive nature (Tönshoff et al., 2000). However, a simple stress equilibrium diagram in that state suggests that there will only be tensile residual stresses in the machined part, provided it is stress free before machining.

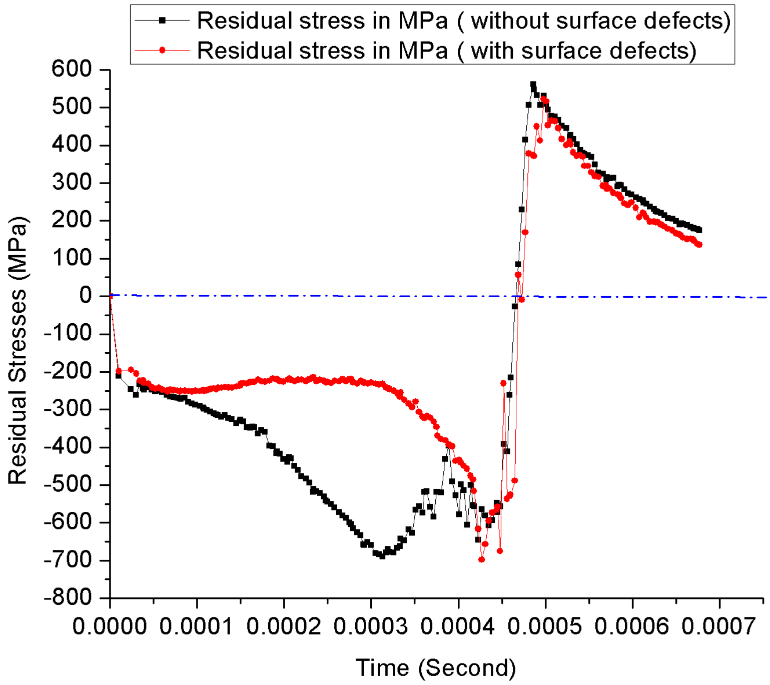

Figure 3.15: Comparison of residual stresses on the machined surface (*x*-direction)

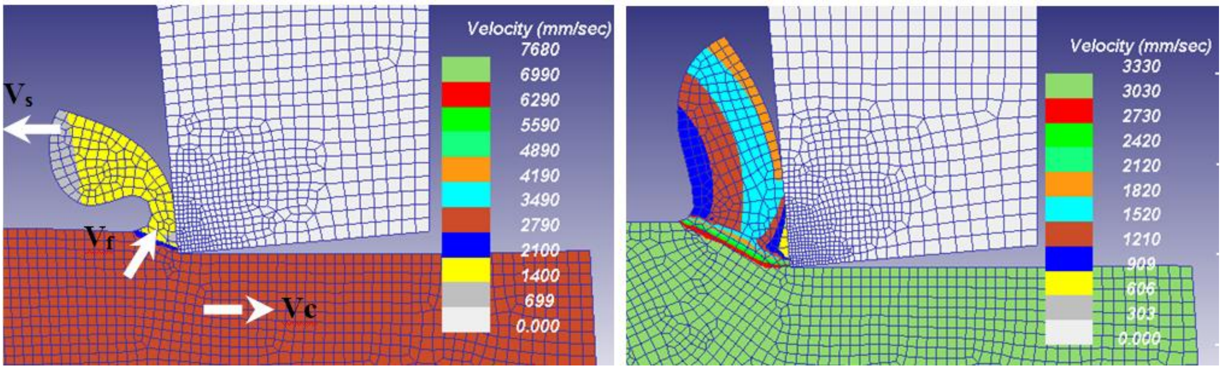

V_s
V_f
Vc
Velocity (mm/sec)
7680
6990
6290
5590
4890
4190
3490
2790
2100
1400
699
0.000
Velocity (mm/sec)
3330
3030
2730
2420
2120
1820
1520
1210
909
606
303
0.000

Figure 3.16: Velocity of cutting chips (V_c: Cutting velocity, V_f: Chip flow velocity, V_s: Shear velocity) during (a) surface defect machining and (b) ordinary HT process

Figure 3.16 presents a comparison of the cutting velocity in the chips obtained from the simulation in both cases. A very high chip flow velocity near the tool-chip interface (2 times higher than the cutting speed) is visible in the case of the SDM method. This is quite plausible, due to the thinning of the cross-section and the breaking of cutting chips; this is also observed experimentally, as is demonstrated further in the next chapter. The small segmented and broken chips are relatively easier to deform in comparison to the long continuous and serrated chips obtained through the conventional HT process. This suggests that the reduced cutting forces are essentially an outcome of this effect.

3.7 Summary

This chapter has detailed the development of a new method named "surface defect machining" and described several aspects and salient features of this method, using the finite element simulation method. The simulation results were validated by published experimental data and a good correlation was obtained. According to results of the theoretical analysis, the following conclusions can be drawn:

1. Surface defects generated on the workpiece allow easy shearing of the material while resulting in simultaneous breaking of the cutting chips into smaller segments. This is in addition to other favourable outcomes, such as reduced cutting forces and reduced shear plane angle.
2. A reduced shear plane angle provides a better machining action and is known to be influenced by varying the cutting tool rake angle or the workpiece hardness. The SDM method is thus found to be capable of reducing the shear plane angle, another advantageous feature of the proposed machining method.
3. During SDM, the machining stresses concentrated in the shear zone cause a reduction in the residual stresses on the machined surface. This provides a product which has good surface integrity compared to that obtained using conventional hard turning.
4. While SDM provides reduced temperatures in the machining zone, a reduced tool-chip interface contact length is found to be responsible for both the low heat dissipation and a consequent gradual increase in the temperature at the cutting edge of tool tip. However, this is acceptable, since the temperature is well within the thermal stability range of CBN tools normally used in hard turning.
5. A high SDM chip flow velocity causes an increase in the cut chip thickness, which, in turn, provides a high strain rate, thus enabling better deformation of the workpiece in the machining zone.

CHAPTER 4 – Experimental study on the SDM approach

4.1 Introduction

The theoretical investigation in the preceding chapter gives very good results regarding SDM applied to hard turning. Therefore, an experimental trial to confirm the previous simulation finding is very important. This chapter aims to present experimental investigations on SDM. Understanding the behaviour of the workpiece material and its optimal cutting parameters is very important. Therefore, in an attempt to explore the versatility of the SDM method, a series of trials were carried out involving the use of randomly selected cutting parameters and eventually a multiple and a quintile regression model was developed to optimize the parameters.

4.2 Machining experiments

In this section, the basis of the experimental trials is explained by describing the workpiece materials, cutting inserts, cutting speed, feed rate and depth of cut. Essentially, the combination matrix of these three parameters is of critical importance in determining the outcome of the process. Proper selection of these three parameters is an essential step to make the process more accurate in terms of the machined quality of the component and other favourable outcomes. The values of these parameters are selected based on the reported technical and published research papers. The conventional hard turning trials were performed on a Mori-Seiki SL-25Y (4-axis) CNC lathe. The workpiece specimen used was AISI 4340 steel hardened up to 69 HRC through a heat treatment process. CBN cutting inserts (type CNMA 12 04 08 S-B) were procured from Warren Tooling Limited, UK, with a rake angle of 0°, clearance angle of 5° and a nose radius of 0.8 mm. Further details of the experiment are given in Table 4.1.

Table 4.1: Experimental parameters

S.NO.	Details	Values
1	Workpiece material	AISI 4340 steel hardened up to 69 HRC
2	Diameter of workpiece before turning	28.8 mm
3	Cutting tool specifications (ISO code)	CNMA 12 04 08 S-B

4	Tool nose radius (R)	0.8 mm
5	Tool rake and clearance angles	0° and 5°

Post-machining non-contact measurement of the surface roughness was carried out using a white light interferometer (Zygo NewView 5000) which is a non-contact measurement instrument. Unlike a Talysurf, it does not use mechanical contact to provide the surface topography, and hence there is no chance of any mechanical/chemical interaction between the workpiece and the apparatus. This approach ensured that the machined surface was free from any sort of damage for post-experiment inspection. Subsequent confirmation of the measurement was done through a Talysurf, after inspection through the interferometer. In the subsequent section, the outcomes of the experimental trials are presented and discussed.

4.2.1 Experimental design to obtain optimized machining parameters

Experimental trials using conventional turning were carried out under the machining conditions shown in Table 4.2, which became the key input to the optimization data. The average surface roughness obtained for the various combinations of tool feed rate (f), depth of cut (d), and cutting speed (V) is also shown in Table 4.2. It can be seen that the best value of the machined surface roughness obtained was 0.452 µm at a feed rate of 0.08 mm/rev, depth of cut of 0.2 mm, and cutting speed of 90 m/min.

Table 4.2: Experimental data obtained from the hard turning trials

V (mm/min)	F (mm/rev)	D (mm)	Ra (µm) Experimental
250	0.15	0.1	1.193
250	0.15	0.192	1.251
250	0.1	0.048	0.781
200	0.1	0.2344	0.772
200	0.1	0.045	0.77
200	0.09	0.0833	0.667
150	0.15	0.2778	1.384
150	0.08	0.1	0.502
150	0.1	0.1333	0.773

120	0.15	0.06	1.361
100	0.1	0.935	0.777
100	0.09	0.2	0.742
100	0.15	0.2	1.316
100	0.09	0.144	0.683
100	0.08	0.542	0.569
100	0.08	0.935	0.582
100	0.09	0.542	0.65
100	0.09	0.935	0.625
100	0.1	0.542	0.677
100	0.1	0.935	0.697
100	0.15	0.542	1.108
100	0.15	0.935	1.134
90	0.08	0.2	0.452
90	0.09	0.2	0.618
90	0.1	0.2	0.703
90	0.15	0.2	1.085
80	0.1	0.2025	0.8
80	0.08	0.2	0.590
80	0.09	0.2	0.678
80	0.1	0.2	0.669
80	0.15	0.2	1.134

4.3 Multiple regression model

First, multiple regression was applied to the data obtained from the experiment to predict the performance parameters of hard turning, as well as for the optimization of the process. In the simplest formulation, average surface roughness (Ra) is considered to be the function of three linear predictors: feed rate (f), depth of cut (d) and cutting speed (V), which was modelled for the ith experiment by assuming a linear function as follows:

$$Ra_i = \alpha + \beta_1 f_i + \beta_2 d_i + \beta_3 v_i + \varepsilon_i \tag{4.1}$$

Equation 4.1 defines a straight line. The parameter α is the constant or intercept, and represents the error of this model estimation. The parameters β_1, β_2, and β_3 represent the expected increment in the response Ra_i per unit change in f_i, d_i, v_i respectively. The linear model in equation 4.1 assumes that the three included variables are the most important determinants of machined surface roughness, and that the error ε_i is normally distributed and uncorrelated to the variables. However, there are steps that should be taken to achieve the surface roughness model. First, the data of the exponential Table 4.3 should be summarised and taken as input of the four normal equations shown in Table 4.4.

Table 4.3: summary of data exponential

Terms	Value	Terms	Value
$\sum f_i$	3.46	$\sum f_i^{\,2}$	0.398
$\sum d_i$	10.663	$\sum d_i^{\,2}$	6.269
$\sum v_i$	3970	$\sum v_i^{\,2}$	581900
$\sum Ra$	26.282	$\sum Ra^2$	23.864
$\sum f_i \times Ra$	3.065	$\sum f_i \times d_i$	1.135
$\sum d_i \times Ra$	8.448	$\sum f_i \times v_i$	439.1
$\sum v_i \times Ra$	3381.598	$\sum d_i \times v_i$	1150.305

Table 4.4: Four normal equations for the model are shown

	Ra		α		$f_i\beta_1$		$d_i\beta_2$		$v_i\beta_3$
1	$\sum Ra$	$=$	$n\alpha$	$+$	$\sum f_i\beta_1$	$+$	$\sum d_i\beta_2$	$+$	$\sum v_i\beta_3$
f_i	$\sum f_i Ra$	$=$	$\sum f_i\alpha$	$+$	$\sum f_i^2\beta_1$	$+$	$\sum f_i d_i\beta_2$	$+$	$\sum f_i v_i\beta_3$
d_i	$\sum d_i Ra$	$=$	$\sum d_i\alpha$	$+$	$\sum d_i f_i\beta_1$	$+$	$\sum d_i^2\beta_2$	$+$	$\sum d_i v_i\beta_3$
v_i	$\sum v_i Ra$	$=$	$\sum v_i\alpha$	$+$	$\sum v_i f_i\beta_1$	$+$	$\sum v_i d_i\beta_2$	$+$	$\sum v_i^2\beta_3$

Second, substituting these values into the normal equations yields the results shown here:

$$26.2816 = 33\alpha + 3.46\beta_1 + 10.6633\beta_2 + 3970\beta_3 \tag{4.2}$$

$$3.065163 = 3.46\alpha + 0.3976\beta_1 + 1.135087\beta_2 + 439.1\beta_3 \tag{4.3}$$

$$8.447919 = 10.6633\alpha + 1.135087\beta_1 + 6.26954\beta_2 + 1150.305\beta_3 \tag{4.4}$$

$$3381.598 = 3970\alpha + 439.1\beta_1 + 1150.305\beta_2 + 581900\beta_3 \tag{4.5}$$

Solving system of the four normal equations can be carried out by a 4x4 matrix system:

$$A = \begin{bmatrix} 33 & 3.46 & 10.6633 & 3970 \\ 3.46 & 0.3976 & 1.135087 & 439.1 \\ 10.6633 & 1.135087 & 6.26954 & 1150.305 \\ 3970 & 439.1 & 1150.305 & 581900 \end{bmatrix}$$

The product of $A^{-1}B$ is the solution of the unknown variables

$$A^{-1}B = \begin{bmatrix} 0.42435476\,4 & -2.42021 & -0.13723814 & -0.00079757\,6 \\ -2.42020826\,3 & 34.46202 & -0.59815755 & -0.00831067\,9 \\ -0.13723814 & -0.59816 & 0.38695651\,2 & 0.00062273\,3 \\ -0.00079757\,6 & -0.00831 & 0.00062273\,3 & 1.22001\text{E}-05 \end{bmatrix} \begin{bmatrix} 26.2816 \\ 3.065163 \\ 8.447919 \\ 3381.598 \end{bmatrix}$$

$$A^{-1}B = \begin{bmatrix} -0.279 \\ 9.455 \\ 0.0539 \\ 5.61\text{E}-05 \end{bmatrix}$$

Substituting these values in equation 4.1 yields:

$$Ra_i = -0.279 + 9.455 f_i + 0.0539 d_i + 5.61\times10^{-5} n_i \quad (4.6)$$

The regression results show that the model can explain 92.5% of variation in the data. The model is therefore a reasonable predictor of surface roughness only when there is no cross interaction between the variables concerned.

Equation (4.6) presupposes that the association between dependent variable Ra_i and the independent variables f_i,d_i,r_i is additive. However, the simultaneous influence of two independent variables (i.e. feed and depth of cut) on surface roughness may not be additive. For example, the impact of feed may depend on the depth of cut. Such an effect is known as an interaction effect, and these effects represent the combined effects of predictors on the dependent variable. In what follows, equation (4.7) is modified to include the interaction of each pair of independent variables, as well as the interaction of all three variables. The equation in (4.6) can be modified as follows:

$$Ra_i = \alpha + \beta_1 f_i + \beta_2 d_i + \beta_3 r_i + \beta_4 f_i * d_i + \beta_5 f_i \times r_i + \beta_6 r_i \times d_i + \beta_7 f_i \times r_i \times d_i + \varepsilon_i \quad (4.7)$$

Table 4.5: Multiple Regression models

Dependent Variable : Surface Roughness					
	Base Model	Interaction Models			
	A	B	C	D	E (better model)
Feed (β_1)	9.455	9.127	7.786	9.345	9.886
	(0.59)	(0.94)	(1.49)	(0.51)	(1.95)
Depth of Cut (β_2)	0.0539	-0.0452	0.0485	-0.271	0.414
	(0.06)	(0.21)	(0.05)	(0.08)	(0.31)
RPM (β_3)	5.61×10^{-5}	5.56×10^{-5}	-8.1×10^{-6}	-9.8×10^{-6}	-1.9×10^{-6}
	(2.6×10^{-5})	(2.5×10^{-5})	(9.6×10^{-5})	(2.2×10^{-5})	(2.2×10^{-5})
Feed × Depth of Cut (β_4)		0.892			-5.91
		(2.21)			(2.91)
Feed × RPM (β_5)			0.00116		-5.0×10^{-5}
			(0.00)		(0.00)
Depth of Cut × RPM (β_6)				0.000223	-0.00019
				(4.3×10^{-5})	(0.00)
Feed × Depth × RPM (β_7)					0.00335
					(0.00)
Constant	-0.279	-0.242	-0.0849	-0.164	-0.223
	(0.08)	(0.08)	(0.14)	(0.05)	(0.19)
Adjusted R^2	0.925	0.924	0.928	0.947	0.95
N	39	39	39	39	39

Values in parentheses indicate Robust Standard Errors of the coefficients

Equation (4.7) represents an extended model where the objective is to explore whether or not the simultaneous effects of the three predictor variables (in pairs and all three together) are significant. In Table 4.5, Models B, C, and D show the interaction effect one pair at a time, and model E shows the interaction effect of all three variables. Adjusted R-squares have been reported for all models – these adjust for the number of explanatory terms in a model (the adjusted R-square value increases only if the new term improves the model more than would be expected by chance). Model B shows that the coefficient of β4 is not significant. Model C shows that the coefficient of β5 is not significant. Hence, models B and C are not significant improvements over model A. However, model D shows that the coefficient of β6 is significant, and therefore it can be asserted that model D is a better model to predict surface roughness than model A. Finally, model E shows that the coefficient of β7 is significant at 99.99%, and therefore model E is also a better model to predict surface roughness. Since Model E can explain a larger variation of data than model D, Model E can therefore be chosen as the preferred model.

Overall, multiple regression results, along with the interaction terms, suggest that the following model (E) is a better predictor of data than model A of equation (4.6).

$$Ra_i = -0.223 + 9.886 f_i + 0.414 d_i - 1.93 \times 10^{-5} r_i - 5.91 f_i \times d_i - 5.02 \times 10^{-5} f_i \times r_i - 0.00188 r_i \times d_i + 0.00335 f_i \times r_i \times d_i \quad (4.8)$$

Equation (4.8) explains 95% of the variation in the data, and therefore is a very good fit with the experimental data.

Overall, Multiple regression analysis helps in identifying two models that can be used for predicting surface roughness. Model A in equation (4.6) is a simpler model, which can be used for quicker prediction of the surface roughness, and can explain 92.5% of variation in the experimental data. Model E in equation (4.8) is a more complex model, but can explain 95% of variation in the experimental data.

4.3.1 Comparison of Multiple Regression

In this section, Multiple Regression results are compared with each other to evaluate their effectiveness in predicting the value of surface roughness. Model A is (simplified multiple regression model), Model E is (complex multiple regression model). These values are correspondingly plotted in figure 4.1, and figure 4.2 to highlight the differences of each model with respect to experimental values.

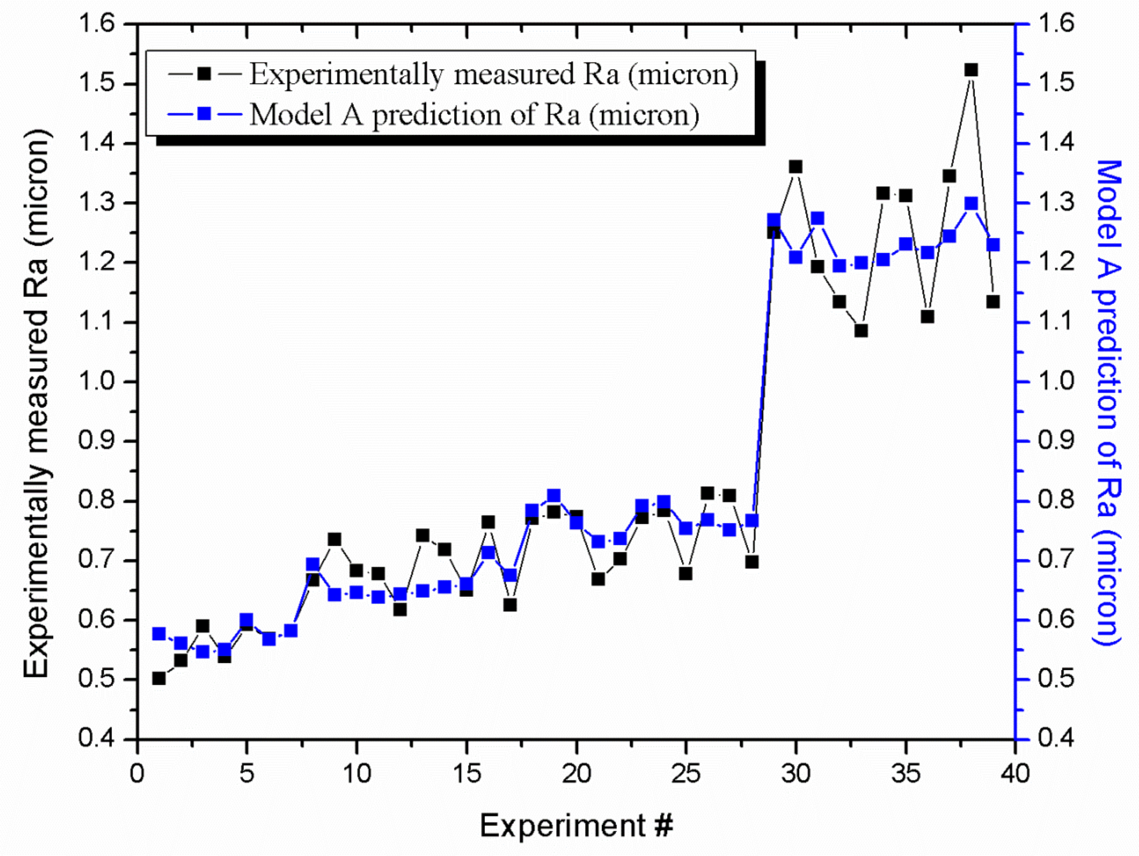

Figure 4.1: Comparison of experimental surface roughness with Multiple Regression Model A

From Figure 4.1, and Figure 4.2, it appears that all three proposed model were quite accurate in predicting the surface roughness, but more accurate only when the surface roughness was below an average value of 1 micron. As the surface roughness tends to get worsen beyond 1 micron, Model E becomes more accurate than Model A because it takes into consideration the pairing of the input variables.

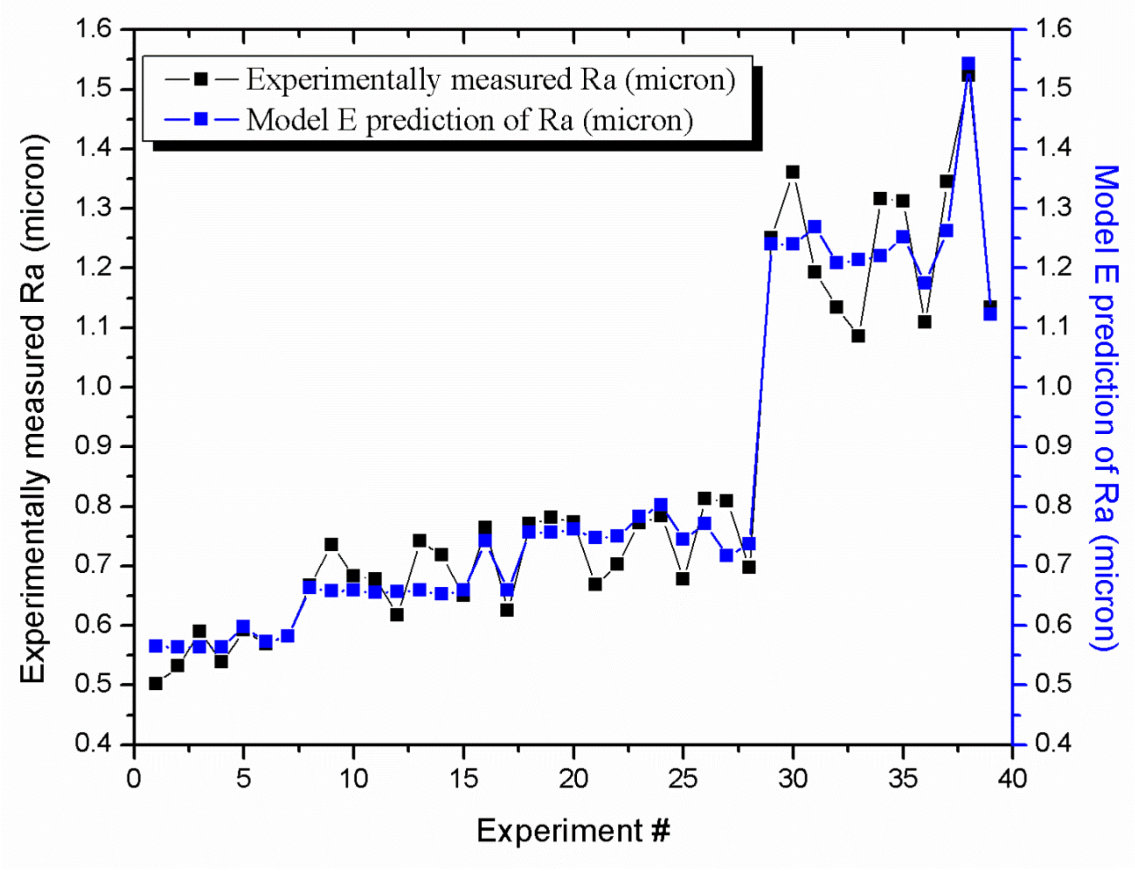

Figure 4.2: Comparison of experimental surface roughness with Multiple Regression Model E

Finally, the standard deviations of the differences of the predicted values from the two models versus the actual values from experiments are shown in Table 4.6.

Table 4.6: Standard deviation of the model with respect to experiments

	Model A	Model E
Standard deviation of experimental values vs. predicted values for the whole experiment	0.0740	0.0565
Standard deviation of experimental values vs. predicted values for Ra below 1 micron	0.0479	0.0447

It can be seen that both for the surface roughness measurement below 1 micron and for the whole set of experiments, Also Model E shows lower standard deviation than Model

A for the whole experiment, but for lower measure of the surface roughness either Model A or Model E can reliably be used.

4.4 Experimental examination of proposed SDM in comparison to conventional hard turning

In this section, the optimal cutting parameters obtained from the previous section have been adopted for experimental studies where both the SDM and conventional methods are used. Among several cutting conditions, the best surface roughness is obtained while using a cutting speed of 90 m/min, a feed rate of 0.08 m/rev and a depth of cut of 0.2 mm. The experimental plan is designed according to the following details:

- Using the same workpiece and cutting tool for both cases.
- Using the same cutting parameters obtained for both cases.
- Preparing the workpiece for SDM by using laser to generate holes on the surface of the workpiece.
- Attaching the cutting holders to the dynamometer and then installing them to the CNC lathe machine.
- Attaching the dynamometer to the data acquisition system and to the PC outside the CNC machine.
- Attaching the thermal camera to a box with optical lenses (the same as the optical lenses of the camera) for protection, and then attaching them to a suction cup to be mounted onto the CNC in a location that allows good measurement to take places.
- Attaching the camera to the PC outside the CNC lathe machine and monitoring the camera and taking a snapshot of the cutting operation instantaneously.
- Measuring the surface roughness for both cases.

4.4.1 Experimental Setup

In this work, the surface defects, in the form of holes on the top of workpiece, were generated using a Trumpf (CO_2) laser machine with a peak power of 2.7 kW. The dimensions of these holes are shown in Table 4.7. The experimental trials were carried out on a Mori-Seiki SL-25Y (4 axis) CNC lathe. A three-component Kistler dynamometer (type 9257BA) was mounted on the tool turret, through a customized fixture, to measure the cutting forces. A thermal camera (FLIR T425) was used to monitor the cutting temperature. The camera was fixed to the lathe using a suction mounted cup and was placed inside a box to protect its lens from the cutting chips. The whole thermal camera assembly was attached to the CNC machine, as shown in Figure 4.3. Two sets of machining trials were carried out in this study. The first set of cutting trials is by a normal hard turning method, while the workpiece with the generated surface defects was cut in the second set of the HT process, in which identical machining operational conditions were used.

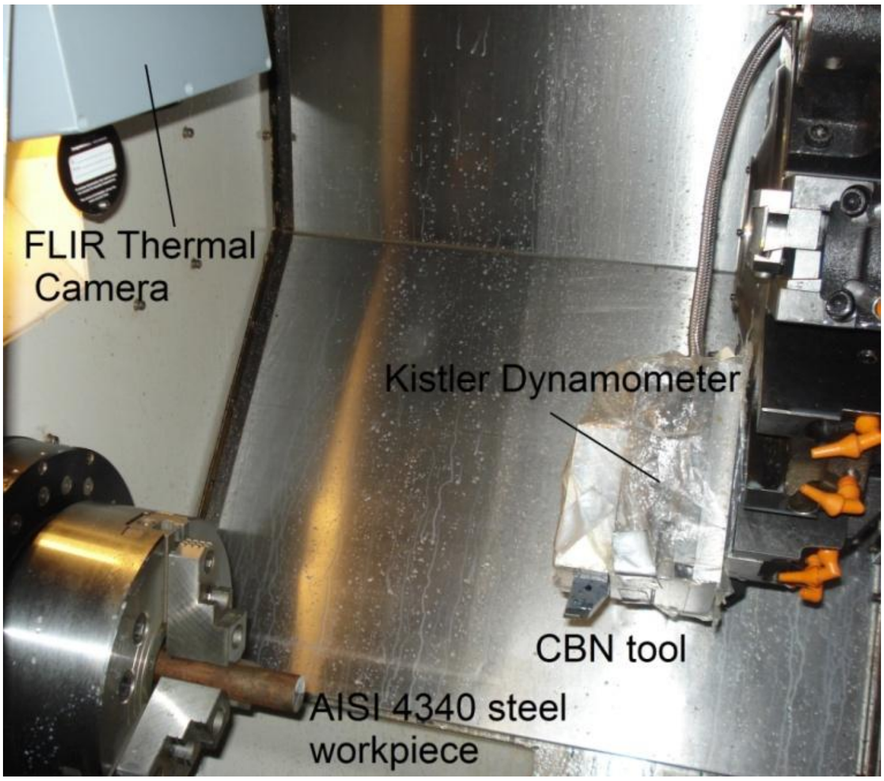

Figure 4.3: Experimental setup

Table 4.7: Experimental parameters

S.NO.	Details	Values
1	Workpiece Material	AISI 4340 steel hardened up to 69 HRC
2	Diameter of workpiece before turning	28.8 mm
3	Cutting tool	CNMA 12 04 08 S-B

	specifications (ISO code)	
4	Tool Nose radius	0.8 mm
5	Tool rake and clearance angles	0° and 5°
6	Feed rate	0.08 mm/rev
7	Depth of cut	0.2 mm
8	Cutting speed	90 m/min
9	Coolant	None
10	Diameter and depth of holes	0.9 mm and 0.17 mm respectively with 6.3 mm interspacing between each hole in the cutting direction and 10mm in the feed direction

4.4.2 Experimental parts assembly

The theoretical study shows a very good result of a promising technique (SDM) that never been used in hard turning elsewhere, therefore, conducting experimental trials was an essential task in order to approve this method. Certainly, experimental work usually faces many challenges, and these challenges have to be solved out in order to put the analysis of the operation on a quantitative basis. In these experiments, overcoming many obstacles was achieved even though the tools and equipment provided were limited to the budget provided and their availability. However, the number of observations that can be made during the cutting process is rather limited; therefore, the output of the experiments should be concentrated towards the most important results such as the determination of cutting forces components and workpiece temperature.

4.4.2.1 Material selection

The workpiece materials and cutting tool insert needs to be selected carefully before the cutting performance. The workpiece should be selected based on some important criteria to be very effective in the cutting performance and to obtain reliable results. Some of these criteria for selecting the workpiece material are listed below:

- The material should be very commonly used in the market.

- It should also have been used in many previous research studies, so the data can be utilized for comparison to this work, if needed.

AISI 4340 steel is one of the most commonly used materials and it has been used widely in many research areas concerning hard turning. The first step for the workpiece used in hard turning is the heat treatment, in order to be ready for machining trials for conventional hard turning.

However, the cutting insert also needs to be selected carefully to obtain satisfactory results. Cubic boron nitride CBN is well known cutting tool material for carrying out the hard turning process. The CBN geometry and types were selected based on the previous research results and expert advice in the field. The details of the cutting inserts and its composition can be referred to its funder for more information. The geometry of the cutting inserts and other information are summarized in Table 4.7.

4.4.2.2 Laser ablation

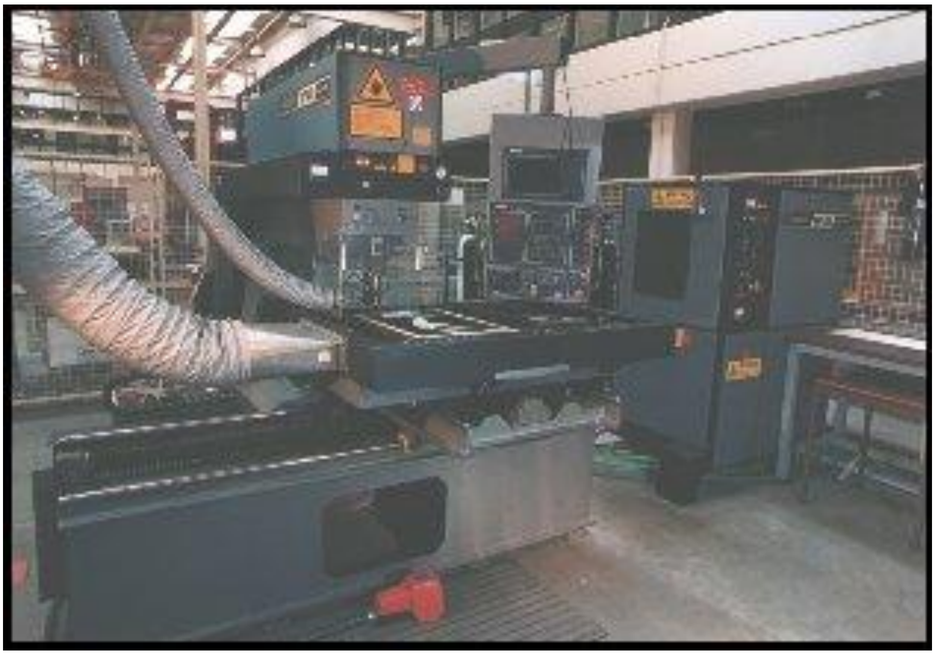

Figure 4.4: Trumpf CO_2 laser machining centre

The surface defects in the form of holes on the top of workpiece were generated by using a Trumpf (CO_2) laser machine shown in Figure 4.4. The hole diameter was nearly 0.92 mm on the top surface and the depth of hole 0.17 mm with 6.3 mm interspacing between each hole in the cutting direction and 10 mm in the feed direction. A snapshot of the workpiece with laser holes is shown in Figure 4.5.

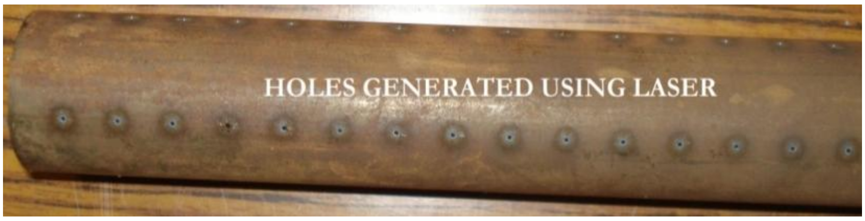
HOLES GENERATED USING LASER

Figure 4.5: Workpiece with holes made by laser

Figure 4.6 is a SEM image of the cross-section of one laser machined hole. The extent of surface damage induced by the laser power was observed to be minimal and it was ensured that this depth is covered by the programmed depth of cut. So it was not of concern. This damage depth is about 15 µm and is not of concern in practice either, because such damage can be recovered during the recrystallization process during the heat treatment process, which is why SDM is particularly useful for machining hard steels without worrying about the depth of damage induced by the laser.

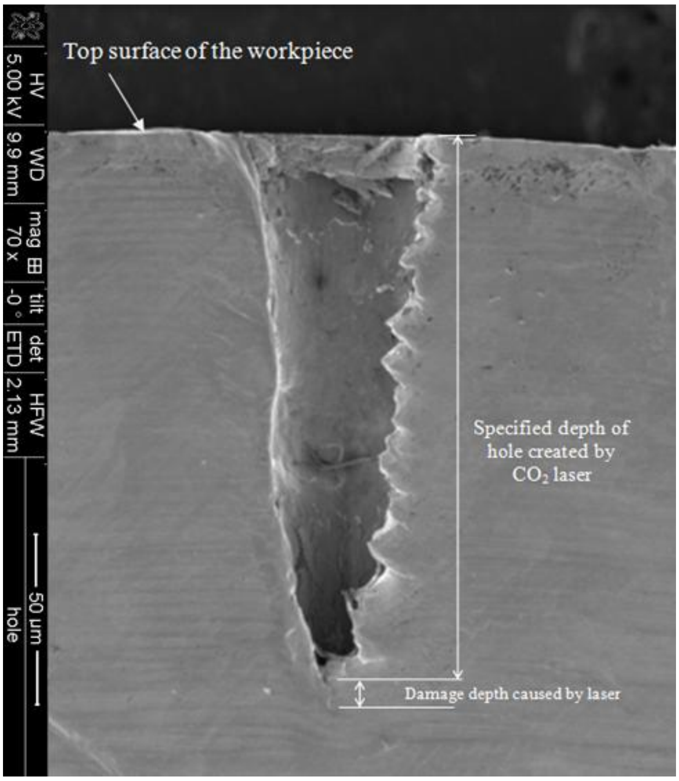
Top surface of the workpiece
Specified depth of hole created by CO₂ laser
Damage depth caused by laser
HV 5.00 kV
WD 9.9 mm
mag 70 x
tilt -0 °
det ETD
HFW 2.13 mm
50 µm
hole

Figure 4.6: SEM image of the cross-section of the surface defect created by the CO_2 laser, highlighting the damage depth caused by laser

4.4.2.3 Dynamometer assembly

One of the obstacles during the experimental work was the attachment of a three-component Kistler dynamometer (type 9257BA) to the CNC lathe machine. The size of the dynamometers is larger than the space of the turret lathe and therefore, a customized fixture, shown in Figure 4.6, was used to fix the dynamometer to the CNC lathe. The overall picture of the whole assembly mounted on the CNC lathe is shown in the Figure 4.7.

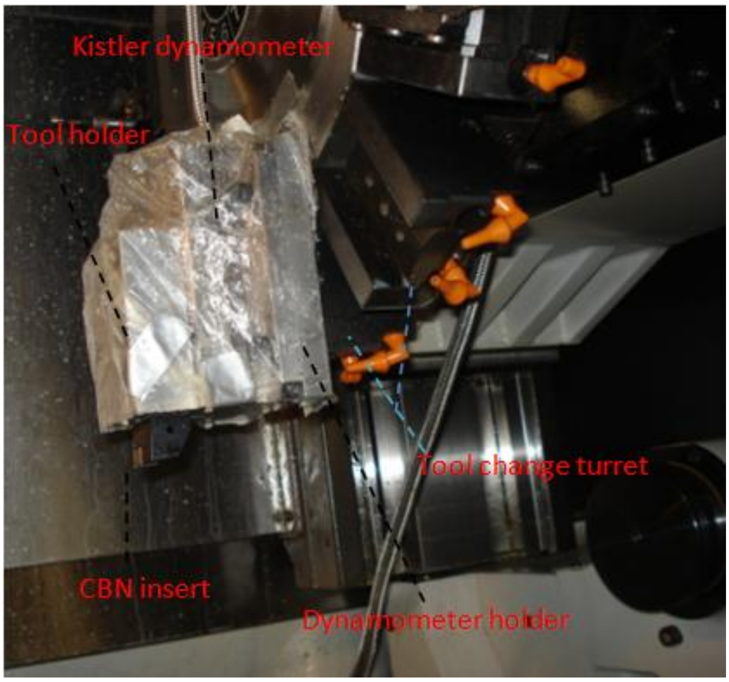

Figure 4.7: Dynamometer assembly via special fixture to the tool holder

4.4.2.4 Thermal camera assembly

The use of the thermal camera for measuring workpiece temperature during machining was believed to be more robust than using the thermocouple. The thermocouple insulation is very difficult and sophisticated to achieve, so a thermal camera can be a good choice. A FLIR T425 thermal camera was used for this study and the challenge lay in the installation of the camera inside the CNC lathe machine, to ensure the safety of the lens of the camera from any possible damage arising due to the randomly flowing cutting chips. A box was designed with an optical lens (of the same material as the thermal camera lens) attached to it, so that the camera was installed safely inside the box when the machining was running. Then the box was attached to a suction cup which could be attached to the CNC lathe very easily and the position of the whole thing could be controlled, as can be seen in Figure 4.8, below.

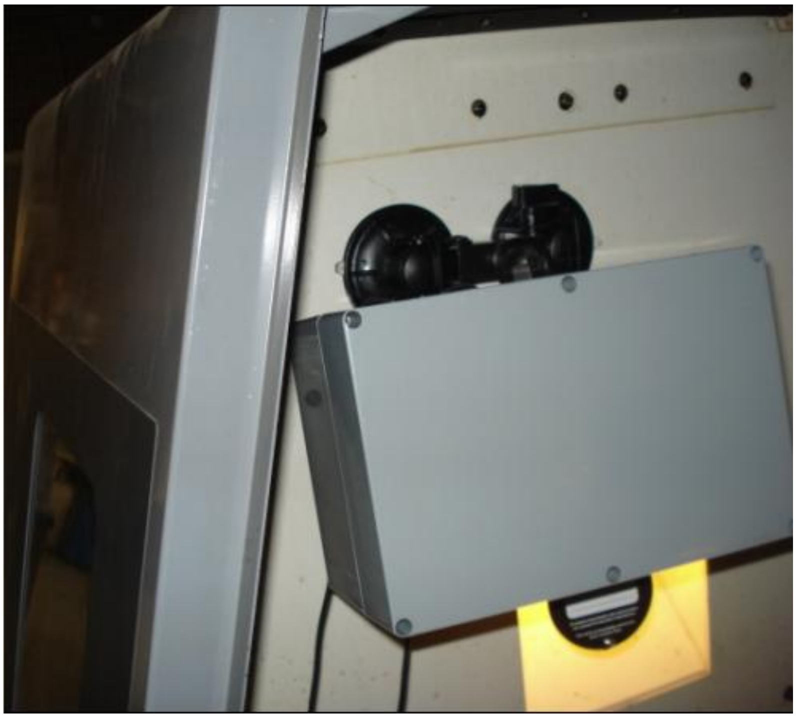

Figure 4.8: Camera positioned inside the box to be protected from the chip, meanwhile, the suction mounted cup is used to fix both the camera and the box and the whole assembly is attached to the CNC wall

4.5 Data collection by the dynamometer

The forces and the temperatures of the workpiece were collected instantaneously by two computers attached to the dynamometers and another one for the thermal camera, as shown in Figure 4.9. Regardless of whether executing the conventional process of hard turning or the proposed method of machining SDM, cutting forces have remained one of the most common machining outcomes used to characterize the performance of the process (Tutunea-Fatan et al., 2011). A comparison of the measured cutting forces i.e. cutting forces (F_c), feed forces (F_f) and principal cutting force (F_z) between the normal hard turning process and proposed machining method is shown in Figure 4.10.

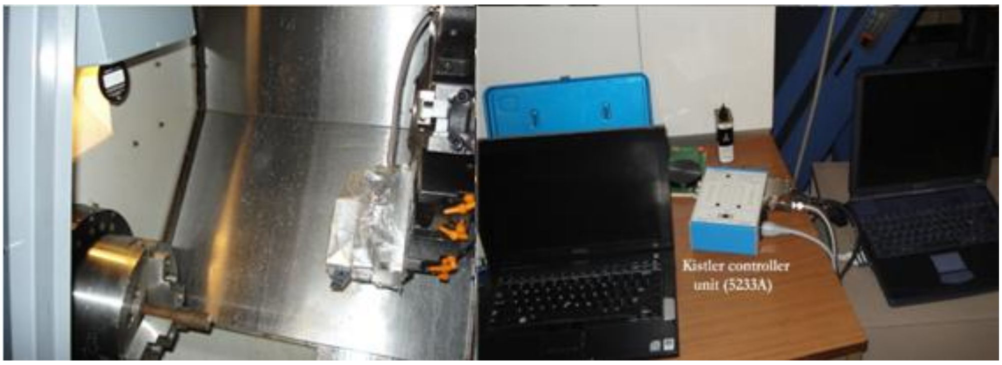

Figure 4.9: Experimental assembly

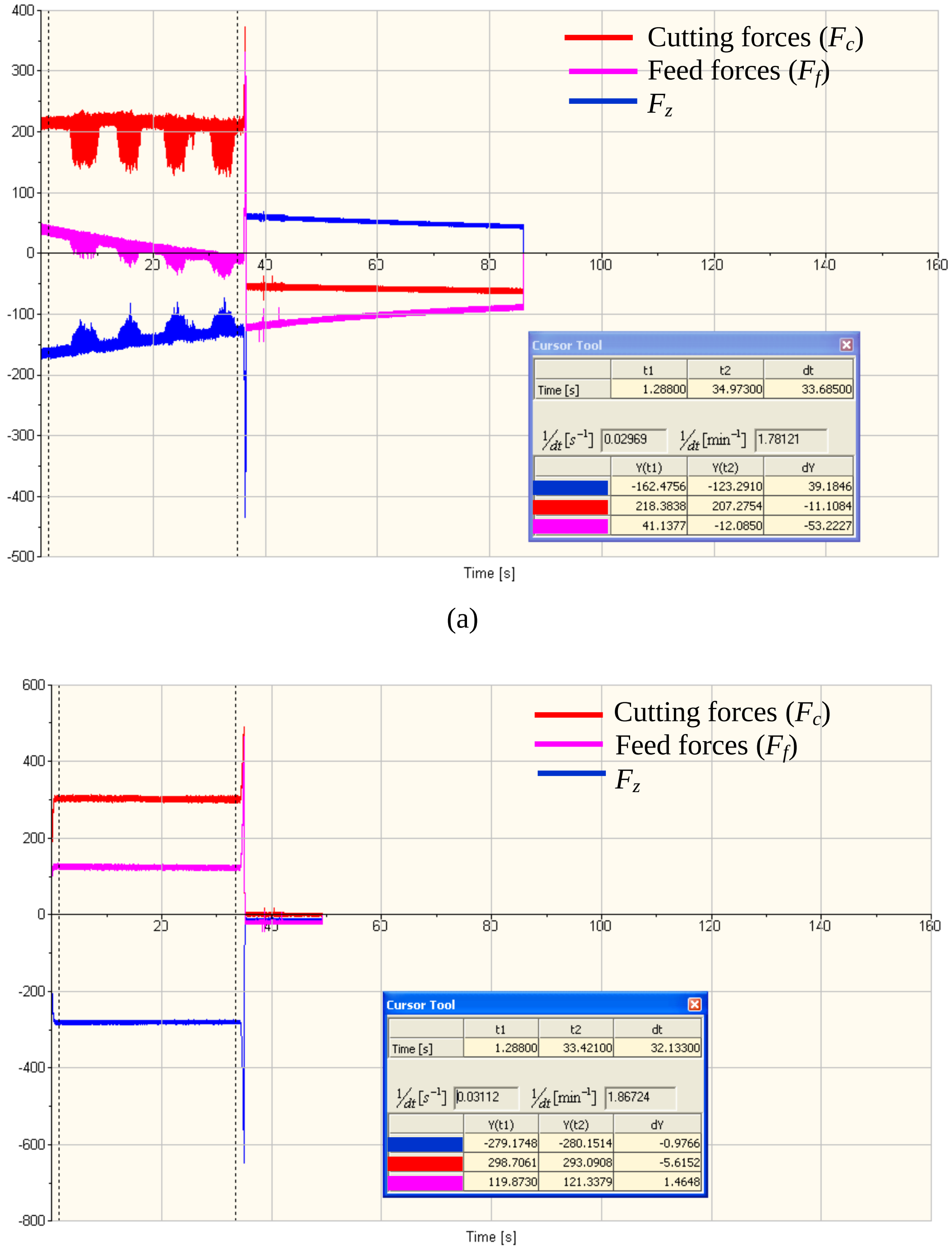

	t1	t2	dt
Time [s]	1.28800	34.97300	33.68500

$^1/_{dt}[s^{-1}]$ 0.02969 $^1/_{dt}[\min^{-1}]$ 1.78121

	Y(t1)	Y(t2)	dY
🟦	-162.4756	-123.2910	39.1846
🟥	218.3838	207.2754	-11.1084
🟪	41.1377	-12.0850	-53.2227

(a)

	t1	t2	dt
Time [s]	1.28800	33.42100	32.13300

$^1/_{dt}[s^{-1}]$ 0.03112 $^1/_{dt}[\min^{-1}]$ 1.86724

	Y(t1)	Y(t2)	dY
🟦	-279.1748	-280.1514	-0.9766
🟥	298.7061	293.0908	-5.6152
🟪	119.8730	121.3379	1.4648

(b)

Figure 4.10: Cutting forces (a) proposed SDM (b) normal hard turning process

It can be seen that the cutting tool experiences intermittent relaxation, which is reflected by the fluctuations of cutting forces when the holes are encountered by the cutting tool. It is anticipated that due to the presence of surface defects or the surface discontinuity, the shearing of the material will become easier. This is because of the fact that the same continuous matter will require more energy for shearing compared to the same discontinuous matter. For this reason, a cutting tool will face lower cutting resistance during the proposed machining method. Earlier, Komanduri et al. (1982) postulated that a reduction in the total length of the shear plane provides this benefit. It was also highlighted earlier that, normally, a high shear plane angle is often observed while machining hard materials (Nakayama et al., 1988), such as in hard turning. It is found that the surface defects actually causes a decrease in the shear plane angle (Bin Rashid et al., 2013). A decrease in the value of the shear plane angle for the same machining parameters signifies the dominance of forces in the feed direction over the forces in the cutting direction i.e. a more efficient cutting action of the cutting tool for the same amount of input energy. This seems to be the plausible reason that the provision of surface defects is found to be responsible for a better machining action and reduced temperature in the machining zone, as shown in section 4.6.

4.6 Temperature in the cutting zone and chip morphology

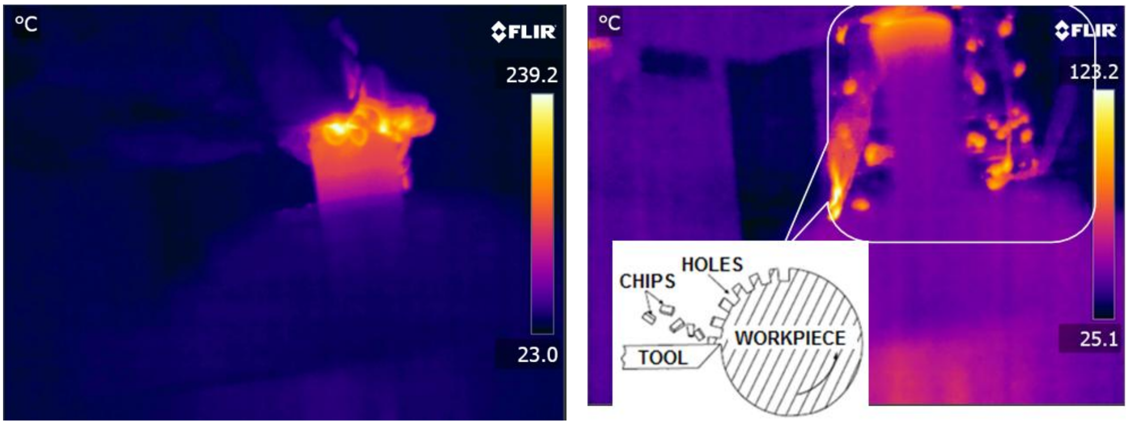

Figure 4.11: Temperatures in the cutting zone (a) conventional HT process (b) SDM

A comparison of the local temperature in the cutting zone, captured through the thermal camera, is shown in Figure 4.11. During the normal hard turning process, the cutting chips appeared to be much hotter, because the local temperature in the cutting zone approached 512 K. In contrast, a reduced temperature of around 400 K was observed during the proposed SDM method. This temperature difference very well explains the positive outcome of the machining, as the reduced temperature is beneficial for both the cutting tool and the workpiece. Besides the reduced cutting temperature, there is also a significant difference in the morphology of the cutting chips. It is noted here that the earlier papers reported that the thermal softening mechanism is responsible for the saw-toothed chip formation mechanism in a hard turning operation. In the current work, however, a lowered temperature in the proposed machining method was observed which suggests that the thermal softening does not alone govern the chip formation mechanism, rather it is the shearing process responsible for the machining action. Shaw (2004) provided further experimental evidence to suggest that the cutting chips are serrated in a conventional hard turning process, which was attributed to the mechanism of concentrated shear. In other words, the cutting chips appear to be continuous in a conventional HT method, as evident from the former part of Figure 4.11a. In contrast, the cutting chips are discontinuous, segmented and are broken into the small pieces, using the SDM method, as shown schematically in Figure 4.11b. Thus, the proposed method also serves the purpose of chip breaker, which inherently favours the SDM process.

4.7 Surface roughness

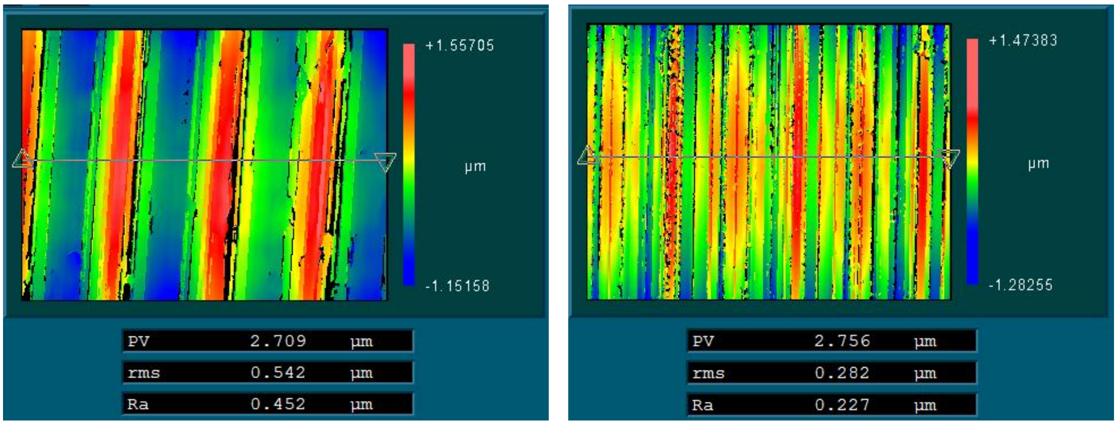

PV 2.709 µm
rms 0.542 µm
Ra 0.452 µm

PV 2.756 µm
rms 0.282 µm
Ra 0.227 µm

Figure 4.12: Surface roughness using (a) conventional HT process (b) proposed method

Figure 4.12 shows a comparison of the surface roughness obtained after machining trials through the normal HT and proposed SDM processes respectively. It can be seen that an average surface roughness (Ra) value of 0.452 µm was obtained using the conventional HT approach. This measurement was found to be in accord with the previously reported experimental results (Grzesik et al., 2007; Poulachon et al., 2001), using similar machining conditions. A theoretical evaluation of the surface roughness based on equation 4.9, specifically meant to calculate theoretical roughness for a CBN cutting insert (SECO, 2003), reveals a closer value to this experimental value (the experimental value is, however, larger than the theoretical estimate most likely due to various sources such as spindle error motions, vibrations and chatter).

$$Ra = \frac{50f^2}{r} = \frac{50 \times 0.08 \times 0.08}{0.8} = 0.4\,\mu m \qquad (4.9)$$

However, compared to the conventional HT method, an improved surface roughness (Ra) value of 0.227 µm was obtained using the proposed machining method, which is believed to be a significant improvement from the commercial perspective, besides an important benchmark for the HT process. Table 4.8 summarizes a comparison of the average surface roughness obtained under the same cutting conditions theoretically and experimentally. The in-depth understanding of the reason underlying the improved surface roughness is not apparent from the previous experimental study. It has been well recognized that the time scales over which machining trials are done are too long to permit any direct observation of the processes occurring at the atomic level.

Table 4.8: A comparison of the average surface roughness

Method used	Average surface roughness Ra (µm)
Regression model A for AISI 4340 equation (4.6)	0.53
Regression model E for AISI 4340 equation (4.8)	0.428
Theoretical roughness for a CBN cutting insert equation (4.9)	0.4
Conventional HT measured experimentally	0.452
SDM measured experimentally	0.227

4.8 Summary

In this chapter a method to improve the attainable surface roughness in the hard turning process has been comprehensively examined through a series of experiments. This method relies on the generation of surface defects on the top of the workpiece. Besides reduced temperature in the cutting zone and reduced average cutting forces, a significant improvement in the surface roughness was observed by using this approach. The advantage of using the suggested method in the domain of hard turning is the fact that the surface defects inherently cause breaking of the chips, which, in turn, serves the purpose of a chip breaker and is hence favourable. Moreover, any sub-surface damage induced by the primary machining operation, like laser ablation, will be recovered during the heat treatment of the ferrous workpiece. The experimental work on surface defect machining of the initial trials is found to be promising. An improved average surface roughness (Ra) value of 0.227 µm in comparison to 0.452 µm from conventional machining on AISI 4340 steel (hardened upto 69 HRC) with a CBN tool was obtained experimentally. One of the most contrasting features of SDM is that both the combination of cutting and rough polishing actions is found to be responsible for the improved surface roughness. In the next chapter the significant cutting parameters are identified and more experimental work will be designed. This will guide the direction of the work in this research and highlight the differences between conventional hard turning and SDM method.

CHAPTER 5 – Optimization of parametric design

5.1 Introduction

Identifying the most effective machining parameter is very important in the study of the influence of machining conditions, as it will greatly save time and cost incurred if all parameters are included. As reported from the literature earlier in this thesis, there were many different opinions on the most significant cutting parameter for surface roughness obtained by hard turning. Therefore, finding the true, most significant parameter experimentally is essential for better understanding the process. It will also help to focus on the influence of a particular parameter on both conventional hard turning and SDM method. Also, since the developments are running in parallel with the technological developments in cutting tool and machine tool technology, the attainable machinable limits are being constantly pushed forward. Therefore, it is very important to examine the current attainable limit of hard turning on a CNC turret lathe en route to that objective. The evaluation of the finished trials based on the quality of machining is normally judged by a tangible examination of surface roughness, and in addition, surface integrity also dictates the functionality and service life of a component under hostile environments and is hence important. In this study, an optimization method will be applied to a set of judiciously chosen parameters by introducing the Taguchi method for identifying the optimal cutting parameters for AISI 4340 steel which was hardened up to 69 HRC. One of the foremost benchmarks set for hard turning was to attain a machined surface finish of 0.1μm Ra, which was previously attainable only from grinding. Therefore, a practical knowledge for determining the proper machining parameters to reach a specified level of surface roughness is essential.

5.2 Taguchi method

The Design of Experiment (DOE) using Taguchi's approach can be used to evaluate the effect of control parameters for parameter optimization. Taguchi's approach allows the study of the whole parameter space with a limited number of experiments, as long as they are carried out in a planned orthogonal array (Ross, 1995). In addition, since only a limited number of experiments are needed, the methodology helps reduce the variability of the response variable, and is therefore an important tool for improving the productivity of the experiments. Taguchi's approach to design of experiments involves the following steps (Taguchi and Konishi, 1987):

1. Select the response variable to be optimized
2. Identify the input variables that affect the response
3. Choose the levels of these factors
4. Select the appropriate orthogonal array
5. Conduct experiments (randomize the experiments so that there is no systematic bias)
6. Analyze the results by signal-to-noise (S/N) ratio or by using analysis of variance (ANOVA)
7. Determine the optimal process parameters.

The sequence of experiments with the combination of parameters and levels is determined by an orthogonal array that determines the number of trials to be performed, ensuring that all levels of all factors are tested in an equal measure. The appropriate array is selected according to the number of factors and levels. For example, consider the problem of optimizing the surface roughness for given feed (*f*), depth of cut (*d*), and (*v*) of cutting speed to improve the surface roughness (*Ra*). If it is decided to run experiments at four different levels for these three factors, then a full factorial search would require a total of $4^3 = 64$ runs. In contrast, Taguchi proposes using an orthogonal array to determine the effects of individual process parameters. For example, an appropriate orthogonal array for such as scenario (e.g. the L'16 array) comprises 16 trials which test 4 levels of up to 5 different experimental factors. Thus, the L'16 orthogonal array only requires 16 runs to complete the optimization of four levels of three factors.

The selection of an appropriate orthogonal array is based on total degree of freedom (DOF) which is computed as:

$$\text{DOF} = (L-1) \text{ for each factor} + (L-1) \times (L-1) \text{ for each interaction} + 1 \qquad (5.1)$$

Taguchi proposes that the parameter design must aim to determine the optimal levels of the control factors such that the response variable is robust to the variability caused by the noise factors. He proposes that there are three specific goals in an experiment:

1. Minimize the response (Smaller is better)
2. Maximize the response (Larger is better)
3. Achieve a desired target value.

For achieving each of these goals, Taguchi defined signal-to-noise (S/N) ratios, which measure the variation present in the response data. The maximization of S/N ratio simultaneously optimizes the quality characteristic and minimizes the effect of noise factors. For each trial in the selected orthogonal array, if the performance measure (*y*) is repeated *n* times, then S/N ratio can be computed as follows:

1. Smaller-the-better :

$$Y = -10\log_{10} + \left[\frac{1}{n}\sum y_i^2\right] dB, \tag{5.2}$$

2. Larger-the-better-:

$$Y = -10\log_{10} + \left[\frac{1}{n}\sum y_i^{-2}\right]^{-2} dB, \tag{5.3}$$

3. Achieving a target:

$$Y = -10\log\left(\frac{s^2}{y^2}\right) \tag{5.4}$$

where s denotes the sample variance. It may be noted that *Y* in the above equation denotes the S/N ratio and not the response parameter.

In summary, it was realized that most of the research studies used almost similar or the same cutting conditions, by neglecting the ongoing developments on the machine tool and cutting tool, and thereby discarding the wisdom of having chosen tighter limits of feed rate. Consequently, the attainable surface roughness achieved did not meet the desired expectations. This motivates the current experimental study.

5.3 Experimental details

In this experimental study, the first step is to develop an orthogonal array by choosing a set of judiciously for cutting parameters. The orthogonal array is shown in Table 5.2. Unlike the previously published literature a much lower feed rate of upto 0.02 mm/rev was chosen in this work for the experimental trials. For the purpose of Taguchi analysis, this study neglects the interactions between the cutting parameters. Consequently, an L_{16} array with three columns and 16 rows came as inputs for the experiments. In Table 5.2, each cutting parameter is assigned to a column with 16 different combinations of feed rates, cutting speeds and depth of cuts.

Table 5.1: Cutting parameters and their levels

Cutting parameters	Unit	Level 1	Level 2	Level 3	Level 4
Feed rate	mm/rev	0.02	0.06	0.1	0.15
Cutting speed	m/min	90	150	200	250
Depth of cut	mm	0.1	0.2	0.3	0.4

Table 5.2: Orthogonal array

Experiment Number	**Feed rate (mm/rev)**	**Cutting speed (m/min)**	**Depth of cut (mm)**	**CBN cutting tool used**
1	0.02	90	0.1	Cutting tool # 1
2	0.02	150	0.2	
3	0.02	200	0.3	
4	0.02	250	0.4	
5	0.06	90	0.2	Cutting tool # 2
6	0.06	150	0.1	
7	0.06	200	0.4	
8	0.06	250	0.3	
9	0.1	90	0.3	Cutting tool # 3
10	0.1	150	0.4	
11	0.1	200	0.1	
12	0.1	250	0.2	
13	0.15	90	0.4	Cutting tool # 4
14	0.15	150	0.3	
15	0.15	200	0.2	
16	0.15	250	0.1	

Thus, these 16 cutting trials enable us to study the entire parameter space using the L_{16} orthogonal array. After designing the experimental array, the next step is to perform the cutting trials. In table 5.2, column 4 is of particular interest. Column 4 is added to this array to add some more value to the experimental results. The interest is to find out economically whether a lower feed rate or a high feed rate is good for tool life. Therefore, four cutting inserts were chosen for the trials instead of sixteen individual cutting inserts. Each cutting insert was used to cut the same cutting length of 80 mm but at four different feed rates as shown in table 5.2.

The machining trials were performed on a Mori-Seiki SL-25Y (4-axis) CNC lathe. The workpiece specimen used was AISI 4340 steel that was hardened up to 69 HRC through a heat treatment process. The cutting tool used was a CBN cutting insert (type CNMA 12 04 08 S-B) purchased from Warren Tooling Limited, UK. The cutting tool had a rake angle of 0°, clearance angle of 5°, and a nose radius of 0.8 mm. Further details of the experiments are provided in Table 5.3.

Table 5.3: Experimental parameters

S.NO.	Details	Values
1	Workpiece material	AISI 4340 steel hardened up to 69 HRC
2	Diameter of workpiece before turning	28.8 mm
3	Cutting tool specifications (ISO code)	CNMA 12 04 08 S-B
4	Tool nose radius (R)	0.8 mm
5	Tool rake and clearance angles	0° and 5°
6	Length of cut	20 mm for each test 1 insert was thus used for a total length of 20×4 = 80 mm length of cut

Thus, the experimental trials will reveal two tangible outcomes i.e. machined surface roughness and the worn CBN tips (which will be used to machine at the different feed rate but the same cutting length). The measurement of the machined surface roughness will be done through a Form Talysurf while a high magnification scanning electron microscope (SEM) (FIB-FEI Quanta 3D FEG) will be used to measure the flank wear length (V_b) to estimate tool wear. In the subsequent section, the outcome of the machining trials is presented and discussed.

5.4 Signal-to-noise (S/N) ratio analysis

Taguchi recommends the use of signal-to-noise (S/N) ratio to measure the quality characteristics deviating from the desired values. The term signal (S) in the S/N ratio represents the desirable value (mean) and the term noise (N) represents the undesirable value (S.D.) for the output characteristic. Therefore, the S/N ratio is actually the ratio of the mean to the S.D. Consequently, a greater S/N ratio corresponds to better quality and hence a greater S/N ratio signifies better parameters. In general there are three categories of quality characteristics which are the-lower-the-better, the-higher-the-better and the-nominal-the-better. Depending on the objective of the task, the characteristic may be chosen accordingly: for example, while evaluating tool life, one may chose the-higher-the-better criterion and contrarily, while evaluating surface roughness, the-lower-the-better criterion is better.

Accordingly, as per the lower-the-better criterion, S/N ratio η is defined as:

$$\eta = -10 \log (\text{M.S.D.}) \qquad (5.5)$$

where $M.S.D. = Si^2$ is the mean-square deviation for the output. Si is characteristic as the value of surface roughness for the ith observation. Table 5.4 shows the experimental results of surface roughness and S/N ratio calculated by the above equation.

Table 5.4: Experimental results for surface roughness and S/N ratio

Experiment number	**Feed Rate (mm/rev)**	**Cutting speed (m/min)**	**Depth of Cut (mm)**	**Measured experimental surface roughness (micron) (Si)**	**Si^2 or M.S.D.**	**S/N ratio (dB)**
Level	**A**	**B**	**C**			
1	0.02	90	0.1	0.0428	0.0018	27.37
2	0.02	150	0.2	0.0478	0.0023	26.41
3	0.02	200	0.3	0.0527	0.0028	25.56
4	0.02	250	0.4	0.0497	0.0025	26.07
5	0.06	90	0.2	0.3281	0.1076	9.68
6	0.06	150	0.1	0.2883	0.0831	10.80
7	0.06	200	0.4	0.2172	0.0472	13.26
8	0.06	250	0.3	0.2065	0.0426	13.70
9	0.1	90	0.3	0.5612	0.3149	5.02
10	0.1	150	0.4	0.6005	0.3606	4.43
11	0.1	200	0.1	0.6351	0.4034	3.94
12	0.1	250	0.2	0.6449	0.4159	3.81
13	0.15	90	0.4	1.0345	1.0702	-0.29
14	0.15	150	0.3	1.0846	1.1764	-0.71

15	0.15	200	0.2	1.1135	1.2399	-0.93
16	0.15	250	0.1	1.1384	1.2960	-1.13
	Total mean					**10.44**

The effect of each cutting parameter at different levels can be calculated by averaging the S/N ratio. For example, the mean S/N ratio for cutting speed at levels 1, 2, 3 and 4 can be computed by averaging the S/N ratio for the experiments (1, 5, 9, 13 for level 1), (2, 6, 10, 14 for level 2), (3, 7, 11, 15 for level 3), and (4, 8, 12, 16 for level 4). For the other cutting parameters, the mean S/N can be calculated in similar way. Table 5.5 shows the summary of the mean S/N ratio for each cutting parameters.

Table 5.5: Response table mean S/N ratio for surface roughness factor

Symbol		**Level 1** (Expt. 1, 2, 3 and 4)	**Level 2** (Expt. 5, 6, 7 and 8)	**Level 3** (Expt. 9, 10, 11, 12)	**Level 4** (Expt. 13, 14, 15 and 16)	**Max-Min**
A	**Feed rate (mm/rev)**	**0.02**	**0.06**	**0.1**	**0.15**	
	Mean S/N ratio	**26.35480665**	**11.86184625**	**4.300174181**	**-0.764926018**	**27.11973267**
		Level 1 (Expt. 1, 5, 9 and 13)	Level 2 (Expt. 2, 6, 10 and 14)	Level 3 (Expt. 3, 7, 11, 15)	Level 4 (Expt. 4, 8, 12 and 16)	
B	**Cutting speed (m/min)**	**90**	**150**	**200**	**250**	
	Mean S/N ratio	**10.44350922**	**10.23**	**10.46**	**10.61**	**0.38**
		Level 1 (Expt. 1, 6, 11 and 16)	Level 2 (Expt. 2, 5, 12 and 15)	Level 3 (Expt. 3, 8, 9, 14)	Level 4 (Expt. 4, 7, 10 and 13)	
C	**Depth of cut (mm)**	**0.1**	**0.2**	**0.3**	**0.4**	
	Mean S/N ratio	**10.24787294**	**9.741916373**	**10.89441033**	**10.86770142**	**1.152493958**

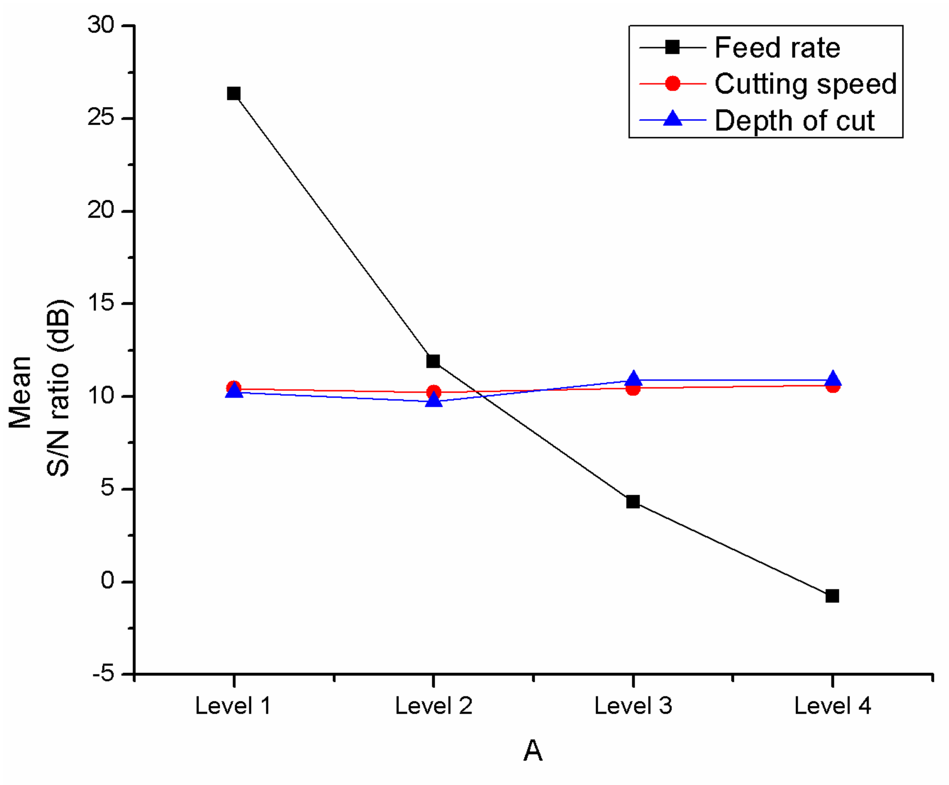

Figure 5.1: Mean S/N ratio for various parameters (feed rate, depth of cut and cutting speed)

Taguchi notes that the greater S/N ratio corresponds to the smaller variance of surface roughness. It can be seen from Figure 5.1 that the maximum S/N ratio for the feed rate was clearly at Level 1 (feed rate of 0.02 mm/rev). Furthermore, variation in the S/N ratio for higher feed rates decreases exponentially, which signifies that feed rate has a very strong influence on the surface roughness: the lower the feed rate the better the machined surface roughness or the higher the feed rate the worse will be the machined surface roughness. However, from Figure 5.1, the influence of cutting speed and depth of cut is not very clear, primarily because the variation in the S/N ratio is not much. This suggests that feed rate is by far the most dominant variable in influencing the machined surface roughness in comparison to the other two machining variables, i.e. cutting speed and depth of cut. To reveal more insights into this, two individual plots were plotted which are shown in Figure 5.2. It can be seen that the maximum S/N ratio for cutting speed is observed to be at Level 4 (cutting speed of 250 mm/min), while maximum S/N ratio for depth of cut is observed to be at Level 3 (depth of cut of 0.3 mm).

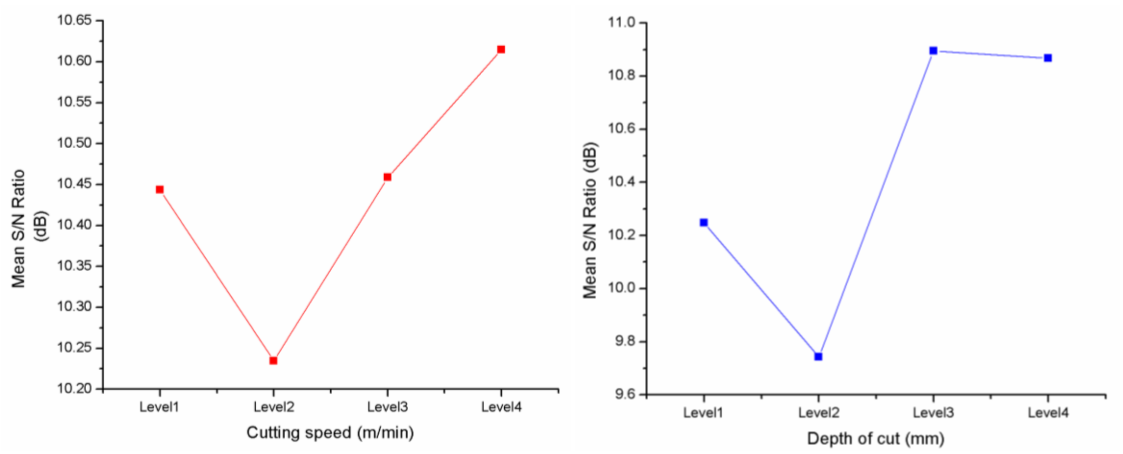

Figure 5.2: Close comparison of S/N ratio for cutting speed and depth of cut

It is also quite surprising that, particularly at level 2, S/N ratio for both cutting speed and depth of cut become the lowest and then rise again. It will be interesting to explore why the S/N ratio drops from Level 1 to Level 2 and then increases again with an increase in Level 3 (this will be expanded in future work). However, Figure 5.1 and Figure 5.2, in conjunction with each other clearly indicate that the optimal cutting parameters are A1, B4, C3 i.e. the optimal machining parameters are the feed rate of 0.02 mm/rev, cutting speed of 250 mm/min and depth of cut of 0.3 mm.

5.5 Analysis of Variance

Analysis of variance (ANOVA) is an established way to assert the dominance of one parameter over the other parameter in influencing the quality characteristic. An important thing needed to do ANOVA is to find out the degree of freedom. In this work, sixteen experiments were done and therefore the total degree of freedom is equal to the number of experiments minus one which gives the degree of freedom as 15. Four levels for each parameter counts for three degree of freedom. The total sum of squared deviations SS_T for each parameter can then be calculated as follows:

$$SS_T = \sum_{i=1}^{m} \eta_i^{\,2} - 1/m\left[\sum_{i=1}^{m} \eta_i / 16\right]^2 \qquad (5.6)$$

For example, feed rate can be calculated as follows:

$$SS_{T\,FEED} = \sum \frac{(1+2+3+4)^2}{4} + \frac{(5+6+7+8)^2}{4} + \frac{(9+10+11+12)^2}{4} + \frac{(13+14+15+16)^2}{4} - \frac{(\sum S/N)^2}{16} \qquad (5.7)$$

$$SS_{T\,Cuttingspeed} = \sum \frac{(1+5+9+13)^2}{4} + \frac{(2+6+10+14)^2}{4} + \frac{(3+7+11+15)^2}{4} + \frac{(4+8+12+16)^2}{4} - \frac{(\sum S/N)^2}{16} \qquad (5.8)$$

$$SS_{TDOC}=\sum\frac{(1+6+11+16)^2}{4}+\frac{(2+5+12+15)^2}{4}+\frac{(3+8+9+14)^2}{4}+\frac{(4+7+10+13)^2}{4}-\frac{(\sum S/N)^2}{16} \quad (5.9)$$

where numbers from 1 to 16 represent the corresponding S/N ratio obtained for each experiment as shown in table 5-4. The total sum of squares can be calculated by:

$$SST_{TOTAL}=\left(\sum(1^2)+(2^2)+(3^2)\cdots+(16^2)\right)-\frac{(\sum S/N)^2}{16} \quad (5.10)$$

The error can then be computed as:

$$SST_{ERROR}=SST_{TOTAL}-SST_{FEED}-SST_{SPEED}-SST_{DEPTH} \quad (5.11)$$

The mean square is equal to half of the sum of squares which can be used to calculate F as follows:

$$F_{FEED}=SST_{FEED}/SST_{ERROR} \quad (5.12)$$

Finally, contribution of the factor can be calculated by:

$$\%\,Contribution=\frac{F}{(\sum F)+1}\times 100\% \quad (5.13)$$

Table 5.6 shows a summary of the ANOVA results for all the experiments. It can be seen from table 5.6 that the feed rate makes the maximum contribution of 99.16%, thus signifying that across all the other cutting parameters, it has the most influence, followed by depth of cut and cutting speed respectively.

Table 5.6: Results of the ANOVA for surface roughness

Symbol	Cutting parameter	Degree of freedom	Sum of squares	Mean square = (Sum of Squares /2)	F (sum of square /Error)	Contribution (%)
A	Feed rate	3	1674.182	837.1	162.39	99.16%
B	Cutting speed	3	0.292	0.146	0.028	0.017
C	Depth of cut	3	3.655	1.827	0.354	0.216
Error (Total-A-B-C)		6	10.31			0.611%
Total Run		15	1688.435			100

5.6 Confirmation experiments

In the previous section, the optimal level of the design parameter was arrived at from the sixteen numbers of experimental arrays which are designed based on the Taguchi method. S/N ratio analysis reveals that the optimal cutting parameters are A1, B4, C3; i.e. the optimal machining parameters are the feed rate of 0.02mm/rev, cutting speed of 250 mm/min, and depth of cut of 0.3 mm. It will thus be of particular interest to find out from the experiments what level of surface roughness can be reached using these machining parameters under the same configuration that was originally used for the other experiments. Accordingly, a confirmatory machining trial was performed to calculate the surface roughness on these optimized machining parameters. Accordingly, the outcome of the experiments i.e. measured surface roughness obtained from the experiment is shown in figure 5.3. An average value of surface roughness of about 48.3 nm was achieved using the optimal parameters. It is noteworthy that this precise range of surface roughness of 48 nm was achieved not by using an ultra-precision lathe but only by a turret lathe, and hence, is indicative of the developments in the machine and cutting tool research that have taken place over the years in the domain of hard turning.

Table 5.7: Output of the confirmatory trial

	Initial cutting parameters	Optimal cutting parameters	
		Prediction	Experiment
Level	A2B2C2	A1B4C3	A1B4C3
Ra μm	0.360	0.0481	0.0483
S/N ratio (db)	8.874	26.355	26.321

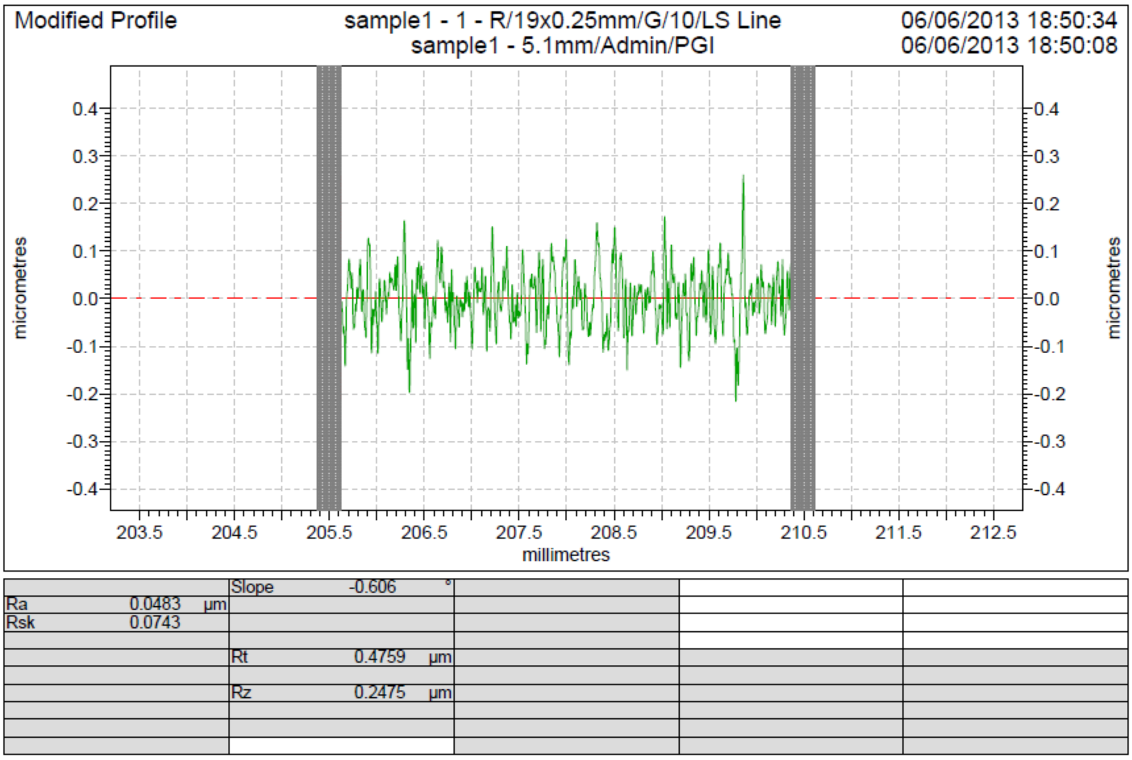

	Slope -0.606 °			
Ra 0.0483 µm				
Rsk 0.0743				
	Rt 0.4759 µm			
	Rz 0.2475 µm			

Figure 5.3: Measurement of the surface roughness using the optimal cutting parameters

Using table 5.4, the following equation can be used for predicting the S/N ratio as follows:

$$\eta_p = \eta_{tm} + \sum_{i=1}^{p} (\eta_m - \eta_{tm}) \tag{5.14}$$

where η_{tm} is the total mean of S/N ratio and is equal to 10.438. As shown in Table 5.5, η_m is the mean S/N ratio at the optimal level for the significant parameter as 26.355 corresponds to A1, 10.615 is for B4, 10.894 for C3 and p is the number of significant cutting parameters affecting the performance characteristic. In this study the only parameter of relevant importance is the feed rate. Accordingly, the predicated Ra can be calculated as:

$$Ra_{prediction} = \sqrt{10^{\left(S/N_{predicted}/-10\right)}} \tag{5.15}$$

A comparison of the predicted and experimental values of the surface roughness using the optimal cutting parameters is shown in Table 5.7. A good agreement between the predicted value and the experimental value can be seen. The increase of the S/N ratio from the initial cutting parameters to the optimal cutting parameters is 17.447 dB and therefore, the surface roughness value can be seen to improve by about 7.45 times.

5.7 Discussion on tool wear

The performance of any mechanical machining process is known to be influenced deeply by the in-process degradation or the wear of the cutting tool. Wear of the cutting tool changes the contact surface of the cutting tool and the workpiece which causes worsening of the machined surface. Wear of the cutting tool is therefore of paramount importance both to the academic and industrial community. Although, it is widely known that tool wear can be initiated either by mechanical or by chemical activities, the main purpose of this work was not to unravel the basic mechanism of tool wear but to examine the influence of the machining parameters, in particular the feed rate, in influencing the tool wear. Table 5.2, in this aspect, became an advantage to this study, as four feed rates are in common with each other. So, sixteen experiments involve the use of four cutting tips only. These four cutting tips were used to cut 80 mm length of cut, each at a different feed rate. Accordingly, Table 5.8 presents the SEM examination results of the cutting tool, which identifies the tools flank wear length, V_b, in each case.

Table 5.8: Experimental measurement of tool flank wear length V_b

Cutting length (experimental trial number)	Tool used at the feed rate of	Tool flank wear (V_b) length	
80 mm (1-4)	0.02 mm/rev	26.12 µm	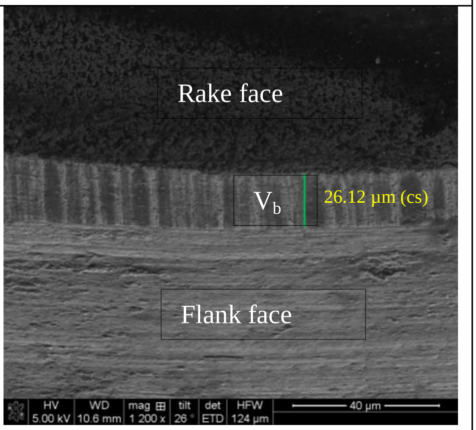 Rake face V_b 26.12 µm (cs) Flank face HV 5.00 kV WD 10.6 mm mag 1 200 x tilt 26 ° det ETD HFW 124 µm 40 µm

80 mm (5-8)	0.06 mm/rev	19.17 µm	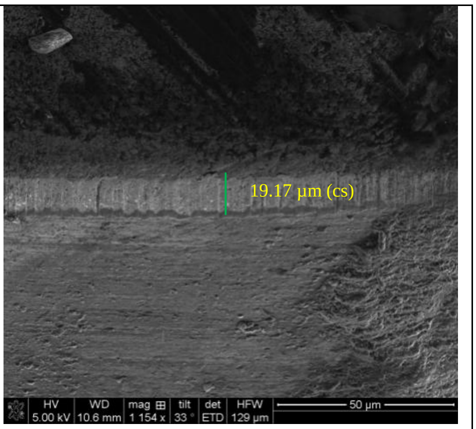 19.17 µm (cs) HV 5.00 kV WD 10.6 mm mag ⊞ 1 154 x tilt 33 ° det ETD HFW 129 µm 50 µm
80 mm (9-12)	0.1 mm/rev	17.11 µm	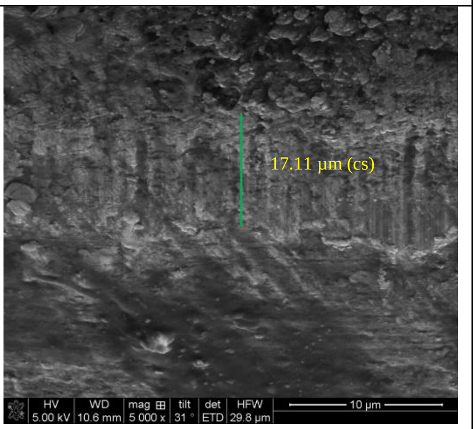 17.11 µm (cs) HV 5.00 kV WD 10.6 mm mag ⊞ 5 000 x tilt 31 ° det ETD HFW 29.8 µm 10 µm
80 mm (13-16)	0.15 mm/rev	16.71 µm	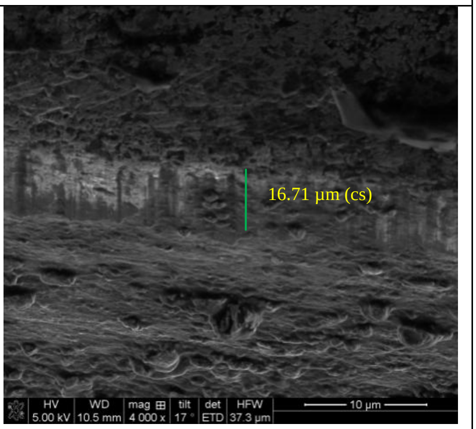 16.71 µm (cs) HV 5.00 kV WD 10.5 mm mag ⊞ 4 000 x tilt 17 ° det ETD HFW 37.3 µm 10 µm

It can be seen from table 5.8, that maximum wear length, V_b, was observed to be about 26.12 µm when cutting was performed at a lower feed rate of 0.02 mm/rev. Similarly, a very low wear length of about 16.71 µm was observed when a high feed rate of 0.15 mm/rev was used and intermittent wear lengths were observed for intermittent feed rates. It is thus clear from this examination that feed rate influences the tool wear. Now, an importance aspect of this particular examination is that a lower feed rate was earlier shown to provide better machined surface roughness, but this comes at an expense of higher wear volume of the cutting tool. On the other hand, at higher feed rates tool wear is low but this produced a poor machined surface. Therefore, in a practical case, the option of choosing the feed rate must consider both machined surface roughness and the wear volume of the cutting tool before finalizing the machining parameters.

5.8 Summary

In this chapter, the Taguchi method was applied to develop an L16 array with individual combinations of feed rate, depth of cut and cutting speed to optimize the surface roughness of AISI 4340 steel (69 HRC). S/N ratio, ANOVA analysis and multiple regression analysis were applied to the machining data to obtain deep insights. A key finding obtained from the hard turning experimental trials reported in this chapter is that an average machined surface roughness of 48 nm, without requiring any additional means, can be achieved in hard turning carried out on a modern CNC turret lathe while using a CBN cutting tool. Based on the foregoing discussions, the following other conclusions can be drawn:

1. S/N ratio analysis shows the dominance of feed rate over other two machining variables depth of cut and cutting speed. The output results of the analysis indicate that the optimal cutting parameters are the use of feed rate of 0.02 mm/rev, cutting speed of 250 mm/min and depth of cut of 0.3 mm.

2. While optimized cutting parameters were arrived at from the S/N ratio, the dominance of each machining variable was not quantitatively clear, for which ANOVA analysis was performed. It was found out that the feed rate can make a contribution of up to 99.16%, whereas other parameters do not carry an appreciable contribution in influencing the machined surface roughness.

3. Multiple Regression Models applied to the 16 experimental datasets obtained from in-house trials revealed the following mathematical equations for predicting the machined surface roughness:

$$Ra = -0.11706992 + 8.148467886\ f + 9.75658 \times 10^{-5} v - 0.20935731\ d$$

4. Finally, it is shown that the lower feed rate, while providing an improved machined surface roughness, also influences and tends to increase the tool wear. Therefore, a trade-off criterion for selection of the appropriate feed rate will come from the cost and quality considerations.

CHAPTER 6 – Obtaining an ultra-precision machined surface by SDM

6.1 Introduction

One of the key findings obtained from the previous chapter shows that the feed rate is the most dominant predictor that dictates the quality of the machined surface. Using this important bit of information, the motivation for this chapter is to use SDM as a probe to realise an ultra-precision machined surface in terms of nanometer level surface roughness and good sub-surface integrity, while using a conventional CNC lathe.

6.2 Details of the machining conditions

In order to test whether the positive outcomes are obtained when applying the surface defect machining (SDM) method as stated above, two sets of machining trials were performed under the same cutting conditions with the same type of work material, using CBN tools. One set of the samples was machined using conventional hard turning and the other sample machined using SDM. All machining variables, such as cutting speed, feed rate, depth of cut and tool geometry, were kept at the same values in both trials. The feed rate varies from 0.08 mm/rev to 0.005 mm/rev, as its significant effect was found experimentally by the Taguchi method in the previous chapter, and the rest of the cutting parameters are fixed. The workpiece used was AISI 4340 steel (69 HRC). The execution of SDM was performed by firstly making surface defects in the form of holes on the top surface of the workpiece using a Trumpf (CO_2) laser machine with a peak power of 2.7 kW. The experimental trials were then carried out on a Mori-Seiki SL-25Y (4 axis) CNC lathe. Other details of machining conditions and tool geometries of the CBN tool inserts are tabulated in Table 6.1. Also, comprehensive details of the experimental setup adopted for this work are described in Chapter 4 and for the purpose of brevity only the relevant results are being reported here.

Table 6.1: Experimental parameters

Number	Details	Values
1	Workpiece Material	AISI 4340 steel hardened up to 69 HRC
2	Diameter of workpiece before turning	28.8 mm

3	Cutting tool specifications (ISO code)	CNMA 12 04 08 S-B
4	Tool Nose radius	0.8 mm
5	Tool rake and clearance angles	0° and 5°
6	Feed rate	0.08,0.03, and 0.005 mm/rev
7	Depth of cut	0.2 mm
8	Cutting speed	90 m/min
9	Coolant	None
10	Diameter and depth of holes	0.9 mm and 0.17 mm respectively with 10 mm interspacing between each hole

6.3 The significant and critical feed rate observation

A lower feed rate is preferred in practical application, to generate a smooth surface, but only upto a certain critical limit beyond which ploughing and consequent worsening of the machined surface become pronounced. Figure 6.1 highlights the variation in the measurement of surface roughness (average machined surface roughness (Ra) and peak to valley measurement (Rz)) obtained by changing the feed rate alone in both sets of experiments. It can be seen that under the current machining conditions and tool geometry used for the experiments, the feed rate of 0.02 mm/rev is critical for attaining the best possible machined surface roughness when using conventional hard turning on the CNC lathe. At this low feed rate of 0.02 mm/rev the Ra is 0.0478 µm, and for further lowering of this value to 0.005 mm/rev produced Ra of 0.0485 µm.

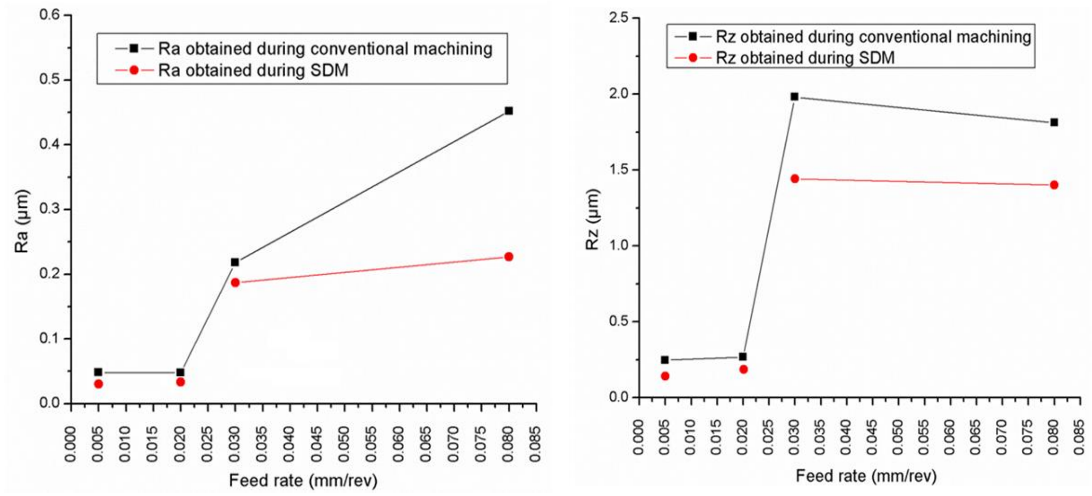

Figure 6.1: Variation in Ra and Rz with respect to the feed rate during conventional machining and SDM

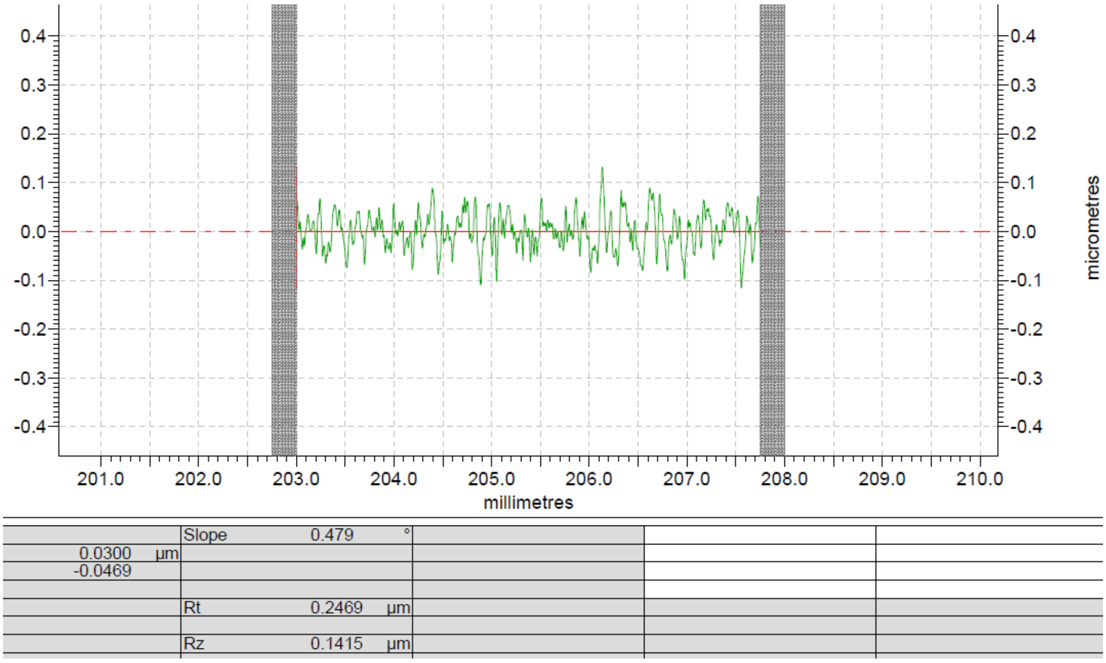

		Slope	0.479	°	
0.0300	µm				
-0.0469					
		Rt	0.2469	µm	
		Rz	0.1415	µm	

(a)

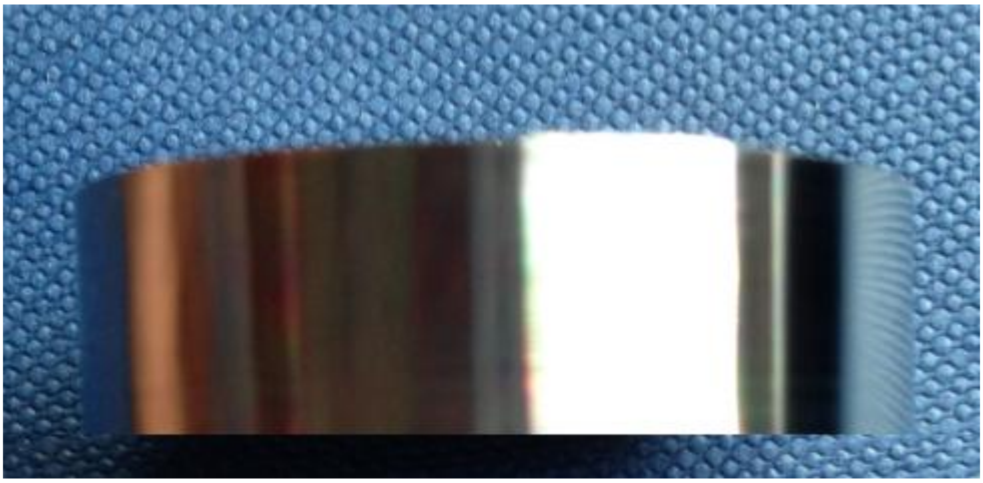

(b)

Figure 6.2: Quality of the machined surface (a) Talysurf measurement of the machined surface roughness (b) mirror finish smooth machined surface

However, lowering of the feed rate beyond the theoretical limits was realized to be a salient feature of the SDM approach. An average value of machined surface roughness (Ra) of 30 nm. Figure 6.2a, is obtained when the SDM method is used on an AISI 4340 steel specimen (shown in Figure 6.2b) with a feed rate lower than 0.02 mm/rev. This gives an important indication that the barrier of critical feed can be broken by adapting the SDM method. This can even potentially enable the turning operation to attain the ultra-precision surface finish that can only be obtained through grinding and polishing processes. Needless to mention that IT4 is currently achievable through tolerance in a state-of-the-art HT processing (Tönshoff et al., 2000). To the author’s knowledge it is the first time that such an optical quality machined surface finish has been obtained in hard turning without using an ultra-precision machine tool. Of particular importance in this regard is the fact that the ASTM standard recommends the surface roughness value (Ra) on the metallic knee joint implants to be lower than 100 nm (Sidpara and Jain, 2012) which is obtained with ease in this work. There is a potential to use hard turning to machine such precise components.

6.4 3D-2D surface topography analyses

In order to gain further insights into the process, the surface topography of the machined surface obtained via conventional machining and the SDM method was carefully studied. Figure 6.3 and Figure 6.4 present a comparison of the surface topography obtained via SDM and conventional machining respectively. Feed rates of 0.03 mm/rev are used in both trials. Clearly the P-V value obtained from SDM method appears to be better than that obtained from the conventional machining method.

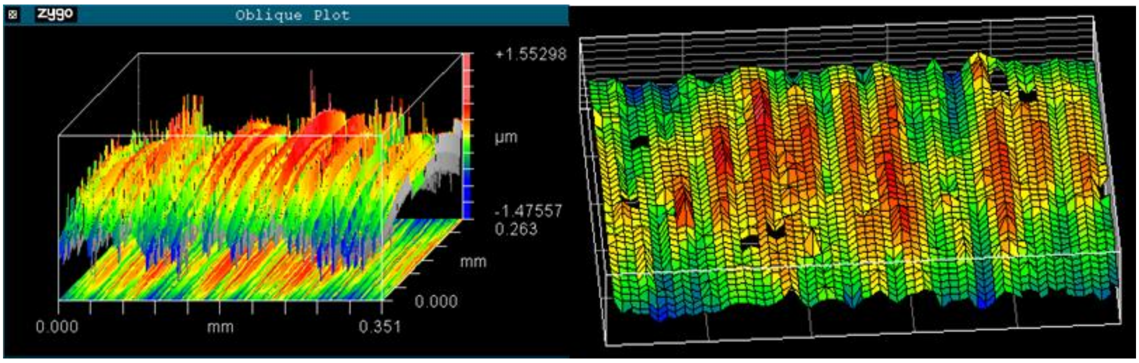

Figure 6.3: Topography of the machined surface when using SDM

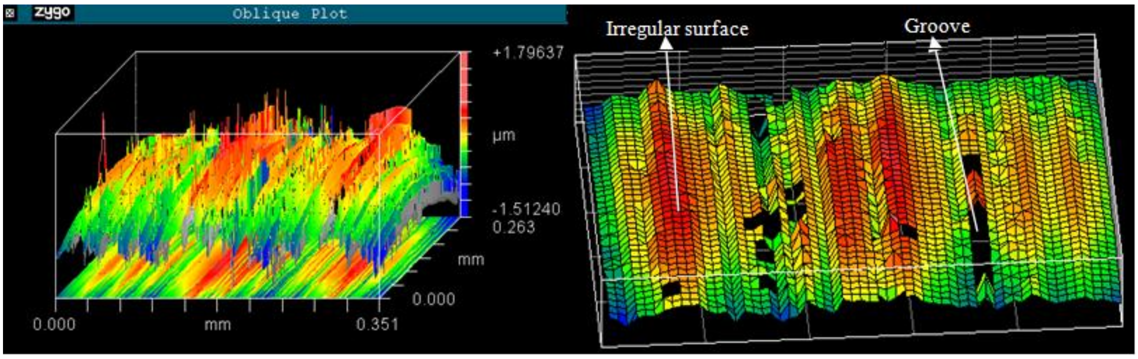

Figure 6.4: Topography of the machined surface when using classical HT

Other than the quantitative improvement in surface roughness, a key difference observed is the presence of grooves/ ridges, irregularities in the machined surface when using conventional machining whereas during SDM a more uniform machined surface is obtained without exhibiting much of variation in the machined surface profile.

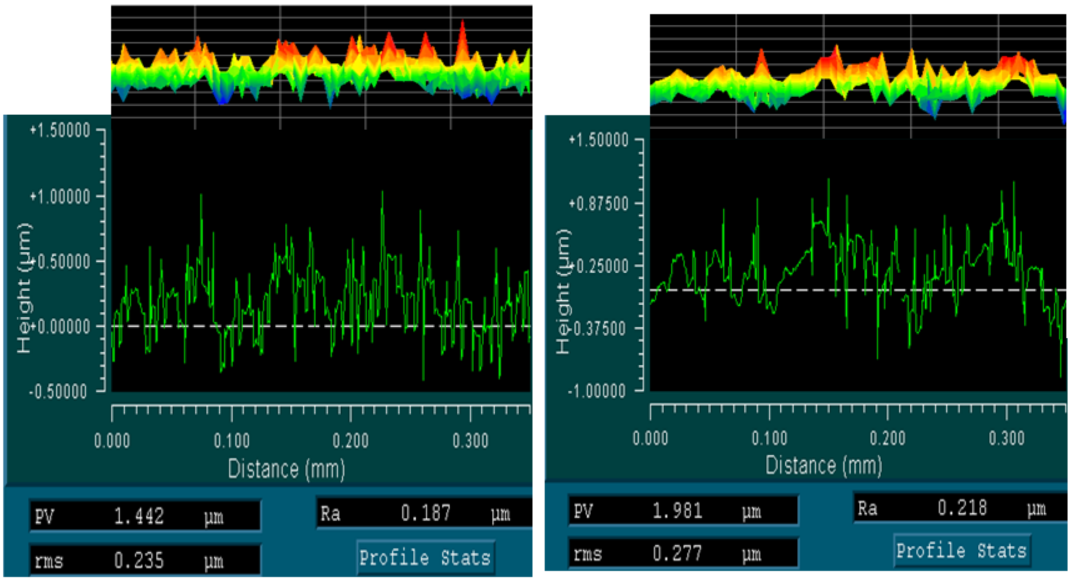
+1.50000
+1.00000
+0.50000
+0.00000
-0.50000
Height (µm)
0.000
0.100
0.200
0.300
Distance (mm)
Profile Stats
+1.50000
+0.87500
+0.25000
-0.37500
-1.00000
Height (µm)
0.000
0.100
0.200
0.300
Distance (mm)
Profile Stats

PV 1.442 µm
rms 0.235 µm
Ra 0.187 µm

PV 1.981 µm
rms 0.277 µm
Ra 0.218 µm

Figure 6.5: 2D profile of the machined surface (a) SDM HT (b) classical HT

Figure 6.5 shows a comparison of the 2D-profile of the machined surface of the two machining methods. The crest and troughs of the machined surface obtained by the SDM method are observed to exhibit more periodicity and uniformity than classical HT. Also, the heights, fluctuations and alterations in the shapes and geometry of the peak appear to be more regular when using the SDM method. The smaller number of intermittent crests and troughs on the machined surface obtained when using SDM makes it clear that the cutting action is more uniform and regular compared to classical HT.

6.5 SEM examination of the machined surface

The 2D profile measurement results are confirmed further by making assessment of the machined surface using a SEM (shown in Figure 6.6). It can be seen that the extent of pile-up and occurrence of side flow during the SDM process is less than that in conventional HT, plausibly resulting in better machined surface roughness.

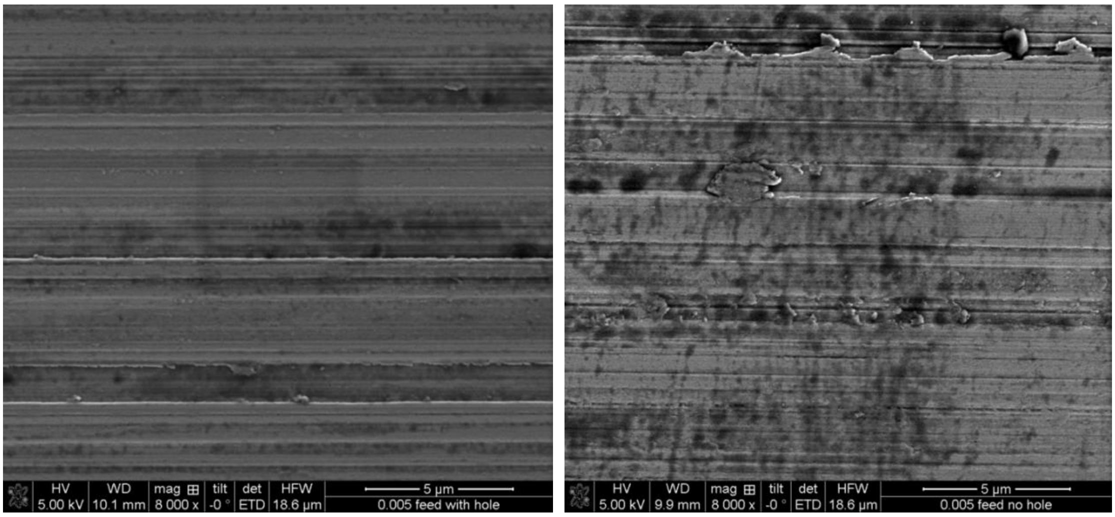
HV 5.00 kV | WD 10.1 mm | mag 8 000 x | tilt -0 ° | det ETD | HFW 18.6 µm
5 µm
0.005 feed with hole
HV 5.00 kV | WD 9.9 mm | mag 8 000 x | tilt -0 ° | det ETD | HFW 18.6 µm
5 µm
0.005 feed no hole

Figure 6.6: Comparison of SEM measurement results of machined surface topography at a feed rate of 0.005 mm/ rev (a) SDM method and (b) conventional HT method

Figure 6.7 presents a comparison of the SEM images of the machined surface obtained from conventional HT method and the SDM method under the same machining conditions with feed rate of 0.03 mm/rev. A significant difference between the qualities of the two machined surfaces is evident from these images.

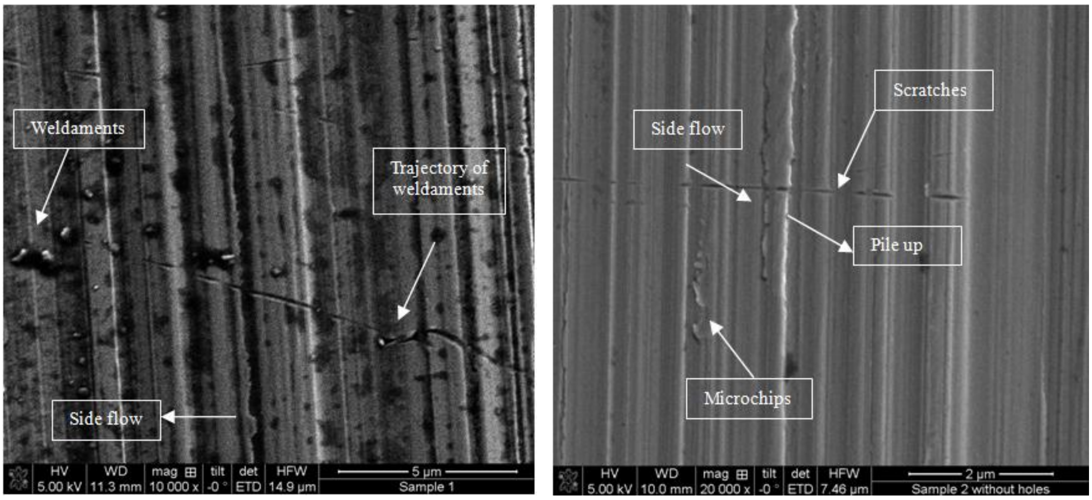
Weldaments
Trajectory of weldaments
Side flow
HV 5.00 kV | WD 11.3 mm | mag 10 000 x | tilt -0 ° | det ETD | HFW 14.9 µm
5 µm
Sample 1
Scratches
Side flow
Pile up
Microchips
HV 5.00 kV | WD 10.0 mm | mag 20 000 x | tilt -0 ° | det ETD | HFW 7.46 µm
2 µm
Sample 2 without holes

(a) Conventional HT method

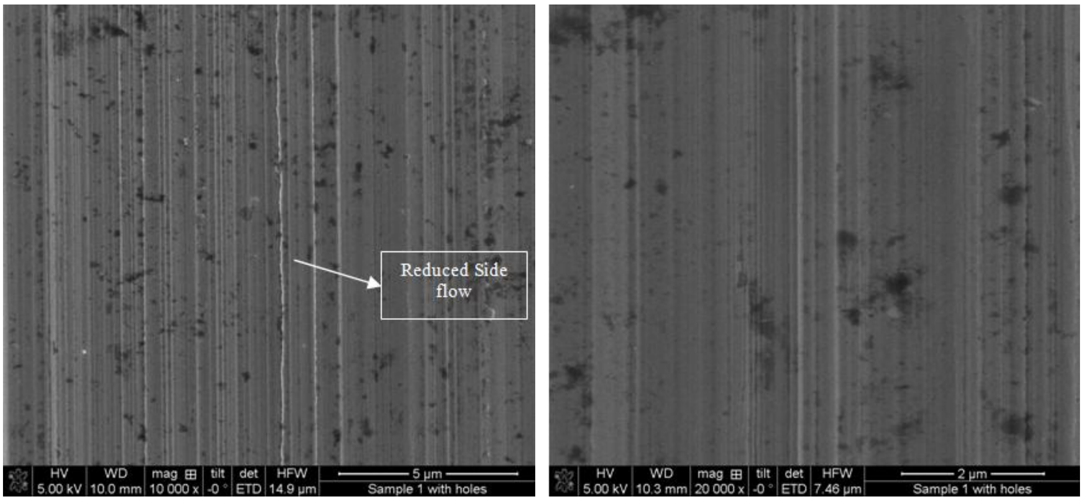

(b) SDM method

Figure 6.7: SEM examination of the machined surface quality obtained from machining at a feed rate of 0.03 mm/ rev

Figure 6.7a reveals appearance of several kinds of surface defects i.e. excessive side flow, presence of microchips on the machine surface, presence of weldaments and penetration of these weldaments in the finish machined surface to form scratches on the machined surface. Such surface defects are precursors to the service life of the machined component. On the other hand, the machined component through the SDM method shows a negligible extent of side flow and no considerable appearance of microchips on the finished surface. Another improvement observed is the amount and appearance of the weldament particles. As discussed earlier, small fractured edges of the steel subjected to an extremely high machining temperature in the cutting zone promotes conditions for welding. The surface machined with SDM is found to be free from such weldaments, which is an outcome of the reduced machining temperature during SDM (Rashid et al., 2013).

6.6 Theoretical analysis via FEA

To augment and further support the experimental findings, finite element analysis was carried out to simulate surface defect machining of D2 steel 63 HRC. These simulations are in continuation to those shown in Chapter 3. The results presented here are for two cases: (i) the depth of surface defects is less than the depth of cut and (ii) depth of surface defect is more than the depth of cut. This will unravel a complete understanding of the whole SDM process.

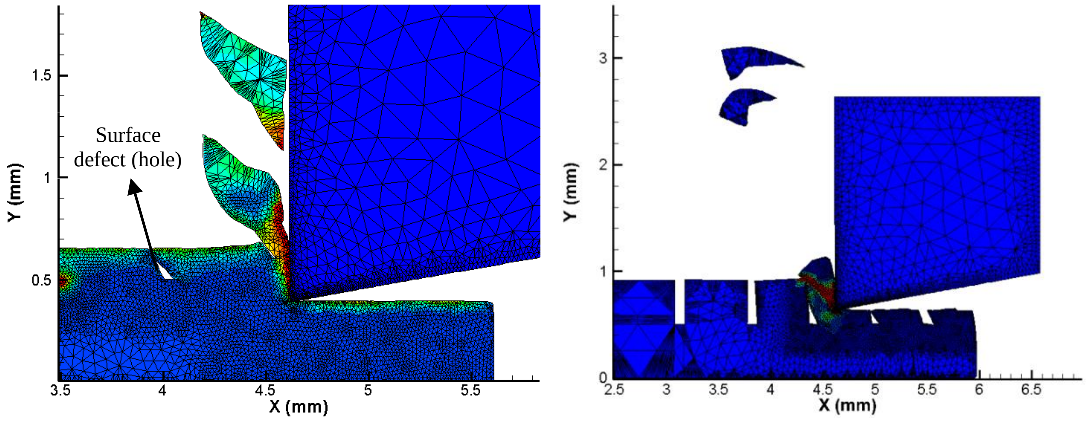

Figure 6.8: Finite element analysis of the surface defect machining of hard steel (a) when depth of surface defects is less than the depth of cut and (b) depth of surface defects is larger than the depth of cut

The simulation results are shown in Figure 6.8, in which the plastic strain during the machining is observed. The most remarkable observation obtained from the finite element analysis on SDM is the significant reduction in the shear plane angle due to the reduction in shear plane area during machining. A decrease in the value of the shear plane angle under the same machining parameters indicates the dominance of cutting forces over feed forces, which justifies the enhanced cutting action of the tool. This means that for the same amount of input energy, cutting action is enhanced. The forces in the direction of the cutting velocity vector are increased. Consequently, the deformation of the material occurs preferentially along the direction of cutting and causes less side flow, resulting in the improved machined surface quality.

6.8 White layer in SDM

The high temperature in the cutting zone will make the machined workpiece surface undergo metallurgical transformations and result in the formation of white layer. White layer on the finished surface has been a precursor for the technological advancement of hard turning. Figure 6.9 highlights the comparison of the formed of white layer measured by SEM for the two samples. The extent of the white layer in conventional hard turning is about 9.06 µm while by using SDM method, it is only 5.72 µm. Clearly, the extent of white layer formation is found to be reduced when using the SDM method. The intensity of the white layer under these two methods is also different. In conventional HT process the machined surface is a mixture of black and white layers and had a few visible surface defects. Using SDM method the intensity of the white layer is more whitish with no appearance of the black layer and minimum surface defects.

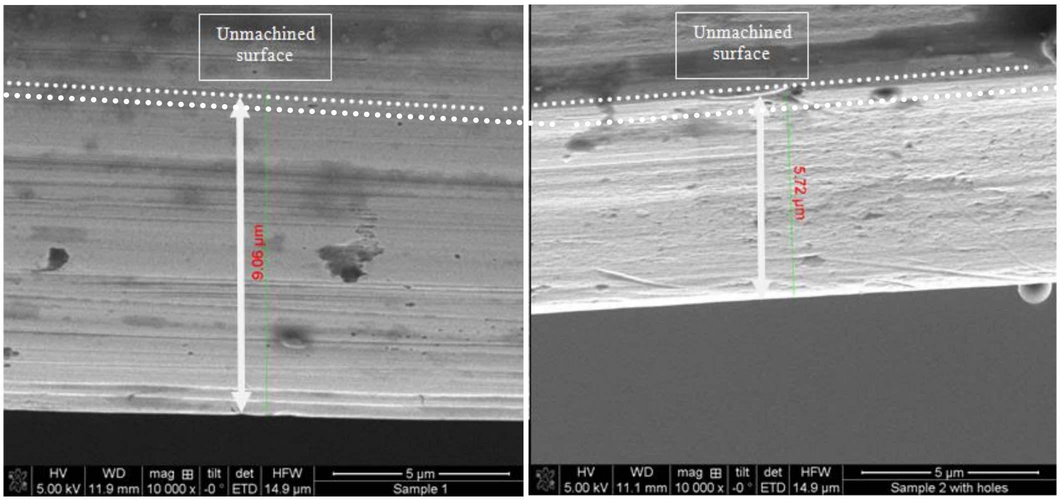
Unmachined surface
9.06 µm
HV 5.00 kV
WD 11.9 mm
mag 10 000 x
tilt -0 °
det ETD
HFW 14.9 µm
5 µm
Sample 1
Unmachined surface
5.72 µm
HV 5.00 kV
WD 11.1 mm
mag 10 000 x
tilt -0 °
det ETD
HFW 14.9 µm
5 µm
Sample 2 with holes

(a) Conventional HT method (b) SDM method

Figure 6.9: Measurement of white layer on the finished machined surface

6.9 Classification of surface and subsurface defects

Based on the comprehensive analysis of the surface defects presented above, it has been schematically shown in Figure 6.10 that surface defects can broadly be classified based on their location on the machined surface, i.e. some of these defects exist above the machined surface while others are located underneath the machined surface. The defects located above the machined surface will tend to increase the extent of the peak of the surface and will contribute to a higher peak value in the P-V measure of the roughness. In contrast, the surface defects below the machined surface will tend to reduce the valley value in the P-V measure of the machined surface roughness. Consequently, these defects pose different threats with respect to their applications, e.g. a higher peak value will lead to the formation of the site to initiate failures by the virtue of fatigue, creep, tribological or chemical wear. On the other hand, the existence of defects below the machined surface, i.e. in the valley, could act as the source for the accumulation of corrosive media leading to corrosion cracking.

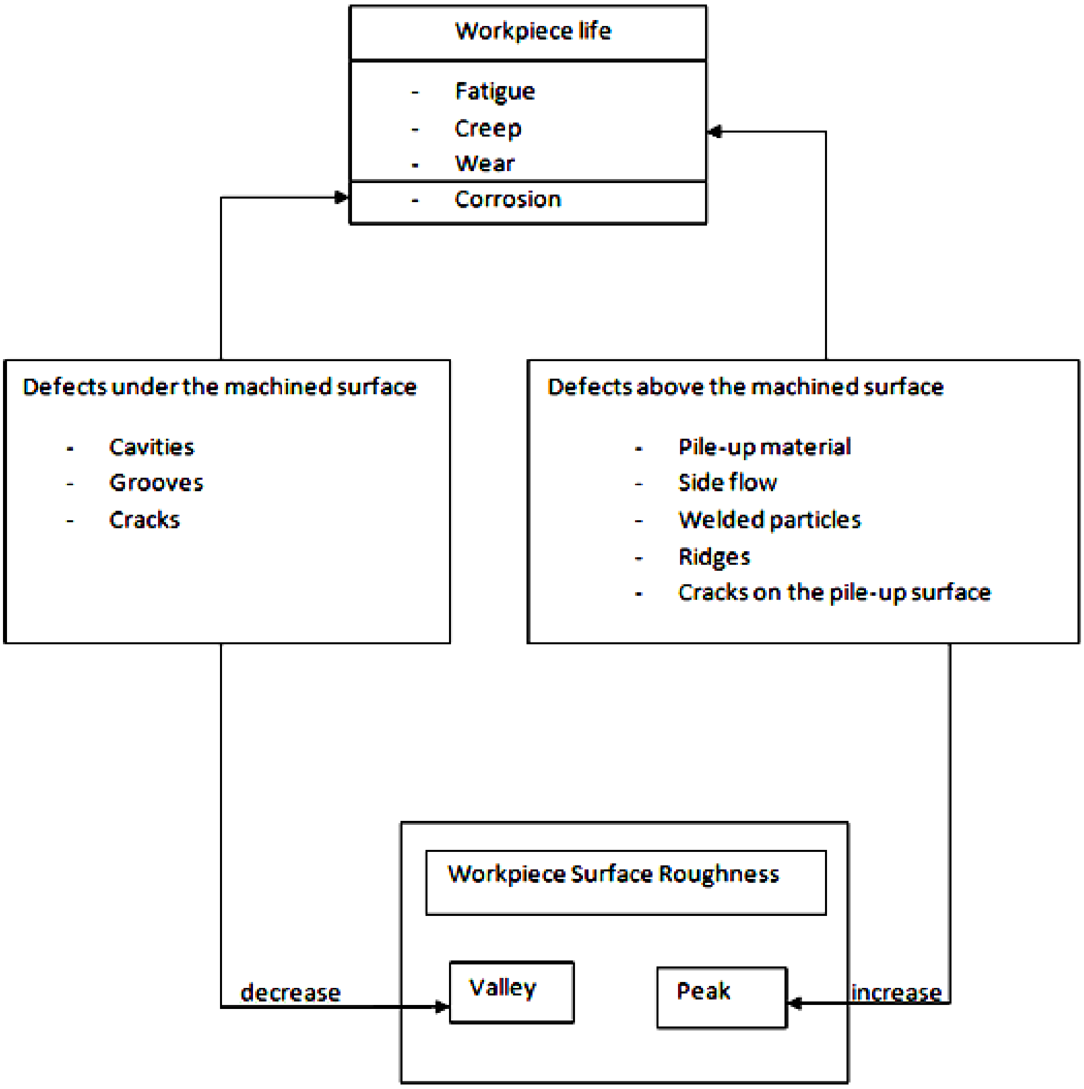
Workpiece life
- Fatigue
- Creep
- Wear
- Corrosion
Defects under the machined surface
- Cavities
- Grooves
- Cracks
Defects above the machined surface
- Pile-up material
- Side flow
- Welded particles
- Ridges
- Cracks on the pile-up surface
Workpiece Surface Roughness
decrease
Valley
Peak
increase

Figure 6.10: Influence of surface defects on altering topography of machined surfaces

6.10 Summary

Rapid advancement in the instrumentation technology has been a key enabling technology to study various machining mechanisms at a much better spatial and temporal resolution than was previously possible. The application of the white light interferometer and scanning electron microscope to study the role of manufacture surface defects in influencing the microscopic mechanics for ease of manufacturing of hard steel is a novel finding in this chapter. Based on the aforementioned results, the following conclusions can be drawn.

1. Conventional machining of hard steels or difficult to machine materials in general involves a wide variety of surface deterioration mechanisms. These types of damage lead to the appearance of surface defects which can broadly be categorized into coarse scale and fine scale surface defects and are sources of observation of a high value of

machined surface roughness. The majority of these defects are associated with the plastic side flow of the material, formation of pile-up edges, weldment particles, formation of grooves and ridges, formation of microchips and tearing of material.

2. The presence of purposely introduced surface defects improves the machinability of difficult to machine materials, through a reduction in shear plane angle and shear plane area, thus permitting reduced side flow with less metallurgical transformations on the finished machined surface and sub-surface.

3. The quality of the machined surface generated by the mechanical machining process is known to be influenced by the feed rate. There are both upper and lower limitations of the feed rate. A lower feed rate is preferred in practical applications to generate a smooth surface but only upto a certain critical limit beyond which ploughing and consequent worsening of the machined surface become pronounced. In the current investigation, lowering of the feed rate beyond the theoretical limits was realized to be a still salient feature of the approach proposed in this work.

4. It has been shown that an increase in the peak and valley of the surface defects poses different threats with respect to the application of the component in practice. An increased peak value of the surface roughness will lead to the formation of the sites to initiate failures by the virtue of fatigue, creep, and tribological or chemical wear. Conversely, a reduced valley in the P-V measure of surface roughness could potentially be the site of accumulation of corrosive media, resulting in corrosion cracking.

CHAPTER 7 – Finite element analysis of multi cutting passes

7.1 Introduction

It is a very common practice on the shop floor that the turned workpiece is machined by multi-passes to its final shape. A question maybe asked: What is the influence of the first cut over the second one? It is not easy to answer the question without using accurate and sophisticated instruments to do that experimentally. But this may, however, reasonably be answered through adaption of an accurate computer simulation based approach. This chapter aims to investigate the influence of previous cut in multi-pass cutting processes by carrying out detailed finite element analysis to compare the two methods, namely, surface defect machining and conventional hard machining. Accordingly, seven workpiece materials of different hardness are selected to perform two sets of simulations.

7.2 Simulation details

In each simulation, two cutting passes were performed to evaluate the cutting performance in these two continuous cuts. The details of the modelling and simulation parameters are summarized in Table 7.1 and Figure 7.1.

Table 7.1: Constitutive equations and machining variables used in the FEA simulation for an elaborative testing on a range of materials

Workpiece details	Geometry	(Length : 4.5 mm and height : 1 mm)
	Element Size	0.02- 0.1 mm
	Number of nodes	72000
Cutting tool details	Material	WC
	Cutting edge radius	0.02 mm
	Rake angle	0°
	Clearance angle	10°
Cutting conditions	Cutting speed	200 m/min
	Depth of cut	0.26 mm

	Length of cut	2.5 mm
Material modelling power law	$\sigma\left(\varepsilon^{\mathrm{P}},\varepsilon^{\bullet},\mathrm{T}\right)=g\left(\varepsilon^{\mathrm{P}}\right)\cdot\Gamma\left(\varepsilon^{\bullet}\right)\cdot\Theta\left(\mathrm{T}\right)$ where, $g\left(\varepsilon^{\mathrm{P}}\right)$ is strain rate hardening, $\Gamma\left(\varepsilon^{\bullet}\right)$ is strain rate sensitivity and $\Theta\left(\mathrm{T}\right)$ is thermal softening.	
Damage function	$D=\sum_{i}\frac{\Delta\varepsilon_{i}^{\mathrm{P}}}{\varepsilon_{fi}^{\mathrm{P}}}$ Where, $\Delta\varepsilon_{i}^{\mathrm{P}}$ is the instantaneous increment of strain, $\varepsilon_{fi}^{\mathrm{P}}$ is the instantaneous strain to failure.	

The outputs of the simulations were compared in terms of cutting forces, workpiece temperature, residual stresses and stresses on the cutting tool. The results obtained are presented in the next sections. Most of the results are in good agreement to what has been discussed in previous chapters.

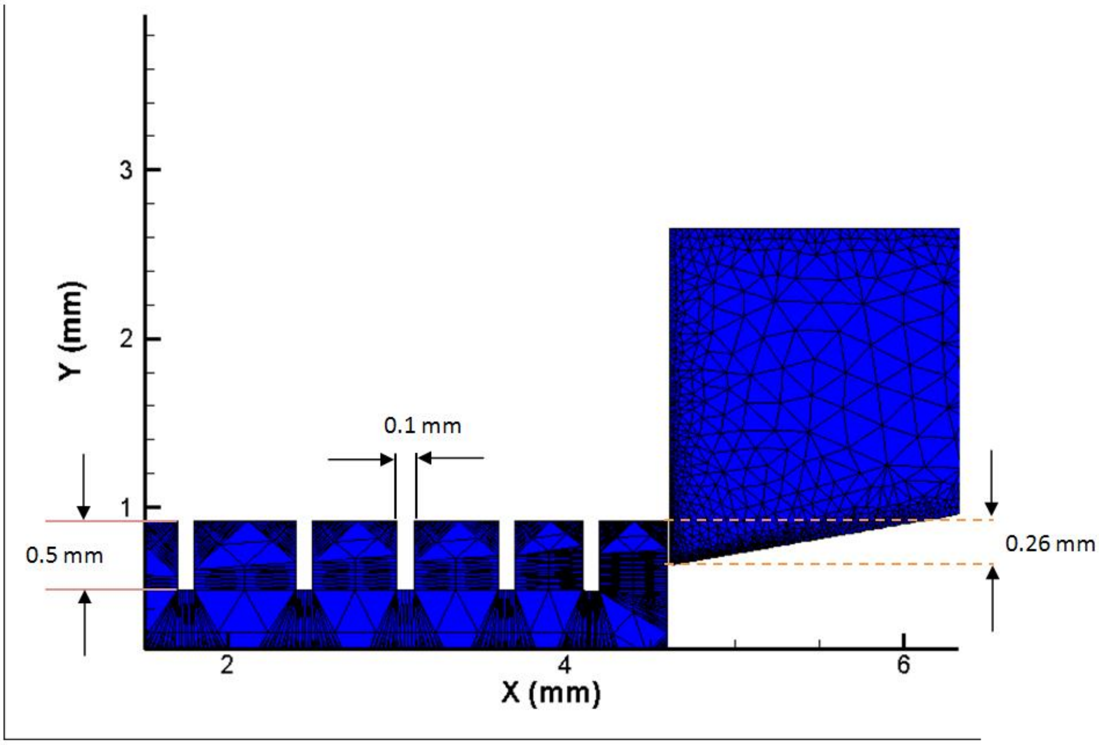

Figure 7.1: Schematic of FEA simulation

7.3 Chip formation mechanism of SDM method

As shown in Table 7.2, the shear angle is found to increase in the second cut from the first cut. This is an outcome of the increased hardness in the second cut due to strain hardening induced in the first cut. This result agrees with earlier (Nakayama, 1997) observations in that, for a given material with different hardness, the shear angle increases if the hardness increases. The simulation results also show different types of cutting chips are formed for different types of steel studied.

Table 7.2: Shear angle alteration from first cut and second cut

materials			Shear angle conventional hard turning first cut	Shear angle conventional hard turning second cut
1	AISI 8617H	59HRC	38.61721	43.10346
2	D2	680bhn	53.24783	54.31363
3	AISI 300m	550bhn	49.53774	50.38929
4	AISI 52100	614bhn	50.75454	51.43163
5	AISI 1053	623bhn	47.34261	55.07246
6	AISI 1070	627bhn	50.39903	52.91946
7	D2	615bhn	41.57877	41.98723

In hard turning, a variety of saw tooth chips can be obtained, depending on many factors such as material properties and cutting conditions. Figure 7.2 shows two different types of saw tooth chip of two different steels exposed to the same cutting conditions.

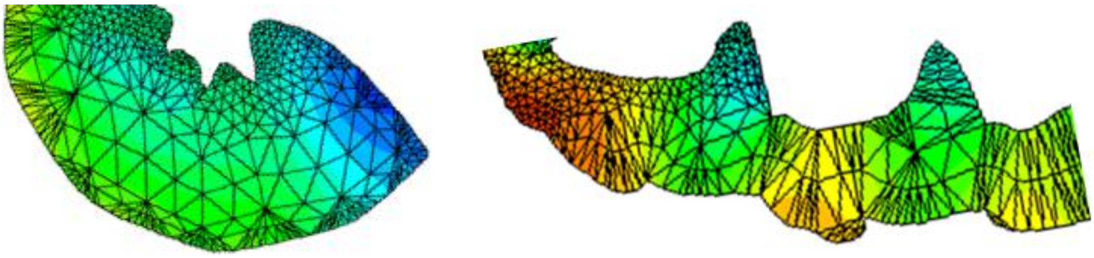

Figure 7.2: Saw tooth chip observed from the FEA simulations

The cyclic chip formation is governed by the shearability of the material which depends on its composition and material properties, including hardness and toughness. The variation in the size and shape of the cutting chips leads to a fluctuation in the cutting forces and eventually in the machining stresses. It is still not clear whether adiabatic shear took place during the cutting process or not, that is yet to be examined. This chapter will only focus on advancing understanding of some other salient aspects of SDM and how the chip formation changes during the multi-pass cutting process. As has been mentioned, the earlier SDM resulted in the generation of broken, small, segmented chips (witnessed using a thermal camera). The simulation results in this chapter also show discontinuous types of chip, similar to those collected experimentally. It came as a surprise to observe from the simulation that a material when heat-treated to exhibit different hardness may show different characteristics of the chip formation mechanism. As shown in Figure 7.3a, D2 of 615bhn hardness showed continuous chip formation when machined by conventional hard turning and in Figure 7.3b, D2 of 680bhn hardness showed saw tooth chip formation when machined by conventional hard turning.

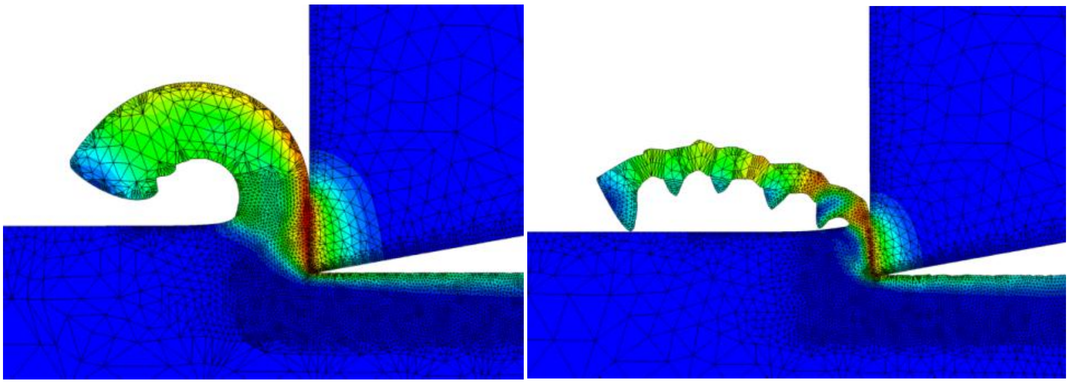

(a) D2 615bhn (b) D2 680bhn

Figure 7.3: Hardness effect on chip formation (a) continuous chip (b) saw tooth chip

Table 7.3: Chip mechanism of D2 steel of two different hardnesses formed by the SDM method

	D2 615bhn	D2 680bhn
1	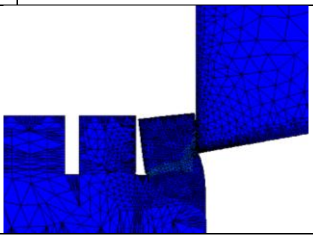	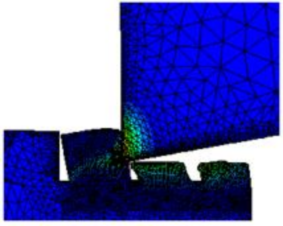

2	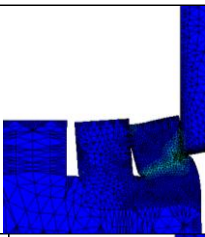	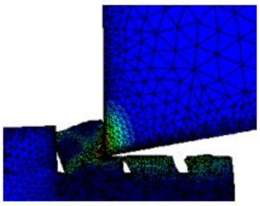
3	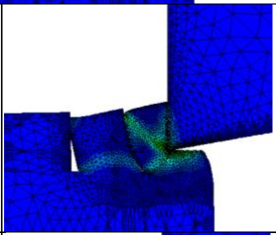	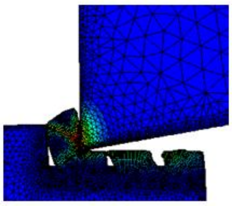
4	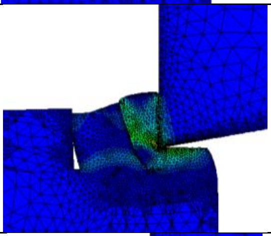	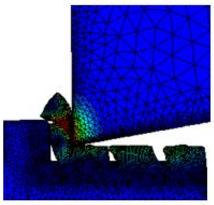
5	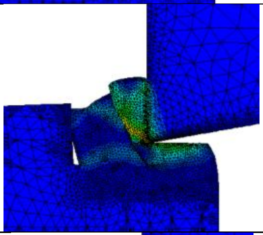	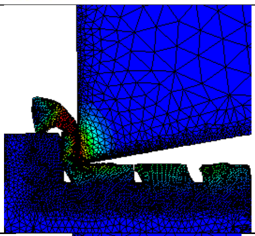
6	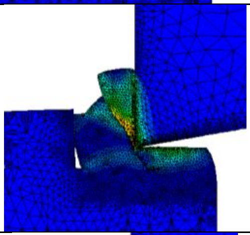	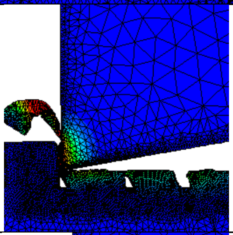
7	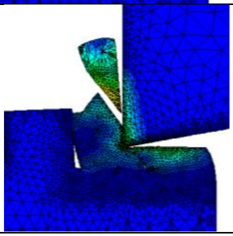	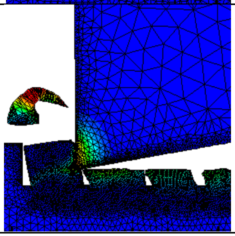

On the other hand, these two materials were also machined using SDM. The snapshot of the simulated chip formations captured for each chip cycle is shown in Table 7.3. The chip mechanism is observed to be significantly different from the counterpart from conventional hard turning.

The snapshot of the D2 680 bhn shown in Table 7.4 shows similar cutting behaviour for the two continuous cuts. The material is deformed and elongated in the second cut. It allows the material to flow along the direction of the hole, which becomes the direction of easy shear and this is the most plausible reason for observing reduced side flow and the surface deteriorations shown previously during the experiments.

Table 7.4: Second cut chip mechanism of SDM

	D2 680bhn		
1	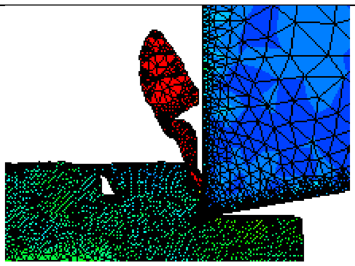	4	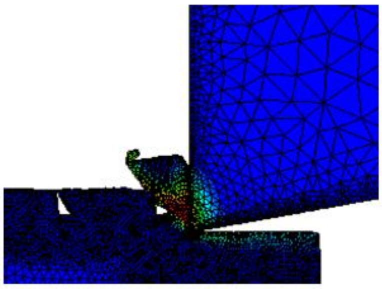
2	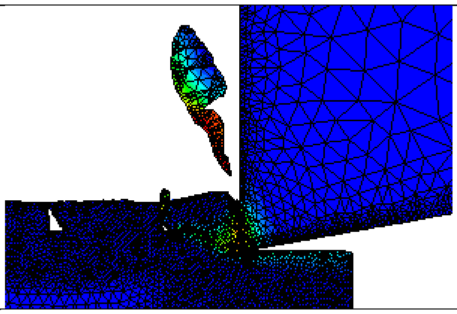	5	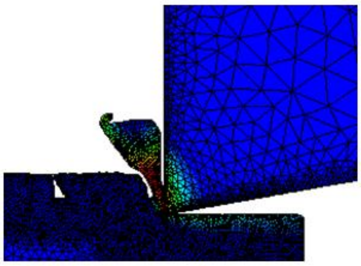
3	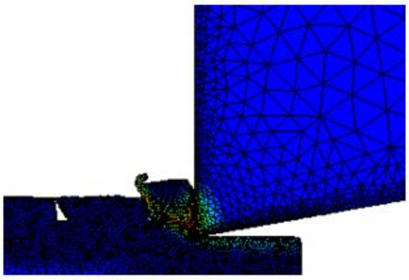	6	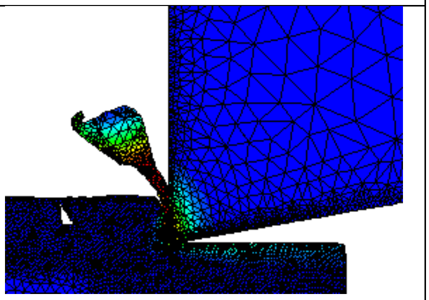
7	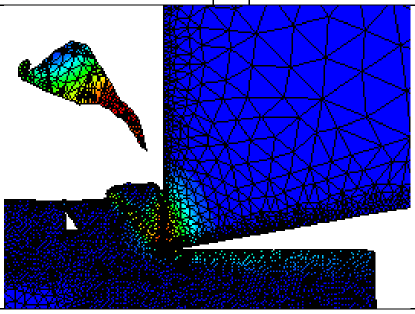		

7.4 Workpiece temperature and residual stresses

Both previous experimental and simulation results show that the workpiece temperature decreases during the SDM for a single machining pass. For better demonstration, two cases are presented here for multi-cutting passes to compare SDM with conventional hard turning. The results are summarized in Table 7.5. The same material (D2) exhibiting different hardness of 615 bhn and 680 bhn was simulated under the same cutting conditions with the SDM and conventional hard turning methods. It was noticeable in all cases that the curve rises from low temperature to its maximum, instantaneously, for both cuts. However, the hardness can result in changes of temperature by using conventional hard turning, which can be seen in Figures 7.4a, b and 7.5a, b. For example, the cutting temperature of D2 680 bhn is higher than D2 615 bhn and the temperature curves show small amplitudes when the hardness is less, but both curves behave in the same pattern in the first and the second cut, regardless of their hardness. Therefore, the effect of thermo-mechanical cyclic loads for a dry cut will be minimal.

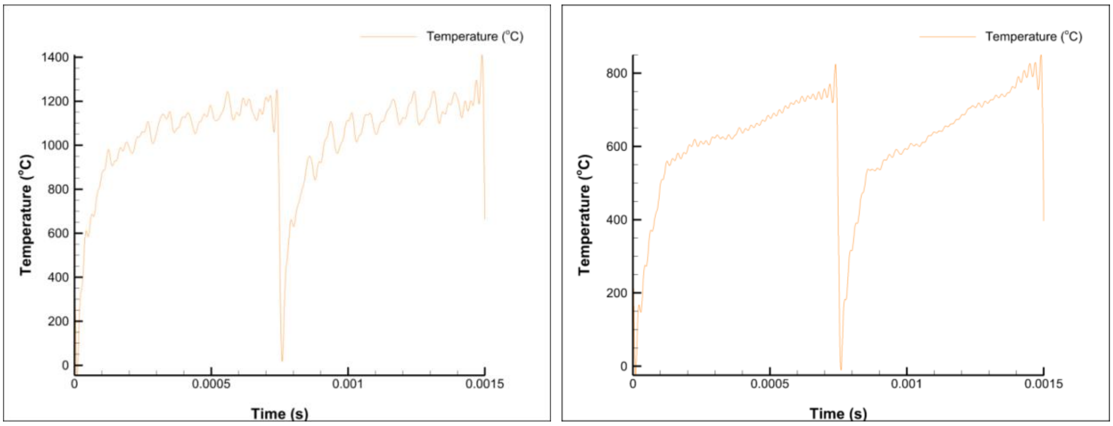

(a) D2 680bhn (b) D2 615bhn

Figure 7.4: Simulation results of the cutting zone temperature: conventional HT

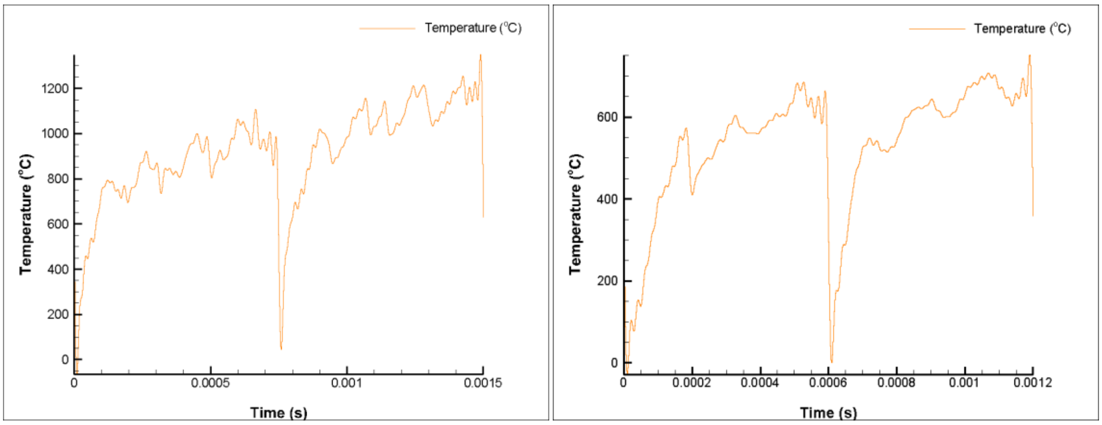

(a) D2 680bhn (b) D2 615bhn

Figure 7.5: Simulation results of the cutting zone temperature: SDM

Table 7.5: Average workpiece temperature obtained after the second cut

Materials		Workpiece temperature	
		Conventional hard turning	SDM method
AISI 8617H	59HRC	1237.35	1133.3
D2	680bhn	1144.19	1082.95

AISI 300m	550bhn	1026.29	783.821
AISI 52100	614bhn	880.497	652.809
AISI 1053	623bhn	862.993	597.06
AISI 1070	627bhn	777.318	555.775
D2	615bhn	740.06	665.145

It is clear from Table 7.5 that workpiece temperature varies from one material to another. Also, the SDM method showed a significant reduction of workpiece temperature. The cutting temperature can be considered as the output of the cutting operation. It is related to the cutting forces, as can be seen from Table 7.6, in that the cutting forces increase with the rising cutting temperature. Cutting temperature can therefore be considered as an index to indicate the machinability of the material i.e. the hard-to-be machined shows higher cutting temperature.

7.4.1 Residual stresses

Figure 7.6 shows the evolution of the residual stresses on the machined surface of the workpiece for the two simulation test cases. The residual stresses were measured with reference to the position of the cutting tool on the workpiece surface, as depicted in the plots. It can be seen from both plots that the compressive stress on the machined surface during conventional machining varies from -20 MPa at the surface top to up to -330 at 0.05 mm depth underneath the machined surface. However, the residual stress shifts to tensile residual stresses from 0.05 mm until it reaches maximum tensile stress of 300 MPa at a depth of 0.15 mm from the machined surface. Conversely, during SDM, the compressive stress initiates at the machined surface from a value of approximately -40 MPa and goes up to -280 MPa at 0.065 mm. Subsequently, a shift from compressive residual stresses to tensile residual stresses occurs at a critical value of 250 MPa, resulting in the workpiece ultimately carrying the compressive residual stresses.

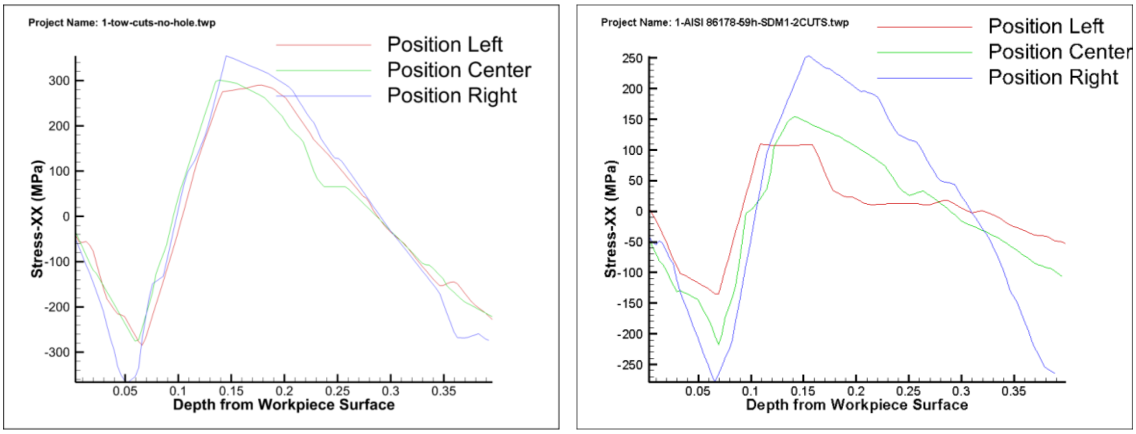

(a) Conventional HT

(b) SDM machining

Figure 7.6: Evolution of residual stresses

7.5 Cyclic cutting forces

Previous research has shown that the cutting force obtained during hard turning exhibits periodic cycles (Vyas and Shaw, 1999; Shaw, 2004).

Thus far, it has not been made clear how these cutting forces can influence the fatigue life of the cutting insert. The cyclic force amplitude can be reduced, depending on the material's properties and cutting parameters, especially cutting speed. Table 7.6 shows the cutting forces for the first cut and the second cut in both conventional and SDM hard turning for the seven different types of steel with different compositions and hardness. The amplitude of the force is observed to vary in each case. The amplitude of the second cut of the conventional hard turning is observed to be higher than the first cut, possibly due to the reduction in the cutting temperature and increase of shear angle. However, when the SDM method is used, the cutting forces and the amplitude are less than in conventional turning. Studying the effect of the performance of the cutting tool, especially fatigue, needs an assessment of the magnitude and repetition cycle of the stresses on the cutting tool. For that purpose the stresses on the cutting tool are obtained and analysed in order to develop a model to predict fatigue crack initiation, which will be discussed in the next section.

Table 7.6: summary of cutting forces obtained from simulated material

	1 Cutting HT forces X		2 Cutting HT forces X		1 Cutting HT forces y		2 Cutting HT forces y		1 Cutting SDM forces X		2 Cutting SDM forces X		1 Cutting SDM forces y		2 Cutting SDM forces y	
Material	**max**	**min**	**max**	**min**	**max**	**min**	**max**	**min**	**max**	**min**	**max**	**min**	**max**	**min**	**max**	**min**
AISI 8617H 59HRC	206	162	214	167.4	69	61.13	72.2	61.4	199.8	77.3	195.8	103.8	84.2	27.8	69.14	49.6
D2 680bhn	232.8	93.4	245.63	97.4	57.63	22.2	57.67	23.9	200.4	34.8	239.14	88.2	57.83	24.8	54.73	37.1
AISI 300m 550bhn	220.91	137.6	229	140.73	59.9	48.5	62.4	49.2	207.8	69	174.8	58	55.4	33.74	56.5	37.6
AISI 52100 614bhn	196.43	97.3	205	99.8	50.9	29	50.9	31	179.5	35	170.8	65	39.4	20.3	41.13	30.8
AISI 1053 623bhn	195.43	90.14	201.7	90.2	49	27.8	49	29.5	156.8	43	155.8	60.6	36.5	21.82	41.1	30.5
AISI 1070 627bhn	174.63	89.2	182.8	92.6	44.8	30.6	47.3	31.2	167	43.4	159	58.6	44.5	21.3	42.8	27.8
D2 615bhn	113.2	109.8	110.8	108	43.63	37.7	42.6	38.53	107.8	38	103.25	53.75	50.3	18.7	38.8	26.8

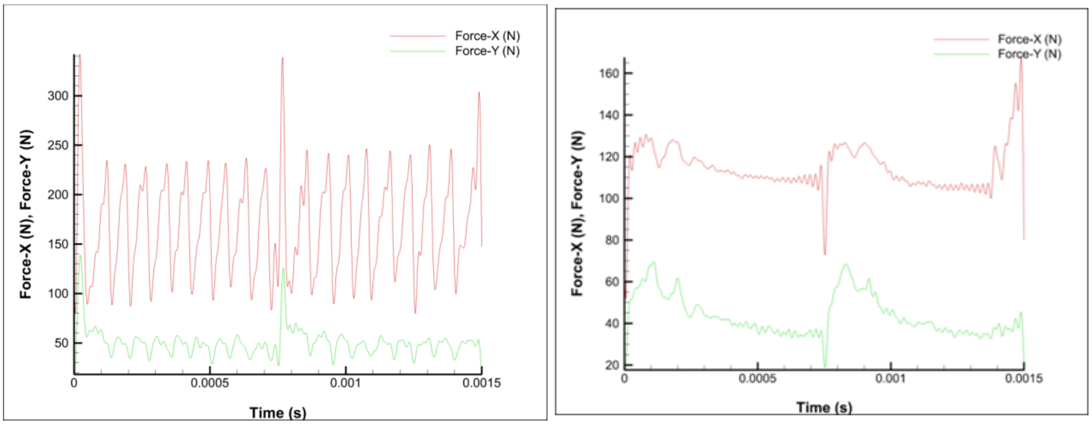

D2 680bhn - saw tooth chip D2 615bhn continuous chip

Figure 7.7: Cyclic force and amplitude for different hardness: conventional HT

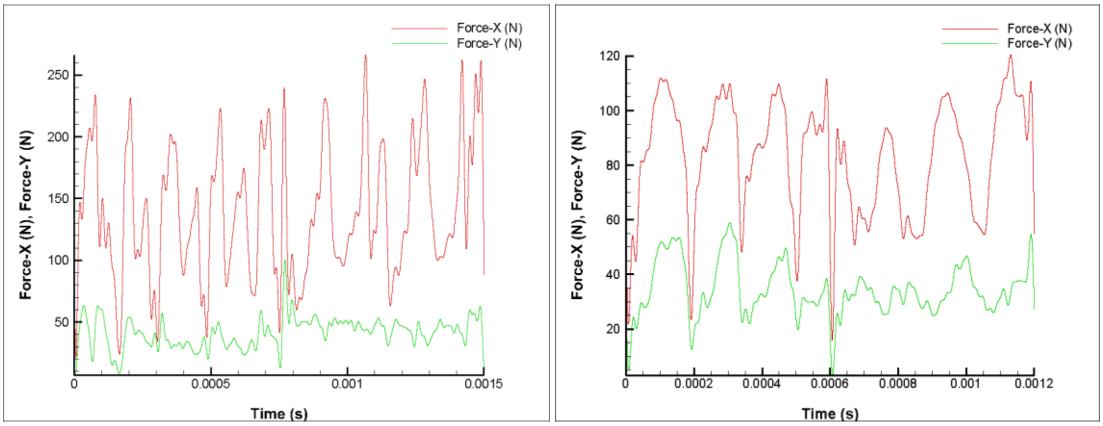

D2 680bhn D2 615bhn

Figure 7.8: Cyclic force and amplitude for different hardness: SDM

7.6 Fatigue crack initiation of the cutting tool

In this section, a theoretical approach is presented to predict the number of cycles of fatigue crack initiation for the cutting tool during the conventional and SDM hard turning process. It is observed from the simulation results that the cutting tool undergoes cyclic loads and cyclic stress in both conventional hard turning and SDM turning methods, as evident from Figures 7.6, 7.7 and Figures 7.8, 7.9.

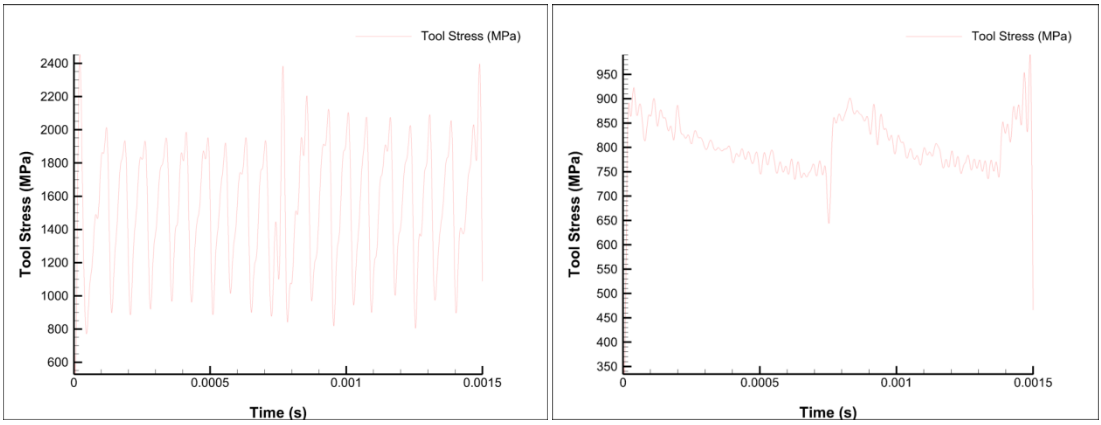

D2

680bhn D2 615bhn

Figure 7.9: Cyclic stress on the cutting tool for different hardness: conventional HT

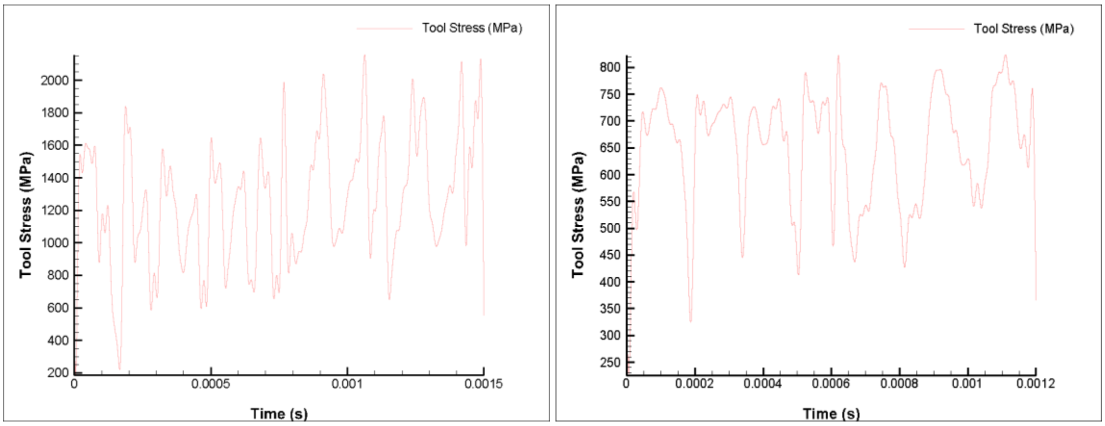

D2 680bhn D2 615bhn

Figure 7.10: Cyclic stress on the cutting tool for different hardness: SDM

This led to further investigation on whether SDM will give rise to fewer or higher numbers of cycles to cause fatigue failure of the tool. In order to illustrate this ambiguity, Forman's equation (Forman et al., 1967) is applied to determine the numbers of cycles needed for fatigue crack initiation on the cutting tool, which can be described as:

$$N_{\mathrm{P}red} = \frac{(1 - R_{rms})K_C - \Delta K_{rms}}{C\,\Delta K_{rms}^{n}} \left(c_f - c_i\right) \tag{7.1}$$

Where, $N_{\mathrm{P}red}$ is the number of load cycles for fatigue crack initiation predicted, R_{rms} is stress ratio, K_C m^0.5 is fracture toughness, ΔK_{rms} is RMS stress intensity factor range, C and n are the coefficient and exponent of Forman's equation, and c_f , c_i are the final and initial crack lengths.

The RMS stress is calculated as follows (Kim et al., 2006):

$$\sigma\max_{rms} = \left[\frac{1}{m}\sum_{i=1}^{m}(\sigma\max)^2\right]^{\frac{1}{2}} \tag{7.2}$$

$$\sigma\min_{rms} = \left[\frac{1}{m}\sum_{i=1}^{m}(\sigma\min)^2\right]^{\frac{1}{2}} \tag{7.3}$$

where: $\sigma\max_{rms}$ and $\sigma\min_{rms}$ are the maximum and minimum stress obtained from the stress on the cutting tool calculated by simulation of both conventional and SDM hard turning, and m is the total number of $\sigma\max_{rms}$ or $\sigma\min_{rms}$ values. Then RMS stress ratio can be found by applying the following relation:

$$R_{rms} = \frac{\sigma\min_{rms}}{\sigma\max_{rms}} \tag{7.4}$$

Fracture toughness K_C m^0.5 is found by applying the following formal:

$$K_C = 1.12\left[\frac{1}{m}\sum_{i=1}^{m}\sigma\max_{rms}\right]\sqrt{3.14\mathrm{a}} \tag{7.5}$$

where a is the crack length.

The RMS stress intensity factor range is calculated by the use of Newman's (Newman, 1973) intensity solution:

$$\Delta K_{rms} = (\sigma \max_{rms} - \sigma \min_{rms}) \cdot \sqrt{\frac{3.14d}{Q}} M_e \tag{7.6}$$

where: d is the crack depth, c is the initial half-crack width and Q is the elastic shape factor for an elliptical crack, which can be found by:

$$Q = 1 + 1.47 \left(\frac{d}{c} \right)^{1.64} \tag{7.7}$$

Me is the elastic magnification factor:

$$Me = \left[M_1 + \left(\sqrt{\frac{Q \cdot C}{d}} - M_1 \right) \left(\frac{d}{t} \right)^p \right] \cdot \left[Sec \frac{3.14 c \cdot d}{W \cdot t} \right]^{\frac{1}{2}} \tag{7.8}$$

where M_1 is the front face correction for the elastic magnification factor:

$$M_1 = 1.13 - 0.1 \left(\frac{d}{c} \right) \tag{7.9}$$

and p the exponent for the elastic magnification factor, can be calculated by:

$$P = 2 + 8 \left(\frac{d}{c} \right)^3 \tag{7.10}$$

All parameters needed for calculating the number of load cycles for fatigue crack initiation are listed in Tables 7.7 and 7.8.

Table 7.7: Summary of the values used in the Forman and Newman's equations

Exponent	Value
a	0.0001 m (Torres et al., 2001)
C and n	4*10^-17, and 5

	(Llanes et al., 2002)
Me	1.015
c	0.000175 m
$c_f - c_i$	0.0001 m (Torres et al., 2001)
d	0.0002 m (Torres et al., 2001)
Q	2.8
K_C	33 MPa m^0.5

Table 7.8 shows the results of $N_{\mathrm{P}red}$ i.e. the predicted number of cycles for fatigue failure of the cutting tool for each type of steel used to simulate both conventional hard turning and the SDM method. The higher value of $N_{\mathrm{P}red}$ means longer fatigue life of the cutting tool and the low value means less fatigue life of the cutting tool. The higher the amplitude of the tool stresses the lower the $N_{\mathrm{P}red}$ value and vice versa. Indeed, SDM shows improved tool life and gives higher $N_{\mathrm{P}red}$ than the conventional hard turning. However, for a material having less hardness, where the saw tooth chip is not the mechanism of deformation, the stress amplitude is low. For example, for D2 of 614 bhn, the $N_{\mathrm{P}red}$ value for conventional turning is slightly higher than for SDM. Consequently, it is asserted that SDM enables the cutting tool to obtain more fatigue life than conventional hard turning, whenever there is a cyclic chip formation resulting in cyclic stress in the cutting tool. Therefore, the fatigue wear is more likely to happen more in conventional hard turning than during SDM.

Table 7.8: Summary of calculated results

materials	$\sigma\max_{rms}$ **MPa HT**	$\sigma\min_{rms}$ **MPa HT**	R_{rms} **HT**	$\sigma\max_{rms}$ **MPa SDM**	$\sigma\min_{rms}$ **MPa SDM**	R_{rms} **SDM**	$N_{\mathrm{P}red}$ **HT**	$N_{\mathrm{P}red}$ **SDM**
AISI 8617H 59HRC	**1650**	**1250**	**0.758**	**1500**	**1100**	**0.733**	**577475245**	**818130748**
D2 680bhn	**1916.489**	**1319.891**	**0.689**	**1522.687**	**932.063**	**0.612**	**49072236**	**163817753**
AISI 300m		**905.7655**	**0.433**	**2019.715**	**897.116**	**0.444**	**905899**	**2207471**

550bhn	**2091.08**							
AISI 52100 614bhn	**1855.36**	**925.1081**	**0.499**	**1594.892**	**718.179**	**0.450**	**10635240**	**28626417**
AISI 1053 623bhn	**1771.896**	**824.4013**	**0.465**	**1529.471**	**665.967**	**0.435**	**13084072**	**35322231**
AISI 1070 627bhn	**1640.03**	**845.3697**	**0.515**	**1403.861**	**623.749**	**0.444**	**38011296**	**69080907**
D2 615bhn	**890**	**740**	**0.831**	**770**	**600**	**0.779**	**1.33121E+11**	**1.02001E+11**

7.7 Summary

In this chapter, an assessment has been made to investigate the influence of previous cut in multi-pass cutting processes by carrying out detailed finite element analysis to compare the performance of the surface defect machining method with a conventional hard turning method. The chip formations generated during the simulations were analysed for the seven different material hardnesses. An analytical analysis was utilized with the support of FEM simulations to predict the fatigue life of the cutting tool. The novelty in the simulation is that, unlike previous simulations, two machining passes were carried out to fully evaluate the effect of the first machining pass over the successive machining pass. For a comprehensive understanding, hard turning of seven different types of steel exhibiting different hardness were simulated. Accordingly, the following points may be concluded:

1. It was noticed that the shear angle increases during the second cut in comparison to the first cut and it is believed to be an outcome of the increased hardness of the workpiece in the second cut.
2. In hard turning, a variety of saw tooth chips can be observed, depending on many factors such as material properties and cutting conditions. Also, the simulation showed discontinuous chips similar to that observed during the experiments.
3. The chip formation mechanism during the SDM method was examined. Other features of SDM machining observed are lower stresses on the cutting tool, lower residual stresses on the machined surface and lower cutting forces than in conventional hard turning.
4. The cyclic cutting forces for conventional hard turning are found to be associated with the chip type formed due to the hardness of the material. The hardness of the steel

will change the form of the cutting chip and this leads to cyclic stress acting on the cutting tool, giving the SDM method advantages over conventional machining by having more fatigue life on the cutting tool.

5. A theoretical analysis was carried out to predict the number of cycles causing fatigue failure of the cutting tool during conventional and SDM hard turning, utilizing Forman’s equation, which showed the SDM method to be superior for tool longevity.

CHAPTER 8– Conclusions and future work

This chapter is divided into three sections covering, respectively, an overall assessment of the contributions made in the thesis, the main conclusions of the work and, finally, the recommendations for future related work.

8.1 Assessment of research contribution

This thesis has provided insights into the current developments that have taken place in the field of hard turning and clarify comprehensively a new method named “surface defect machining”.

The novelty and contribution arising from this research lies in:

- The innovation in the development of a method to create manufacture surface defects on the top of the workpiece using CO_2 high power laser and to apply it successfully in the area of hard turning because any laser induced damage is recoverable during the heat treatment process.
- The method has demonstrated to be of tremednous advantage for all scales ranging from macro/- to micro/- to nano/-. While experiments revealed an Ra value of 30 nm on 69 HRC hard steel parts.
- The lowering of the critical feed rate came as a remarkable finding. This would eventually provide the roadmap to bridge the gap of cutting and grinding processes in terms of attainable surface roughness.
- An analysis is presented to estimate the fatigue life expectency of the cutting tool and was applied to compare the peformance of the tool during SDM and conventional machining approaches. SDM showed longevity of the tool life thereby once again confirming the direct desirable advantages of the SDM method.

8.3 Conclusions of the research

This research aimed to develop a new way to machine hard steels in order to improve the outcome of the machining process, especially for difficult-to-machine materials. The phenomenological understanding of the SDM method to machine hardened steel was investigated comprehensively and compared at all scales with the conventional machining process, using experimental trials and computer simulations. The most striking observation of SDM was to change the mechanism of chip morphology from jagged to discontinuous. This ties in with the fact that SDM enables ease of deformation by shearing the material at reduced input energy. Also, due to the large proportion of stress concentration in the cutting zone - rather than the sub-surface – it enables the machined surface to carry a lesser extent of the residual stresses on the machined surface. This provides a product which has good surface integrity compared to that obtained using conventional hard turning. These advantages point to the fact that a component machined using the SDM method should exhibit improved quality of the machined surface, which was eventually realized to be true. Accordingly, the major findings of this work can be summarized as follows:

1. The purposely generated surface defect on the top surface of the workpiece prior to machining allows easy shearing of the material during cutting, which provides an important unique advantage of chip breaking during hard turning. This is in addition to other favourable outcomes, such as reduced cutting forces, reduced shear plane angle and reduced machining temperature.
2. SDM provides and results in a reduced shear plane angle which enables a better machining action to be obtained, and which was earlier thought to be influenced only by varying the cutting tool rake angle or the workpiece hardness.
3. During SDM, machining stresses are observed to be concentrated in the shear zone, causing a reduction in the residual stresses on the machined surface. This results in a product which has good surface integrity compared to that obtainable by using conventional hard turning.
4. While SDM provides reduced machining temperature in the cutting zone, a reduced tool-chip interface contact length is found to be responsible for both the low heat dissipation and a consequent gradual increase in the temperature at the cutting edge of tool tip; however, this is found to be acceptable, since the temperature is well within the thermal stability range of CBN tools.

5. Relatively higher velocity of chip flow is observed to be a significant advantage

to cause an increase in the cut chip thickness, which, in turn, provides a high strain rate, thus enabling better deformation of the workpiece in the machining zone.

6. One of the most notable features of SDM is that the combination of both cutting and rough polishing actions is found to proceed in tandem with each other, which is responsible for the improved surface roughness.
7. It has been shown that an increase in the peak and valley of the surface defects poses different threats with respect to the application of the component in practice. An increased peak value of the surface roughness will lead to the formation of sites to initiate failures by the virtue of fatigue, creep, tribological or chemical wear. Conversely, a reduced valley in the P-V measure of surface roughness could potentially be the site of accumulation of corrosive media, resulting in corrosion cracking.
8. The quality of the machined surface generated by the mechanical machining process is known to be influenced by the feed rate. There are both upper and lower limitations of the feed rate. A lower feed rate is preferred in practical applications to generate a smooth surface, but only upto a certain critical limit beyond which ploughing and consequent worsening of the machined surface becomes pronounced. In the current investigation, lowering the feed rate beyond the theoretical limits is realized to be a still salient feature of the approach proposed in this work.
9. This is merely a mock up study to demonstrate the effectiveness of the proposed method termed here for the first time as SDM. Within the scope defined for the project, a comprehensive analysis has been provided including summary of development, novelty, and application of the idea. Aside from that, simulation lends further credence both at micro and at nanoscale to the experimental data provided in this thesis. Within the stipulated scope of work, all analysis were done and while the idea of comparing the cost is good, it's not something which can be done with the limited data presented in the work. Even if it's done, it would not be a correct project of the cost for the fact that the fixed cost and variable cost for generation one hole or several holes in assemble line and tooling and setup cost will hugely vary. Moreover, before such a costing comparison, it would be fairer to first optimize the machining parameters to harness the maximum efficiency from SDM. Based on the limited project

experience, the costing should thus be done only on case to case basis. As of this thesis the merits of the SDM are well explained.

8.4 Recommendations for future work

This work is the fundamental investigation of the new “surface defect machining” (SDM) for hard turning. Further development of this technique towards commercialization of this process can be made through a more rigorous scientific or commercial analysis, by looking into cost aspects. Nevertheless, the following still remained as areas for future investigation:

1. Surface defect generation method

The performance of the SDM method relies highly on the topology of the surface defects generated on the workpiece surfaces. Such defects can be generated in many ways, depending on the time and cost considerations. Creation of such defects in a controlled way depending on the kind of material, so that their influence does not go past the intended depth of cut is an area of future research which might be of high relevance, especially in ultra-high precision manufacturing. Moreover, such defects can be created by many methods apart from a laser machine, and this is also an area of future research as to which method suits which material as the best and most economic solution.

2. Study on influence of tool wear

This study should be conducted to evaluate the performance of tool wear in depth and to investigate all types of wear using SDM and conventional hard turning, even diamond turning. Studies on white layer thickness and tool wear during single point diamond turning could be potential areas to enable expand of applicability of SDM into the area of nanometric cutting of hard, brittle materials.

3. Optimization of surface defects

The parameter affecting SDM should be investigated to find the optimal parameters and the influence on each one. The size, inclination and the interspacing of the surface defects is an area which can be investigated to harness the process efficiency to the maximum extent.

4. Use of solid particle coolant

Solid particles can be used by filling up the holes to give further reduction of the temperature in the cutting area. This may reduce the thickness of white layer.

5. Machining white layer with diamond

It is a very interesting idea to study the tool wear of a diamond cutting tool when it is used to remove the white layer. This could result in a new way of machining hard steel to generate a thick white layer and then using diamond tool for finishing.

~~6.~~1.Using different cutting tool materials and geometry

SDM should be applied with different cutting tool materail to reduce the cost of the CBN tool. Also, the tool wear rate should be studied from the economic aspects as well.

List of References:

AOUICI, H., YALLESE, M. A., CHAOUI, K., MABROUKI, T. & RIGAL, J.-F. 2012. Analysis of surface roughness and cutting force components in hard turning with CBN tool: Prediction model and cutting conditions optimization. *Measurement,* 45**,** 344-353.

ARRAZOLA, P. & OZEL, T. 2008. Numerical modelling of 3D hard turning using arbitrary Lagrangian Eulerian finite element method. *International Journal of Machining and Machinability of Materials,* 4**,** 14-25.

ARAMCHAROEN, A. & MATIVENGA, P. 2008. White layer formation and hardening effects in hard turning of H13 tool steel with CrTiAlN and CrTiAlN/MoST-coated carbide tools. *The International Journal of Advanced Manufacturing Technology,* 36**,** 650-657.

ARSECULARATNE, J. A., ZHANG, L. C. & MONTROSS, C. 2006. Wear and tool life of tungsten carbide, PCBN and PCD cutting tools. *International Journal of Machine Tools and Manufacture,* 46**,** 482-491.

ASILTÜRK, I. & AKKUŞ, H. 2011. Determining the effect of cutting parameters on surface roughness in hard turning using the Taguchi method. *Measurement,* 44**,** 1697-1704.

ASLAN, E., CAMUŞCU, N. & BIRGÖREN, B. 2007. Design optimization of cutting parameters when turning hardened AISI 4140 steel (63 HRC) with Al/TiCN mixed ceramic tool. *Materials & design,* 28**,** 1618-1622.

BAILEY, J. 1976. Surface integrity in machining AISI 4340 steel. *J. Eng. Ind. (Trans. ASME, B),* 98**,** 999-1007.

BAILEY, J. A. 1974. On surface damage during machining of AISI 4340 steel. *Wear,* 27**,** 161-173.

BAILEY, J. A. 1977. Surface damage during machining of annealed 18% nickel maraging steel Part 1—Unlubricated conditions. *Wear,* 42**,** 277-296.

BÄKER, M. 2006. Finite element simulation of high-speed cutting forces. *Journal of Materials Processing Technology,* 176**,** 117-126.

BÄKER, M., RÖSLER, J. & SIEMERS, C. 2003. The influence of thermal conductivity on segmented chip formation. *Computational Materials Science,* 26**,** 175-182.

BARRY, J. & BYRNE, G. 2002. TEM study on the surface white layer in two turned hardened steels. *Materials Science and Engineering A,* 325**,** 356-364.

BARTARYA, G. & CHOUDHURY, S. K. 2012. State of the art in hard turning. *International Journal of Machine Tools and Manufacture,* 53, 1-14.

BRINKSMEIER, E., CAMMETT, J., KÖNIG, W., LESKOVAR, P., PETERS, J. & TÖNSHOFF, H. 1982. Residual stresses—measurement and causes in machining processes. *CIRP Annals-Manufacturing Technology,* 31, 491-510.

BIL, H., KıLıÇ, S. & TEKKAYA, A. E. 2004. A comparison of orthogonal cutting data from experiments with three different finite element models. *International Journal of Machine Tools and Manufacture,* 44, 933-944.

BIN RASHID, W., GOEL, S., LUO, X. & RITCHIE, J. M. 2013. The development of a surface defect machining method for hard turning processes. *Wear*.

BOUACHA, K., YALLESE, M. A., MABROUKI, T. & RIGAL, J.-F. 2010. Statistical analysis of surface roughness and cutting forces using response surface methodology in hard turning of AISI 52100 bearing steel with CBN tool. *International Journal of Refractory Metals and Hard Materials,* 28, 349-361.

BRESSELER, B., EL-WARDANY, T. & ELBESTAWI, M. 1997. Material side flow in high speed finish boring of case hardened steel. *In:* 1st French and German Conference on High Speed Machining, 1997. 196-206.

BROSKEA, T. 2001. Analyzing PCBN tool wear. *Modern Machine Shop (USA),* 73, 86-93.

CAI, M., LI, X. & RAHMAN, M. 2007a. Characteristics of “dynamic hard particles” in nanoscale ductile mode cutting of monocrystalline silicon with diamond tools in relation to tool groove wear. *Wear,* 263, 1459-1466.

CAI, M., LI, X. & RAHMAN, M. 2007b. Study of the mechanism of groove wear of the diamond tool in nanoscale ductile mode cutting of monocrystalline silicon. *Journal of Manufacturing Science and Engineering,* 129, 281-286.

CHAO, B. & TRIGGER, K. 1951. Cutting temperatures and metal-cutting phenomena. *Trans. ASME,* 73, 771.

CHILDS, T. 1998. Material property needs in modeling metal machining. *Machining Science and Technology,* 2, 303-316.

CHILDS.T, M. K., OBIKAW.T, YAMANE.Y, 2000. *Metal Machining Theory and Applications*.

CHOU, Y.-S. 1994. *Wear mechanisms of cubic boron nitride tools in precision turning of hardened steels.* Ph.D, Purdue University.

CHOU, Y. K., EVANS, C. J. & BARASH, M. M. 2003. Experimental investigation on cubic boron nitride turning of hardened AISI 52100 steel. *Journal of Materials Processing Technology,* 134**,** 1-9.

CHOU, Y. K. & EVANS, C. J. 1999. White layers and thermal modeling of hard turned surfaces. *International Journal of Machine Tools and Manufacture,* 39**,** 1863-1881.

CHRYSSOLOURIS, G. 1982. Turning of hardened steels using CBN tools. *Journal of Applied Metalworking,* 2**,** 100-106.

CHUZHOV, L., DEVOR, R., KAPOOR, S. & BAMMANN, D. 2002. Microstructure-level modeling of ductile iron machining. *Journal of Manufacturing Science and Engineering,* 124**,** 162-169.

CHUZHOY, L., DEVOR, R. & KAPOOR, S. 2003a. Machining simulation of ductile iron and its constituents, part 2: numerical simulation and experimental validation of machining. *Journal of Manufacturing Science and Engineering,* 125**,** 192-201.

CHUZHOY, L., DEVOR, R., KAPOOR, S., BEAUDOIN, A. & BAMMANN, D. 2003b. Machining simulation of ductile iron and its constituents, part 1: Estimation of material model parameters and their validation. *Journal of Manufacturing Science and Engineering,* 125**,** 181-191.

CIRSTOIU, C. A. 2005. Influence of feed rate on surface roughness in turning processes with different tool inserts. *University" Politehnica" of Bucharest Scientific Bulletin, Series D: Mechanical Engineering,* 67**,** 63-70.

COELHO, R. T., NG, E.-G. & ELBESTAWI, M. A. 2007. Tool wear when turning hardened AISI 4340 with coated PCBN tools using finishing cutting conditions. *International Journal of Machine Tools and Manufacture,* 47**,** 263-272.

ÇYDAŞ, U. 2010. Machinability evaluation in hard turning of AISI 4340 steel with different cutting tools using statistical techniques. *Proceedings of the Institution of Mechanical Engineers, Part B: Journal of Engineering Manufacture,* 224**,** 1043-1055.

DANIEL P. SOROKA, H. I. 2013. Hard Turning and The Machine Tool. Elmira, NY.

DAVIES, M. A. & BURNS, T. J. 2001. Thermomechanical oscillations in material flow during high-speed machining. *Philosophical Transactions of the Royal Society of London. Series A: Mathematical, Physical and Engineering Sciences,* 359**,** 821-846.

DAVIES, M. A., BURNS, T. J. & EVANS, C. J. 1997. On the Dynamics of Chip Formation in Machining Hard Metals. *CIRP Annals - Manufacturing Technology,* 46**,** 25-30.

DAVIES, M. A., FICK, S. E. & EVANS, C. J. 1996. Dynamic measurement of shear band formation in precision hard turning. *Liber Amicorum, Professor Paul Vanherck, etenschapper, Ingenieur en Pedagoog, ISBN 90-73802-56-3, Katholieke Universiteit Leuven.*

DAVIM, J. P. 2001. A note on the determination of optimal cutting conditions for surface finish obtained in turning using design of experiments. *Journal of Materials Processing Technology,* 116**,** 305-308.

DAVIM, J. P. 2003. Design of optimisation of cutting parameters for turning metal matrix composites based on the orthogonal arrays. *Journal of Materials Processing Technology,* 132**,** 340-344.

DAVIM, J. P. & FIGUEIRA, L. 2007. Machinability evaluation in hard turning of cold work tool steel (D2) with ceramic tools using statistical techniques. *Materials & design,* 28**,** 1186-1191.

DAWSON, T. G. & KURFESS, T. R. 2001. Tool life, wear rates, and surface quality in hard turning. *TRANSACTIONS-NORTH AMERICAN MANUFACTURING RESEARCH INSTITUTION OF SME***,** 175-182.

DOGRA, M., SHARMA, V. & DUREJA, J. 2011. Effect of tool geometry variation on finish turning - A Review. *Engineering Science and Technology Review,* 4**,** 13.

DOGRA, M., SHARMA, V., SACHDEVA, A., SURI, N. & DUREJA, J. 2010. Tool wear, chip formation and workpiece surface issues in CBN hard turning: A review. *International Journal of Precision Engineering and Manufacturing,* 11**,** 341-358.

DORNFELD, D., MIN, S. & TAKEUCHI, Y. 2006. Recent Advances in Mechanical Micromachining. *CIRP Annals - Manufacturing Technology,* 55**,** 745-768.

EL-WARDANY, T. & ELBESTAWI, M. 1998. Phenomenological analysis of material side flow in hard turning: causes, modeling, and elimination. *Machining Science and Technology,* 2**,** 239-251.

EL-WARDANY, T., MOHAMED, E. & ELBESTAWI, M. 1993. Material side flow in finish turning of hardened steel with ceramic tools. *ASME-PUBLICATIONS-PED,* 67**,** 159-159.

EL-WARDANY, T. I., KISHAWY, H. A. & ELBESTAWI, M. A. 2000a. Surface integrity of die material in high speed hard machining, part 1: Micrographical analysis. *Journal of Manufacturing Science and Engineering-Transactions of the Asme,* 122**,** 620-631.

EL-WARDANY, T. I., KISHAWY, H. A. & ELBESTAWI, M. A. 2000b. Surface integrity of die material in high speed hard machining, part 2: Microhardness variations and residual stresses. *Journal of Manufacturing Science and Engineering-Transactions of the Asme,* 122**,** 632-641.

FENG, C.-X. & WANG, X.-F. 2003. Surface roughness predictive modeling: neural networks versus regression. *IIE Transactions,* 35**,** 11-27.

FORMAN, R. G., KEARNEY, V. & ENGLE, R. 1967. Numerical analysis of crack propagation in cyclic-loaded structures. *Journal of Basic Engineering,* 89**,** 459.

GOEL, S., RASHID, W. B., LUO, X., AGRAWAL, A. & JAIN, V. 2013. A theoretical assessment of surface defect machining and hot machining of nanocrystalline silicon carbide. *Wear,* 302**,** 1124-1135.

GRZESIK, W. 2011. *Mechanics of Cutting and Chip Formation, in Machining Hard Materials* Springer London.

GRZESIK, W., RECH, J. & WANAT, T. 2007. Surface finish on hardened bearing steel parts produced by superhard and abrasive tools. *International Journal of Machine Tools and Manufacture,* 47**,** 255-262.

GUO, Y., WARREN, A. & HASHIMOTO, F. 2010. The basic relationships between residual stress, white layer, and fatigue life of hard turned and ground surfaces in rolling contact. *CIRP Journal of manufacturing science and technology,* 2**,** 129-134.

GUO, Y., ANURAG, S. & JAWAHIR, I. 2009. A novel hybrid predictive model and validation of unique hook-shaped residual stress profiles in hard turning. *CIRP Annals-Manufacturing Technology,* 58**,** 81-84.

GUO, Y. & SAHNI, J. 2004. A comparative study of hard turned and cylindrically ground white layers. *International Journal of Machine Tools and Manufacture,* 44**,** 135-145.

GUO, Y. & BARKEY, M. E. 2004. Modeling of rolling contact fatigue for hard machined components with process-induced residual stress. *International Journal of Fatigue,* 26**,** 605-613.

GUO, Y. & LIU, C. 2002a. FEM analysis of mechanical state on sequentially machined surfaces. *Machining Science and Technology,* Vol. 6, No. 1, pp. 21-4.

GUO, Y. & YEN, D. W. 2004. Hard turning versus grinding—the effect of process-induced residual stress on rolling contact. *Wear,* 256**,** 393-399.

GUO, Y. B. & LIU, C. R. 2002b. 3D FEA modeling of hard turning. *Journal of Manufacturing Science and Engineering-Transactions of the Asme,* 124**,** 189-199.

HUA, J. & SHIVPURI, R. 2004. Prediction of chip morphology and segmentation during the machining of titanium alloys. *Journal of Materials Processing Technology,* 150**,** 124-133.

HUA, J., SHIVPURI, R., CHENG, X., BEDEKAR, V., MATSUMOTO, Y., HASHIMOTO, F. & WATKINS, T. R. 2005. Effect of feed rate, workpiece hardness and cutting edge on subsurface residual stress in the hard turning of bearing steel using chamfer+ hone cutting edge geometry. *Materials Science and Engineering: A,* 394**,** 238-248.

HUANG, Y. 2002. *Predictive Modeling of Tool Wear Rate with Applications to CBN Hard Turning.* PhD Dissertation, Georgia Institute of Technology, Georgia.

HUANG, Y. & DAWSON, T. G. 2005. Tool crater wear depth modeling in CBN hard turning. *Wear,* 258**,** 1455-1461.

Hardinge Inc., H. 2014. http://www.hardinge.com/index.asp?pageID=64&cID=54.

JACOBSON, M. 2002. Surface integrity of hard-turned M50 steel. *Proceedings of the Institution of Mechanical Engineers, Part B: Journal of Engineering Manufacture,* 216**,** 47-54.

JASPERS, S. & DAUTZENBERG, J. 2002. Material behaviour in conditions similar to metal cutting: flow stress in the primary shear zone. *Journal of Materials Processing Technology,* 122**,** 322-330.

JOHNSON, G. R. & COOK, W. H. 1985. Fracture characteristics of three metals subjected to various strains, strain rates, temperatures and pressures. *Engineering Fracture Mechanics,* 21**,** 31-48.

KALPAKJIAN, S. & SCHMID, S. R. 2006. *Manufacturing Engineering and Technology,* Pearson Prentice Hall.

KIRBY, E. D. 2006. A parameter design study in a turning operation using the Taguchi method. *The Technology Interface/ Fall 2006.*

KIM, S. T., TADJIEV, D. & YANG, H. T. 2006. Fatigue life prediction under random loading conditions in 7475-T7351 aluminum alloy using the RMS model. *International Journal of Damage Mechanics,* 15**,** 89-102.

KISHAWY, H. & ELBESTAWI, M. 2001. Tool wear and surface integrity during high-speed turning of hardened steel with polycrystalline cubic boron nitride tools.

Proceedings of the Institution of Mechanical Engineers, Part B: Journal of Engineering Manufacture, 215**,** 755-767.

KISHAWY, H. & ELBESTAWI, M. 1999. Effects of process parameters on material side flow during hard turning. *International Journal of Machine Tools and Manufacture,* 39**,** 1017-1030.

KLOCKE, F., RAEDT, H.-W. & HOPPE, S. 2001. 2D-FEM simulation of the orthogonal high speed cutting process. *Machining Science &Technology*, Vol. 5, no. 3, pp. 117-124.

KO, T. J. & KIM, H. S. 2001. Surface Integrity and Machineability in Intermittent Hard Turning. *The International Journal of Advanced Manufacturing Technology,* 18**,** 168-175.

KOMANDURI, R. & SHAW, M. 1975. Wear of synthetic diamond when grinding ferrous metals. *Nature*, 255, 211-213.

KOMANDURI, R. S., T . HAZRA, J . VON TURKOVICH, B F . FLOM, D G 1982. On the Catastrophic Shear Instability in High-Speed Machining of an AISI 4340 Stee. *Trans. ASME,* 104**,** 10.

KOMANDURI, R., LEE, M., FLOM, D. G., THOMPSON, R. A., JONES, M. G. & DOUGLAS, R. J. 1982. Pulse laser pretreated machining. US Patent No. 4356376 against application no. 263235, Assignee: General Electric Company, N.Y., United States of America, 6th October 1982.

KÖNIG, W., BERKTOLD, A. & KOCH, K. F. 1993. Turning versus Grinding - A Comparison of Surface Integrity Aspects and Attainable Accuracies. *CIRP Annals - Manufacturing Technology,* 42**,** 39-43.

KOPAC, J., KOROSEC, M. & KUZMAN, K. 2001. Determination of flow stress properties of machinable materials with help of simple compression and orthogonal machining test. *International Journal of Machine Tools and Manufacture,* 41**,** 1275-1282.

KOSKILINNA, J. 2007. *Quantum chemical studies on atomic-scale tribology of diamond and boron nitride,* University of Joensuu.

KUMAR, S., FALLBÖHMER, P. & ALTAN, T. 1997. Computer Simulation of Orthogonal Metal Cutting Process: Determination of Material Properties and Effects of Tool Geometry on Chip Flow. *TRANSACTIONS-NORTH AMERICAN MANUFACTURING RESEARCH INSTITUTION OF SME***,** 33-38.

LAHIFF, C., GORDON, S. & PHELAN, P. 2007. PCBN tool wear modes and mechanisms in finish hard turning. *Robotics and Computer-Integrated Manufacturing,* 23**,** 638-644.

LEI, S., SHIN, Y. & INCROPERA, F. 1999. Thermo-mechanical modeling of orthogonal machining process by finite element analysis. *International Journal of Machine Tools and Manufacture,* 39**,** 731-750.

LIN, C. 2004. Use of the Taguchi method and grey relational analysis to optimize turning operations with multiple performance characteristics. *Materials and Manufacturing Processes,* 19**,** 209-220.

LIU, K. & MELKOTE, S. N. 2006. Effect of plastic side flow on surface roughness in micro-turning process. *International Journal of Machine Tools and Manufacture,* 46**,** 1778-1785.

LLANES, L., TORRES, Y. & ANGLADA, M. 2002. On the fatigue crack growth behavior of WC–Co cemented carbides: kinetics description, microstructural effects and fatigue sensitivity. *Acta Materialia,* 50**,** 2381-2393.

LUNDBLAD, M. Year. Influence of cutting speed on residual stresses in the work piece. *In:* Second international seminar on improving machine tool performance, held at La Baule, France, 2000.

LUO, S. Y., LIAO, Y. S. & TSAI, Y. Y. 1999. Wear characteristics in turning high hardness alloy steel by ceramic and CBN tools. *Journal of Materials Processing Technology,* 88**,** 114-121.

MANDAL, N., DOLOI, B. & MONDAL, B. 2012. Force prediction model of Zirconia Toughened Alumina (ZTA) inserts in hard turning of AISI 4340 steel using response surface methodology. *International Journal of Precision Engineering and Manufacturing,* 13**,** 1589-1599.

MANNA, A. & BHATTACHARYYA, B. 2004. Investigation for optimal parametric combination for achieving better surface finish during turning of Al/SiC-MMC. *The International Journal of Advanced Manufacturing Technology,* 23**,** 658-665.

MARUSICH, T. & ORTIZ, M. 1995. Modelling and simulation of high-speed machining. *International Journal for Numerical Methods in Engineering,* 38**,** 3675-3694.

MATHEW, P. & ARYA, N. 1993. Material Properties from Machining. *Dynamic Loading in Manufacturing and Service: Preprints of Papers***,** 33.

MATSUMOTO, Y., HASHIMOTO, F. & LAHOTI, G. 1999. Surface Integrity Generated by Precision Hard Turning. *CIRP Annals - Manufacturing Technology,* 48**,** 59-62.

MATSUMOTO, Y., BARASH, M. & LIU, C. 1986. Effect of hardness on the surface integrity of AISI 4340 steel. *J. Eng. Ind.(Trans. ASME),* 108**,** 169-175.

MATSUMOTO, Y., BARASH, M. & LIU, C. 1987. Cutting mechanism during machining of hardened steel. *Materials Science and Technology,* 3**,** 299-305.

MEHRBAN, M., NADERI, D., PANAHIZADEH, V. & NAEINI, H. M. 2008. Modelling of Tool Life in Turning Process Using Experimental Method. *International journal of material forming,* 1**,** 559-562.

M.G. COCKCROFT, D. J. L. 1968. Ductility and the workability of metals. *J. Inst. Met,* 96**,** 33-39.

MITAL, A. & MEHTA, M. 1988. Surface finish prediction models for fine turning. *International Journal of Production Research,* 26**,** 1861 - 1876.

MOYLAN, S., KOMPELLA, S., CHANDRASEKAR, S. & FARRIS, T. 2001. A nano-indentation study of the mechanical propeties of thin surface layers affected by manufacturing processes. *Tribology Series,* 39**,** 895-903.

NAKAI, T. N., S. TOMITA, K. GOTO, M June 1991. Hard Turning by PCBN *Superabrasives '91.* Chicago, Illinois; USA.

NARULKAR, R. 2009. *Investigation on the mechanism of wear of single crystal diamond tool in nanometric cutting of iron using molecular dynamics (MD) and the development of generalized potential energy surfaces (GPES) based on ab initio calculations.*

NAKAYAMA, K., ARAI, M. & KANDA, T. 1988. Machining characteristics of hard materials. *CIRP Annals-Manufacturing Technology,* 37**,** 89-92.

NAKAYAMA, K. 1997. Topics on fundamentals of precision machining. *Machining Science and Technology,* 1**,** 251-262.

NEWMAN, J. 1973. Fracture analysis of surface-and through-cracked sheets and plates. *Engineering Fracture Mechanics,* 5**,** 667-689.

NG, E.-G., ASPINWALL, D., BRAZIL, D. & MONAGHAN, J. 1999. Modelling of temperature and forces when orthogonally machining hardened steel. *International Journal of Machine Tools and Manufacture,* 39**,** 885-903.

NG, E.-G., EL-WARDANY, T. I., DUMITRESCU, M. & ELBESTAWI, M. A. 2002. Physics-based simulation of high speed machining. *Machining Science and Technology,* 6**,** 301-329.

NOUARI, M., LIST, G., GIROT, F. & COUPARD, D. 2003. Experimental analysis and optimisation of tool wear in dry machining of aluminium alloys. *Wear,* 255**,** 1359-1368.

OXLEY, P. L. B. & YOUNG, H. 1989. The mechanics of machining: an analytical approach to assessing machinability: hattp://ntur.lib.ntu.edu.tw/handle/246246/217047 [accessed 1989-07]

OYANE, M., TAKASHIMA, F., OSAKADA, K. & TANAKA, H. Year. The behaviour of some steels under dynamic compression. *In:* 10th Japan Congress on Testing Materials, 1967.

ÖZEL, T. 2003. Modeling of hard part machining: effect of insert edge preparation in CBN cutting tools. *Journal of Materials Processing Technology,* 141**,** 284-293.

ÖZEL, T. & ALTAN, T. 2000. Determination of workpiece flow stress and friction at the chip–tool contact for high-speed cutting. *International Journal of Machine Tools and Manufacture,* 40**,** 133-152.

ÖZEL, T., HSU, T.-K. & ZEREN, E. 2005a. Effects of cutting edge geometry, workpiece hardness, feed rate and cutting speed on surface roughness and forces in finish turning of hardened AISI H13 steel. *The International Journal of Advanced Manufacturing Technology,* 25**,** 262-269.

ÖZEL, T., HSU, T.-K. & ZEREN, E. 2005b. Effects of cutting edge geometry, workpiece hardness, feed rate and cutting speed on surface roughness and forces in finish turning of hardened AISI H13 steel. *The International Journal of Advanced Manufacturing Technology,* 25**,** 262-269.

ÖZEL, T. & KARPAT, Y. 2005. Predictive modeling of surface roughness and tool wear in hard turning using regression and neural networks. *International Journal of Machine Tools and Manufacture,* 45**,** 467-479.

ÖZEL, T., KARPAT, Y., FIGUEIRA, L. & DAVIM, J. P. 2007. Modelling of surface finish and tool flank wear in turning of AISI D2 steel with ceramic wiper inserts. *Journal of Materials Processing Technology,* 189**,** 192-198.

PEKELHARING, A. & GIESZEN, C. 1971. Material side flow in finish turning. *Annals of the CIRP,* 20**,** 21-22.

POULACHON, G., MOISAN, A. & JAWAHIR, I. S. 2001. Tool-wear mechanisms in hard turning with polycrystalline cubic boron nitride tools. *Wear,* 250**,** 576-586.

POULACHON, G. & MOISAN, A. L. 2000. Hard Turning: Chip Formation Mechanisms and Metallurgical Aspects. *Journal of Manufacturing Science and Engineering,* 122**,** 406-412.

RAMESH, A. 2002. *Prediction of Process-Induced Microstructural Changes and Residual Stresses in Orthogonal Hard Machining.* Ph.D. Dissertation, Georgia Institute of Technology.

RAVINDRA, D. 2011. *Ductile mode material removal of ceramics and semiconductors.* PhD, Western Michigan University.

RASHID, W. B., GOEL, S., LUO, X. & RITCHIE, J. M. 2013. An experimental investigation for the improvement of attainable surface roughness during hard turning process. *Proceedings of the Institution of Mechanical Engineers, Part B: Journal of Engineering Manufacture,* 227**,** 338-342.

ROSS, P. J. 1995. Taguchi techniques for quality engineering (2nd ed'95).

TAGUCHI, G. & KONISHI, S. 1987. *Orthogonal arrays and linear graphs: tools for quality engineering*, American Supplier Institute Allen Park, MI.

SADAT, A. 1990. Effect of high cutting speed on surface integrity of AISI 4340 steel during turning. *Materials Science and Technology,* 6**,** 371-375.

SADAT, A. & BAILEY, J. 1987. Residual stresses in turned AISI 4340 steel. *Experimental Mechanics,* 27**,** 80-85.

SANDVIKENS 2013. Switch to hard-part turning. http://www2.coromant.sandvik.com/coromant/pdf/Hard_part_turning/C-1040-069.pdf Printed in Sweden, AB Sandvikens Tryckeri. © AB Sandvik Coromant 2005.10.

SARTKULVANICH, P., KOPPKA, F. & ALTAN, T. 2004. Determination of flow stress for metal cutting simulation—a progress report. *Journal of Materials Processing Technology,* 146**,** 61-71.

SATA, T. 1966. Surface finish in metal cutting. *CIRP ANN,* 12**,** 190-197.

SCHWACH, D. W. & GUO, Y. 2006. A fundamental study on the impact of surface integrity by hard turning on rolling contact fatigue. *International journal of Fatigue,* 28**,** 1838-1844.

SELVAM, M. & RADHAKRISHNAN, V. 1973. Influence of side-flow and built-up edge on the roughness and hardness of the surface machined with a single point tool. *Wear,* 26**,** 393-403.

SECO 2003. Secomax PCBN Technical Guide (www.secotools.com). SECO Tools AB, SE-737 82 Fagersta, Sweden: Sweden. p. 41.

SHATLA, M., KERK, C. & ALTAN, T. 2001a. Process modeling in machining. Part I: determination of flow stress data. *International Journal of Machine Tools and Manufacture,* 41**,** 1511-1534.

SHATLA, M., KERK, C. & ALTAN, T. 2001b. Process modeling in machining. Part II: validation and applications of the determined flow stress data. *International Journal of Machine Tools and Manufacture,* 41**,** 1659-1680.

SHATLA, M. N. 1999. *Prediction of forces, stressses, temperatures and tool wear in metal cutting.* Ohio State University.

SHAW, M. C. 2004. *Metal cutting principles,* Oxford Series on Advanced Manufacturing, Editor: J.R. Crookall, M.C. Shaw, and N.P. Suh. New York: Oxford University Press.

SHAW, M. C. & VYAS, A. 1998. The Mechanism of Chip Formation with Hard Turning Steel. *CIRP Annals - Manufacturing Technology,* 47**,** 77-82.

SIDPARA, A. M. & JAIN, V. 2012. Nanofinishing of freeform surfaces of prosthetic knee joint implant. *Proceedings of the Institution of Mechanical Engineers, Part B: Journal of Engineering Manufacture,* 226**,** 1833-1846.

SINGH, D. & RAO, P. 2007. A surface roughness prediction model for hard turning process. *The International Journal of Advanced Manufacturing Technology,* 32**,** 1115-1124.

STEVENSON, R. 1997. Study on the correlation of workpiece mechanical properties from compression and cutting tests. *Machining Science and Technology,* 1**,** 67-79.

SUNDARAM, R. & K LAMBERT, B. 1981. Mathematical models to predict surface finish in fine turning of steel. Part II. *THE INTERNATIONAL JOURNAL OF PRODUCTION RESEARCH,* 19**,** 557-564.

SUNDARAM, R. & LAMBERT, B. 1981. Mathematical models to predict surface finish in fine turning of steel. Part I. *THE INTERNATIONAL JOURNAL OF PRODUCTION RESEARCH,* 19**,** 547-556.

SURESH, P., VENKATESWARA RAO, P. & DESHMUKH, S. 2002. A genetic algorithmic approach for optimization of surface roughness prediction model. *International Journal of Machine Tools and Manufacture,* 42**,** 675-680.

SURESH, R., BASAVARAJAPPA, S., GAITONDE, V. N., SAMUEL, G. & DAVIM, J. P. 2013. State-of-the-art research in machinability of hardened steels. *Proceedings of the Institution of Mechanical Engineers, Part B: Journal of Engineering Manufacture,* 227**,** 191-209.

SURESH, R., BASAVARAJAPPA, S. & SAMUEL, G. 2012. Some studies on hard turning of AISI 4340 steel using multilayer coated carbide tool. *Measurement,* 45**,** 1872-1884.

SUN, S., BRANDT, M. & DARGUSCH, M. 2010. Thermally enhanced machining of hard-to-machine materials—A review. *International Journal of Machine Tools and Manufacture,* 50**,** 663-680.

T. SATA & SHAW, M. C. 1964. Behavior of cellular materials undergoing plastic flow. *CIRP Annals* 12**,** 190.

TAMIZHARASAN, T., SELVARAJ, T. & HAQ, A. N. 2006. Analysis of tool wear and surface finish in hard turning. *The International Journal of Advanced Manufacturing Technology,* 28**,** 671-679.

THAMIZHMANII, S., SAPARUDIN, S. & HASAN, S. 2007. Analyses of surface roughness by turning process using Taguchi method. *Journal of Achievements in Materials and Manufacturing Engineering,* 20**,** 503-506.

THIELE, D. M., N.PEASCOE, A.WATKINS, R. 2002. Effect of Cutting-Edge Geometry and Workpiece Hardness on Surface Residual Stresses in Finish Hard Turning of AISI 52100 Steel. *Manufacturing Science and Engineering,* 122.

THIELE, J. D. & N MELKOTE, S. 1999. Effect of cutting edge geometry and workpiece hardness on surface generation in the finish hard turning of AISI 52100 steel. *Journal of Materials Processing Technology,* 94**,** 216-226.

THIELE, J. D. & N. MELKOTE, S. 1999. Effect of cutting edge geometry and workpiece hardness on surface generation in the finish hard turning of AISI 52100 steel. *Journal of Materials Processing Technology,* 94**,** 216-226.

TÖNSHOFF, H. K., ARENDT, C. & AMOR, R. B. 2000. Cutting of Hardened Steel. *CIRP Annals - Manufacturing Technology,* 49**,** 547-566.

TORRES, Y., CASELLAS, D., ANGLADA, M. & LLANES, L. 2001. Fracture toughness evaluation of hardmetals: influence of testing procedure. *International Journal of Refractory Metals and Hard Materials,* 19**,** 27-34.

TUTUNEA-FATAN, O., FAKHRI, M. & BORDATCHEV, E. 2011. Porosity and cutting forces: from macroscale to microscale machining correlations. *Proceedings of the Institution of Mechanical Engineers, Part B: Journal of Engineering Manufacture,* 225**,** 619-630.

UMBRELLO, D., HUA, J. & SHIVPURI, R. 2004. Hardness-based flow stress and fracture models for numerical simulation of hard machining AISI 52100 bearing steel. *Materials Science and Engineering: A,* 374**,** 90-100.

VERNON, A. & ÖZEL, T. 2003. Factors affecting surface roughness in finish hard turning. *In:* 17th International Conference on Production Research, Blacksburg, Virginia, 2003.

VYAS, A. & SHAW, M. 1999. Mechanics of saw-tooth chip formation in metal cutting. *Journal of Manufacturing Science and Engineering,* 121**,** 163-172.

WAN, Y., CHENG, K., LIU, Z. & YE, H. 2013. An investigation on machinability assessment of difficult-to-cut materials based on radar charts. *Proceedings of the Institution of Mechanical Engineers, Part B: Journal of Engineering Manufacture,* 227**,** 1916-1920.

WARREN, A. & GUO, Y. 2009. Characteristics of residual stress profiles in hard turned versus ground surfaces with and without a white layer. *Journal of Manufacturing Science and Engineering,* 131.

WILLIAM, D. 2007. *Materials Science and Engineering an Introduction,* John Wiley and Sons.

WU, D. & MATSUMOTO, Y. 1990. The effect of hardness on residual stresses in orthogonal machining of AISI 4340 steel. *Journal of Engineering for Industry (Transactions of the ASME),* 112**,** 245-252.

WU, M., GURUZ, M., DRAVID, V., CHUNG, Y., ANDERS, S., FREIRE, F. & MARIOTTO, G. 2000. Formation of carbon nitride with superlattice coatings. *Applied Physics Letters,* 76**,** 2692-2694.

XUEPING, Z., ERWEI, G. & RICHARD LIU, C. 2009. Optimization of process parameter of residual stresses for hard turned surfaces. *Journal of Materials Processing Technology,* 209**,** 4286-4291.

YANG, W. & TARNG, Y. 1998. Design optimization of cutting parameters for turning operations based on the Taguchi method. *Journal of Materials Processing Technology,* 84**,** 122-129.

YEN, Y.-C. 2004. *Modeling of metal cutting and ball burnishing-prediction of tool wear and surface properties.* Ohio State University.

YIH-FONG, T. 2006. Parameter design optimisation of computerised numerical control turning tool steels for high dimensional precision and accuracy. *Materials & design,* 27**,** 665-675.

YONG, H. & STEVEN, L. 2005. Modeling of cutting forces under hard turning conditions considering tool wear effect. *ASME,* 127.

ZHANG, J. 2005. *Process optimization for machining of hardened steels.* Ph.D. Dissertation, Georgia Institute of Technology.

ZHANG, X., LIU, C. R. & YAO, Z. 2007. Experimental study and evaluation methodology on hard surface integrity. *The International Journal of Advanced Manufacturing Technology,* 34**,** 141-148.

ZHOU, J., BUSHLYA, V. & STAHL, J. 2011. An investigation of surface damage in the high speed turning of Inconel 718 with use of whisker reinforced ceramic tools. *Journal of Materials Processing Technology*.

Appendices

A. Comparison between surface defects machining and vibration assisted machining

Vibration assisted machining (VAM) and surface defects machining (SDM)	Similarities	Differences
Cutting forces on tool	Reduced cutting forces provide better surface finish and tool longevity.	Not applicable
Overall cutting load on tool	Not applicable	In VAM, periodic reduction in cutting load occurs at specified amplitude whereas in SDM cutting load reduces where dislocations in the form of holes are encountered.
Volume of material removal	Not applicable	Although, tool is periodically rotated to reduce the cutting load, the total material to be removed during VAM process remains unchanged. In SDM, due to the vacancies made in the form of holes, some of the volume of the material to be removed reduces.
Tool contact with chips	Not applicable	In VAM cutting tool loses contact with the chips on specified amplitude whereas in SDM cutting chips remains in continuous contact with the tool.
Operational time	Not applicable	No cutting action took place

		while the tool is disengaged in VAM whereas in SDM continuous cutting takes place.
Requirement of machine tool	Not applicable	Separate machine tool required to execute VAM whereas with an addition of independent process, conventional machine tool is good enough for SDM process.

B. CNC G code program used in the experiments

```
%
O2321(WALEED TEST SAMPLES)
G80
G40
M69
G113
G107C0.
G18U0.W0.
N1(BAR-ROUGHING)
G30U0.W0.
M320
M46
M9
G50S1200
G00G96G99G40S90T606M3
G80
X32.Z3.0
G01G42X29.6F0.14
Z-20.5
G40X33.0
G00Z1.
G30U0.W0.
G97
G80
M5
M320
M46
G97
G23
M00
G40
M69
G113
G107C0.
G18U0.W0.
N1(BAR-FINISH CBN TOOL)
G30U0.W0.
G80
M320
M46
M9
G50S1000
G00G96G99G40S250T707M3
G80
X32.Z2.0
G01G42X29.4F0.15
Z-20.0
G40X33.0
G00Z2.0
G30U0.W0.
G97
G80
M5
M320
M46
G23
M00
N2(PART OFF 2.5MM WIDE BLADE)
G80
G40
M69
G113
G107C0.
G18U0.W0.
G99
G30U0.W0.
M320
M46
G50S1000
G00T808
G97S300M3
X33.0Z2.
Z-22.5
F0.04M08
G01X32.
G00U0.2
G01X31.
G00U0.2
G01X30.
G00U0.2
G01X29.
G01X28.
G00U0.2
G01X27.
G00U0.2
G01X26.
G00U0.2
G01X25.
G00U0.2
G01X24.
G00U0.2
G01X23.
G00U0.2
G01X22.
G00U0.2
G01X21.
G00U0.2
G01X20.
G00U0.2
G01X19.
G00U0.2
G01X18.
G00U0.2
G01X17.
G00U0.2
G01X16.
G00U0.2
G01X15.
G00U0.2
G01X14.
G00U0.2
G00U0.2
G01X13.
G00U0.2
G01X12.
G00U0.2
G01X11.
G00U0.2
G01X10.
G00U0.2
G01X9.
G00U0.2
G01X8.
G00U0.2
G01X7.
G00U0.2
G01X6.
G00U0.2
G01X5.
G00U0.2
G01X4.
G00U0.2
G01X3.
G00U0.2
M73
G97S300
G01X-0.2F0.03

G00X33.
M74
M9
G30U0.W0.
G80
M5
M320
M46
G97
G23
M30
%
```

C. Materails properties (Hardness and Composition)

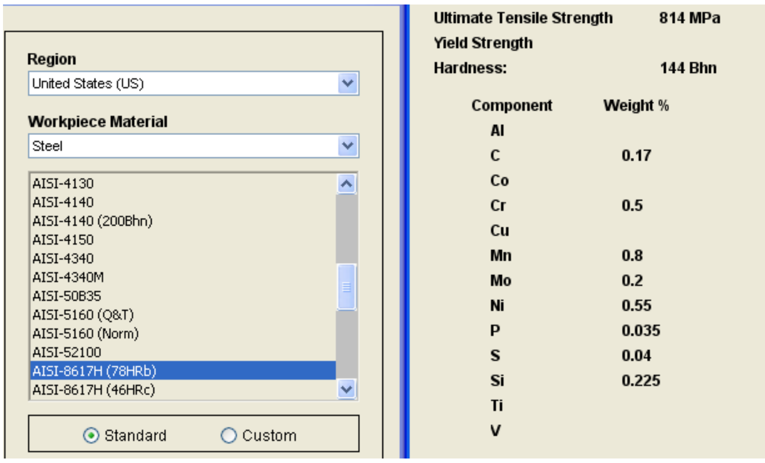

Region
United States (US)

Workpiece Material
Steel

AISI-4130
AISI-4140
AISI-4140 (200Bhn)
AISI-4150
AISI-4340
AISI-4340M
AISI-50B35
AISI-5160 (Q&T)
AISI-5160 (Norm)
AISI-52100
AISI-8617H (78HRb)
AISI-8617H (46HRc)

● Standard ○ Custom

Ultimate Tensile Strength	814 MPa
Yield Strength	
Hardness:	144 Bhn

Component	Weight %
Al	
C	0.17
Co	
Cr	0.5
Cu	
Mn	0.8
Mo	0.2
Ni	0.55
P	0.035
S	0.04
Si	0.225
Ti	
V	

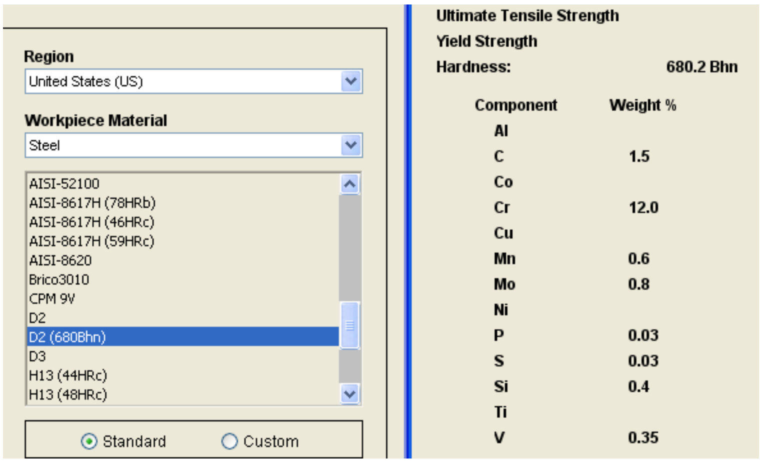

Region
United States (US)

Workpiece Material
Steel

AISI-52100
AISI-8617H (78HRb)
AISI-8617H (46HRc)
AISI-8617H (59HRc)
AISI-8620
Brico3010
CPM 9V
D2
D2 (680Bhn)
D3
H13 (44HRc)
H13 (48HRc)

● Standard ○ Custom

Ultimate Tensile Strength	
Yield Strength	
Hardness:	680.2 Bhn

Component	Weight %
Al	
C	1.5
Co	
Cr	12.0
Cu	
Mn	0.6
Mo	0.8
Ni	
P	0.03
S	0.03
Si	0.4
Ti	
V	0.35

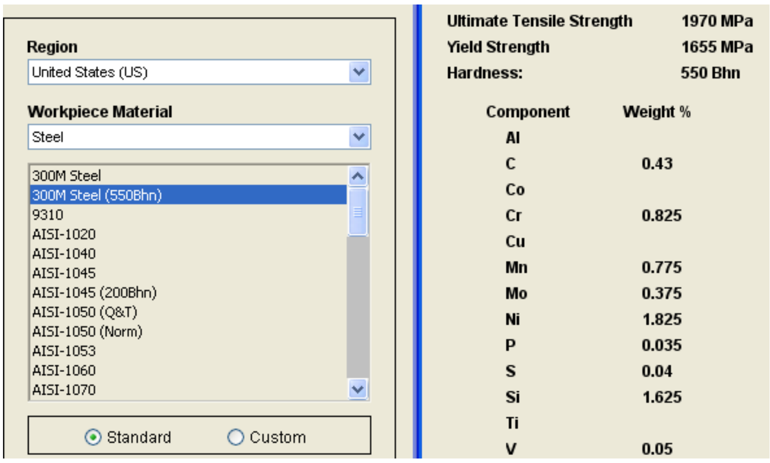

Region
United States (US)

Workpiece Material
Steel

300M Steel
300M Steel (550Bhn)
9310
AISI-1020
AISI-1040
AISI-1045
AISI-1045 (200Bhn)
AISI-1050 (Q&T)
AISI-1050 (Norm)
AISI-1053
AISI-1060
AISI-1070

● Standard ○ Custom

Ultimate Tensile Strength	1970 MPa
Yield Strength	1655 MPa
Hardness:	550 Bhn

Component	Weight %
Al	
C	0.43
Co	
Cr	0.825
Cu	
Mn	0.775
Mo	0.375
Ni	1.825
P	0.035
S	0.04
Si	1.625
Ti	
V	0.05

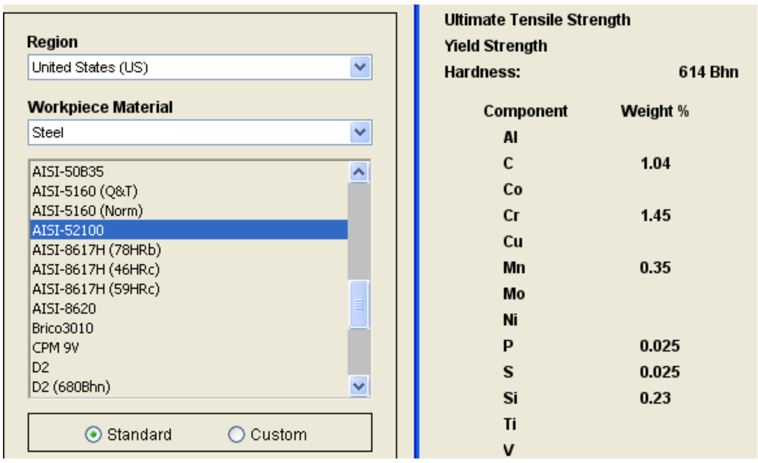
Region: United States (US)

Workpiece Material: Steel

AISI-50B35
AISI-5160 (Q&T)
AISI-5160 (Norm)
AISI-52100
AISI-8617H (78HRb)
AISI-8617H (46HRc)
AISI-8617H (59HRc)
AISI-8620
Brico3010
CPM 9V
D2
D2 (680Bhn)

● Standard ○ Custom

Ultimate Tensile Strength
Yield Strength
Hardness: 614 Bhn

Component	Weight %
Al	
C	1.04
Co	
Cr	1.45
Cu	
Mn	0.35
Mo	
Ni	
P	0.025
S	0.025
Si	0.23
Ti	
V	

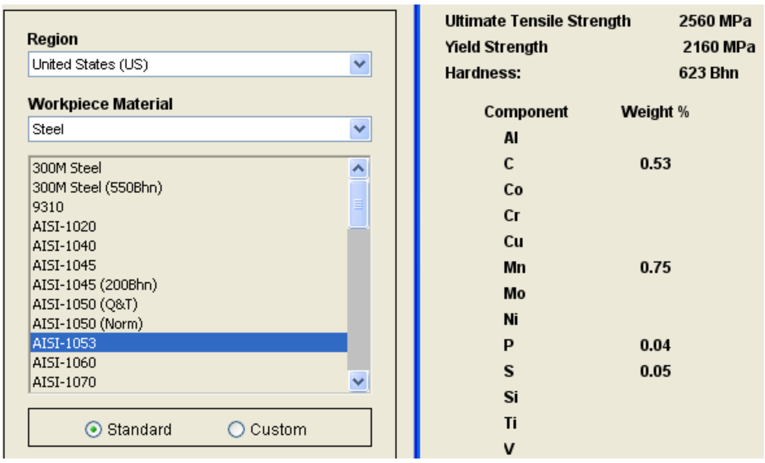
Region: United States (US)

Workpiece Material: Steel

300M Steel
300M Steel (550Bhn)
9310
AISI-1020
AISI-1040
AISI-1045
AISI-1045 (200Bhn)
AISI-1050 (Q&T)
AISI-1050 (Norm)
AISI-1053
AISI-1060
AISI-1070

● Standard ○ Custom

Ultimate Tensile Strength 2560 MPa
Yield Strength 2160 MPa
Hardness: 623 Bhn

Component	Weight %
Al	
C	0.53
Co	
Cr	
Cu	
Mn	0.75
Mo	
Ni	
P	0.04
S	0.05
Si	
Ti	
V	

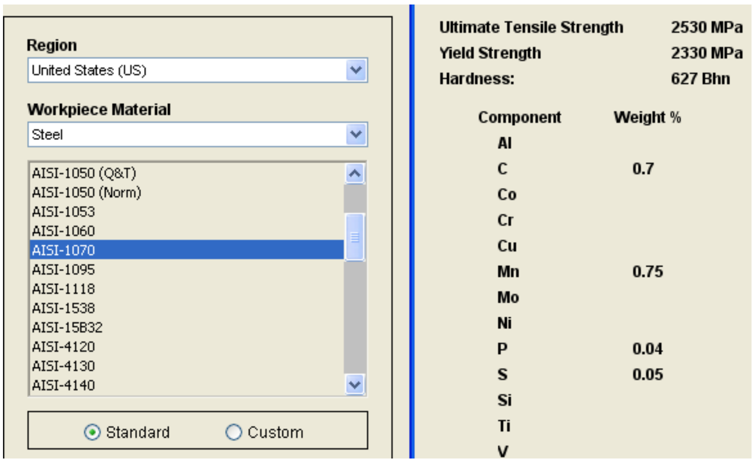
Region: United States (US)

Workpiece Material: Steel

AISI-1050 (Q&T)
AISI-1050 (Norm)
AISI-1053
AISI-1060
AISI-1070
AISI-1095
AISI-1118
AISI-1538
AISI-15B32
AISI-4120
AISI-4130
AISI-4140

● Standard ○ Custom

Ultimate Tensile Strength 2530 MPa
Yield Strength 2330 MPa
Hardness: 627 Bhn

Component	Weight %
Al	
C	0.7
Co	
Cr	
Cu	
Mn	0.75
Mo	
Ni	
P	0.04
S	0.05
Si	
Ti	
V	

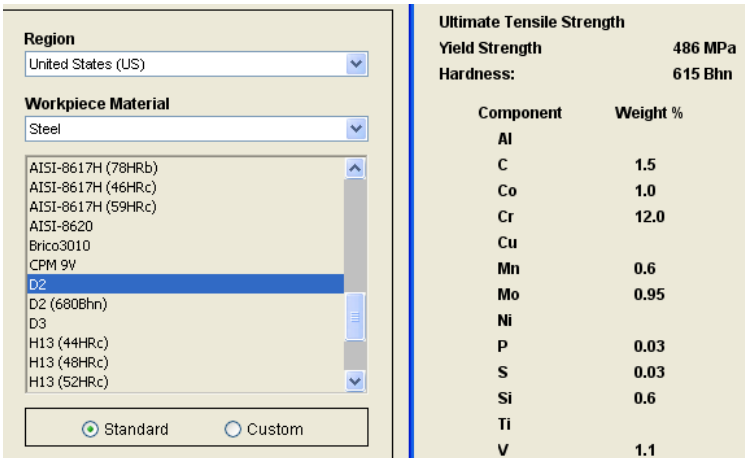
Region: United States (US)

Workpiece Material: Steel

AISI-8617H (78HRb)
AISI-8617H (46HRc)
AISI-8617H (59HRc)
AISI-8620
Brico3010
CPM 9V
D2
D2 (680Bhn)
D3
H13 (44HRc)
H13 (48HRc)
H13 (52HRc)

● Standard ○ Custom

Ultimate Tensile Strength
Yield Strength 486 MPa
Hardness: 615 Bhn

Component	Weight %
Al	
C	1.5
Co	1.0
Cr	12.0
Cu	
Mn	0.6
Mo	0.95
Ni	
P	0.03
S	0.03
Si	0.6
Ti	
V	1.1